

Development of a CRISPR-imaging toolset for imaging of genomic loci in living plants

**Dissertation
zur Erlangung des
Doktorgrades der Agrarwissenschaften (Dr. agr.)**

der

**Naturwissenschaftlichen Fakultät III
Agrar- und Ernährungswissenschaften,
Geowissenschaften und Informatik**

der Martin-Luther-Universität Halle-Wittenberg

vorgelegt von

Solmaz Khosravi
Geb. am 21.03.1981 in Tehran, Iran

Gutachter:

1. Prof. Dr. Andreas Houben
2. Dr. Frank Hartung

Tag der öffentlichen Verteidigung: 26. April 2021, Halle (Saale)

تقدیم بہ پدر و مادر عزیزم

*To two treasures of my life
my dear husband Christian and
my dear daughter Anita Sophie*

Acknowledgements

First, I would like to thank my supervisor Prof. Andreas Houben for allowing me to work on this hot topic and to enrich my knowledge about live-cell imaging. Dear Andreas, I appreciate your constant professional supervision of my work. With you, I learned not only how to be a good scientist but also how to keep a balance between my professional and my social life. Thank you for everything!

I also thank the collaboration partners of this project at KIT, Prof. Holger Puchta and especially Patrick Schindele. Working with you was for me a great honour and I learned a lot during my stay at KIT. Thank you!

Then, I would like to thank all CSF group members without whom I would not have been able to complete this research on time. My sincere thanks to dear Christin-Sophie Gaede, Oda Weiss, Sylvia Swetik and katrin Kumke. I thank you all for addressing all my questions and requests during performing my thesis! Also, thanks to Christine Helmold for helping me with stable transformation of Nicotiana.

I also appreciate Jana Lorenz at miosis group for providing me the restriction enzymes that I needed suddenly in critical moments of my cloning work. With your support Jana, the cloning steps of this work went on more fast. Thank you!

Furthermore, I would like to thank Dr. Twan Rutten for his great work on CSLM. With no doubt, your precious work to capture the required pictures and movies had a great influence for publishing our data.

Additionally, I would like to thank Dr. Veit Schubert and Dr. Evgeny Gladilin for helping me to work with Imaris and analysing the data obtained from Imaris.

My special thanks to Dr. Steven Dreissig for all the scientific discussions we had through this work. Your ideas and suggestions always helped me a lot. Thank you!

Additionally, I would like to thank Dr. Takayoshi Ishii and Dr. Dimitri Demodov for spending your time to answer questions and discussions during this work. Thank you both!

Also, I would like to appreciate Dr. Frank Dunemann and his team at JKI, Quedlinburg for performing the carrot transformation.

My special thanks to Dr. Jörg Fuchs, for his valuable comments on my PhD defense presentation.

My great thanks to Dr. Britt Leps for supporting me all these years for facing the challenges of my social life. Your experience and wisdom always saved me. You filled for me part of my family who is far away from me. Thank you for everything!

At least but not last, I also would like to appreciate my husband Christian hertig for his spiritual and scientific support during performing this challenging topic and also my little angel Anita

Sophie for her patience that gave me a peaceful time to be able to focus on writing my thesis and manuscript and putting an end to this research. I would also like to thank my parents who without their support I could never reach this step of my life. Thank you all!

Table of Contents

| | |
|---|----|
| List of abbreviations | 1 |
| 1. Introduction..... | 3 |
| 1.1. Organization of chromatin in interphase | 3 |
| 1.2. Different approaches for imaging of chromatin dynamic..... | 4 |
| 1.2.1. Imaging methods based on fixed specimens..... | 4 |
| 1.3. Live imaging methods..... | 7 |
| 1.3.1. Labelling of chromatin proteins in living cells | 7 |
| 1.3.2. Application of repressor/operator systems to visualize genomic regions | 8 |
| 1.3.4. ANCHOR for imaging of untargeted single-copy sequences in living cells..... | 9 |
| 1.3.5. Application of zinc finger proteins to visualize high copy repeats in living cells.... | 10 |
| 1.3.6. Transcription activator-like effector (TALE) for live-cell imaging | 11 |
| 1.3.7. CRISPR/Cas9 for live-cell imaging in plants..... | 12 |
| 2. Aims..... | 20 |
| 3. Materials and Methods | 21 |
| 3.1. Plant material and transformation | 21 |
| 3.1.1. <i>Arabidopsis thaliana</i> plant material and stable transformation | 21 |
| 3.1.2. <i>Nicotiana benthamiana</i> plant material for transient and stable transformation .. | 21 |
| 3.1.3. <i>Daucus carota</i> plant material and stable transformation | 21 |
| 3.2. Induction of transgene expression with β -estradiol | 21 |
| 3.3. Cloning and construct generation | 22 |
| 3.3.1. CRISPR live-cell imaging vectors | 22 |
| 3.3.2. Cloning of entry vector to destiny dCas9 vector | 23 |
| 3.3.3. Control vectors..... | 24 |
| 3.4. Protospacer design | 24 |
| 3.4.1. Targeting telomeric regions in <i>N. benthamiana</i> and <i>A. thaliana</i> | 25 |

| | |
|--|----|
| 3.4.2. Targeting centromeric regions in <i>A. thaliana</i> | 25 |
| 3.4.3. Targeting 5S rDNA, 45S rDNA and ITS regions in <i>N. benthamiana</i> | 26 |
| 3.5. Preparation of dCas9 constructs under the control of different promoters | 28 |
| 3.5.1. Isolation and cloning of the 35s promoter | 28 |
| 3.5.2. Isolation and cloning of the RPS5a promoter | 28 |
| 3.5.3. Isolation and cloning of XVE inducible promoter | 28 |
| 3.6. Improving the gRNA scaffold | 28 |
| 3.6.1. Insertion of aptamer sequences into the sgRNA scaffold | 28 |
| 3.6.2. Changing the sgRNA scaffold | 29 |
| 3.6.3. Altering the copy number of aptamers | 29 |
| 3.7. Immunostaining and fluorescence <i>in situ</i> hybridization (FISH) | 29 |
| 3.8. Microscopy | 31 |
| 3.9. Protease inhibitor test | 31 |
| 3.10. Analysis of telomere signals | 32 |
| 3.10.1. Labelling efficiency and signal/background noise | 32 |
| 3.10.2. Dynamics of telomeres | 32 |
| 3.11. Analysis of stably transformed plants | 33 |
| 3.11.1. DNA extraction | 33 |
| 3.11.2. PCR | 33 |
| 3.11.3. RNA extraction | 33 |
| 3.11.4. cDNA synthesis | 33 |
| 3.11.5. real-time PCR | 34 |
| 3.11.6. Immunostaining of dCas9 | 34 |
| 3.12. Comparison of XVE and ubiquitin promoter activity by real-time PCR | 34 |
| 4. Results | 36 |
| 4.1. Improving live imaging of telomeres with aptamer-based CRISPR/dCas9 vectors | 36 |

| | |
|--|----|
| 4.1.1. Aptamer-based labelled SpdCas9 (dCas9:2xMS/3xPP7:FP) vs. directly fused dCas9 to FP (dCas9:FP) for targeting the telomeric regions in <i>N. benthamiana</i> | 36 |
| 4.1.2. Changing the sgRNA scaffold | 39 |
| 4.1.3. Effect of aptamer copy numbers on labelling efficiency of telomeres | 40 |
| 4.1.4. Comparing the effect of different promoters to express dCas9 | 41 |
| 4.1.5. Analysis of telomere signals..... | 43 |
| 4.2. Targeting 5S rDNA, 45S rDNA and ITS regions in <i>N. benthamiana</i> | 44 |
| 4.2.1. Labelling of 5S rDNA | 45 |
| 4.2.2. Labelling of 45S rDNA | 46 |
| 4.2.3. Labelling of 45S rDNA ITS regions | 47 |
| 4.3. Application of CRISPR-imaging in stably transformed plants..... | 47 |
| 4.4. Application of Cas12 (Cpf1) for live-cell imaging of telomeres in <i>N. benthamiana</i> | 52 |
| 4.5. RNA targeting with dCas13..... | 53 |
| 5. Discussion | 56 |
| 5.1. Improving live imaging of telomeres with aptamer-based CRISPR/dCas9 vectors..... | 56 |
| 5.2. Targeting 5S rDNA, 45S rDNA and ITS regions in <i>N. benthamiana</i> | 57 |
| 5.3. Why does CRISPR imaging not work in stably transformed plants? | 59 |
| 5.4. Application of Cas12a (Cpf1) for live-cell imaging of telomers in <i>N. benthamiana</i> | 60 |
| 5.5. RNA targeting with Cas13 | 60 |
| 6. Outlook..... | 62 |
| 7. Summary..... | 64 |
| 8. Zusammenfassung..... | 66 |
| 9. References..... | 68 |
| 10. Curriculum vitae | 76 |
| 11. Eidesstattliche Erklärung / | 81 |
| Declaration under Oath..... | 81 |

12. Appendix I..... 82

List of abbreviations

Bimolecular fluorescence complementation (BiFC)

Bovine serum albumin (BSA)

Chromosome conformation capture (3C)

Chromosome territory (CT)

Clustered regularly interspaced short palindromic repeats (CRISPR)-associated caspase 9 (CRISPR/Cas9)

Cooled charge-coupled device (CCD)

CRISPR RNA (crRNA)

Cyan fluorescent protein (CFP)

dead Cas9 (dCas9)

Fluorescence *in situ* hybridization (FISH)

Fluorescent repressor- operator system (FROS)

Green fluorescent protein (GFP)

Nuclear export signal (NES)

Nuclear localization signal (NLS)

Nucleolar organizer regions (NORs)

Phosphate buffer solution, pH 7.4 (PBS)

Protospacer adjacent motif (PAM)

Red fluorescent protein (RFP)

Ribosomal DNA (rDNA)

RNA-guided endonuclease – *in situ* labeling (RGEN-ISL)

Room temperature (RT)

Saline sodium citrate (SSC)

Trans-activating CRISPR RNA (tracrRNAs)

Transcription activator-like effector (TALE)

Two and three dimensional (2D and 3D)

Yellow fluorescent protein (YFP)

Zinc finger proteins (ZFP)

1. Introduction

1.1. Organization of chromatin in interphase

The nuclear genome in eukaryotic cells is packed into a structure called chromatin. In 1928, Heitz observed for the first time intensively stained and condensed chromatin areas in interphase cells and termed it 'heterochromatin' (Heitz, 1928). While heterochromatin is poor in genes, the decondensed area of chromatin called 'euchromatin' is enriched with potentially active genes. In most organisms, heterochromatin is mainly localized towards the nuclear periphery. Euchromatin is located in the interior region of the nucleus (de Nooijer et al., 2009).

Heterochromatin is subdivided into constitutive and facultative heterochromatin. Constitutive heterochromatin is composed of repetitive sequences and is very stable. Facultative heterochromatin is formed under specific conditions, including developmental processes or tissue differentiation (Nishibuchi and Déjardin, 2017). The main constitutive heterochromatic regions in plants are located at centromeres, pericentromeres, telomeres, and nucleolar organizer regions (NORs) (Del Prete et al., 2014). The autosomal imprinted genomic loci in maize and *A. thaliana* are examples of facultative heterochromatin in plants (Alleman and Doctor, 2000)

The basic unit that causes chromatin compaction is the nucleosome, which plays a role in the regulation of gene expression. However, the amount of condensation that is needed for chromatin to fit in an interphase nucleus or a metaphase chromosome shows that there are extra higher-order levels of organization for chromatin. Any reproducible conformation of nucleosomes in 3D space is recognized as higher-order of chromatin, for example, the organization of chromatin fibre to mitotic/meiotic chromosome. Studies on 3D spatial location and transcriptional competence of genes concerning their chromosome territories have provided insights on the importance of this level of chromatin organization on the regulation of gene expression (Rosa and Shaw, 2013). The chromatin organization in interphase nuclei shows that chromosomes occupy distinct regions in the interphase nucleus, which are termed chromosome territories (Bovery, 1909; Rabl, 1885). The discovery of chromosome territories resulted in the finding that the chromatin organization is involved in the regulation of gene expression (Abranches et al., 1998; Wegel et al., 2009).

So far, different techniques have been developed to decipher how the chromatin structure is organized. Fluorescence *in situ* hybridization (FISH) is one of the primary techniques which was developed for this purpose. However, FISH requires the fixation of cells, which causes DNA and protein denaturation (Hoshi et al., 2011). Therefore, the chromatin structure is perturbed during FISH and is not the best indicator of its natural template (Schubert and Shaw, 2011). On the other hand, FISH can not be applied for *in vivo* monitoring of chromatin dynamics because of the fixation of cells and high-temperature treatment of cells required for hybridisation. To overcome this problem, live chromatin imaging techniques were developed to enable studying of biological compartments in their native context (Bystricky, 2015).

1.2. Different approaches for imaging of chromatin dynamic

1.2.1. Imaging methods based on fixed specimens

Experimental approaches that have been extensively used to investigate the chromosome structure in eukaryotes are DNA FISH (Bridger and Volpi, 2010), chromosome conformation capture (3C) and its derivatives (de Wit et al., 2012). FISH includes fixing and permeabilizing of cells, followed by the hybridization of fluorescently labelled DNA probes to a specific part of a chromosome. Before using single-stranded DNA probes, the sample must be denatured to allow that the probe can base-pair with the target DNA (Fig. 1). Consequently, the target region can be directly visualized by fluorescence microscopy. FISH enables the localization of the target locus to be studied in the context of the overall nuclear architecture and with respect to other genomic loci (Chaumeil et al., 2008). FISH can be performed in two and three dimensions (2D and 3D) (Cremer et al., 2007; Garimberti and Tosi, 2010). The fixation and permeabilizing procedures of cells differ between 2D and 3D FISH. In 2D FISH, the nucleus is flattened due to the treatment applied; therefore, standard microscopy can be used for imaging. In 3D FISH, the cellular morphology is conserved. Thus, imaging is performed in 3D by adjusting the focus in the Z direction. While 2D FISH is used more for comparing chromosomal positioning or positions of loci within chromosomes, 3D FISH can be applied for quantitative measurement of the three-dimensional distance between two targeted loci inside single cells. However, it should be considered that performing 3D FISH is technically more challenging (Giorgetti and Heard, 2016).

On the other hand, 3C and its derivatives are based on biochemical assays in which chromatin is first chemically crosslinked with formaldehyde. Crosslinking happens between loci that are

nearby in 3D space from a few nanometers up to a few hundred nanometers. Next, the crosslinked chromatin is digested, and afterwards, the DNA will be ligated. Depending on different 3C techniques, ligated products are detected by PCR or sequencing. It should be considered that finding a clear description of what is “sufficiently close” for crosslinking is not an easy task (de Wit and de Laat, 2012). While FISH has the power of single-cell analysing of gene positioning, 3C based methods enable the detection of physical proximity between multiple genomic loci (and eventually across an entire genome) simultaneously (Giorgetti and Heard, 2016).

Although FISH and 3C-based techniques have been successfully used for deciphering the chromatin organization, the necessary fixation steps in these techniques cause them to be just used in fixed cells. On the other hand, the chromatin structure is affected by the harsh treatments during fixation, which is not the real indicative of chromatin structure in living cells. Therefore, it would be of great importance to establish live-cell imaging techniques for studying the chromatin organization in plants.

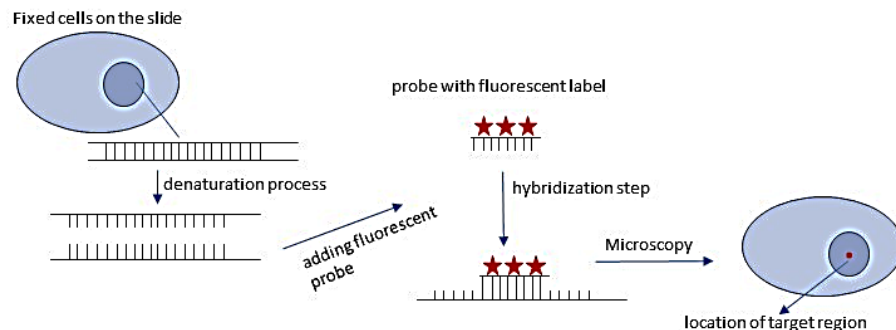


Fig. 1. FISH steps for labelling genomic regions in fixed nuclei or chromosomes. The fixed material is treated with heat and/or chemicals to denature DNA. Afterwards, the single-stranded target region is reachable by a labelled single-stranded probe. The probe can hybridize with the target sequence and the position of hybridization can be visualized by microscopy.

More recently, the use of fluorophore-coupled single guide RNA (sgRNA) in combination with Halo-tag coupled nuclease-deficient recombinant Cas9 (dCas9), together termed as Cas9-mediated FISH, allowed the labelling of repetitive DNA elements in fixed mammalian cells (Deng et al., 2015). Further development of this method, which does not require the laborious *in vitro* RNA synthesis or application of a Halo-tag approach and therefore simplifies the handling of the enzyme-RNA complex-based labelling of fixed nuclei and chromosomes, was

described by Ishii and colleagues (2019). The 'RNA-guided endonuclease – *in situ* labelling (RGEN-ISL)- method preserves the natural spatio-temporal organization of the chromatin and allows specific and simultaneous *in situ* detection of multi-colored genomic sequences by applying a complex of a two-part guide RNA and recombinant Cas9 endonuclease (Fig. 2). RGEN-ISL does not require the transformation of an organism with any kind of construct, enzymatic *in vitro* RNA synthesis and modified Cas9 proteins. The application of differentially labelled trans-activating CRISPR RNA (tracrRNAs) allows the multiplexing of RGEN-ISL. Real-time visualization of the Clustered Regularly Interspaced Short Palindromic Repeats/-associated caspase 9 - mediated (CRISPR/Cas9) DNA labelling process revealed the fast kinetics of the reaction. Using maize as an example, a combination of RGEN-ISL, immunostaining and 5-ethynyl-2'-deoxyuridine (EdU) labelling was used to visualize *in situ* specific repeats, histone marks and DNA replication sites, respectively (Němečková et al., 2019). To evaluate the influence of denaturation on the morphology of chromatin, RGEN-ISL was performed first and analysed by 3D super-resolution microscopy (3D-SIM). Afterwards, the same specimen was used for FISH. Using standard microscopy, the overall morphology of chromosomes and nuclei was similar for both methods. However, the application of 3D-SIM revealed subtle differences. It seemed, that FISH impaired and flattened the chromatin. In the case of RGEN-ISL, the chromatin structure remains more compact. Hence, RGEN-ISL is the method of choice for the visualization of repeats if the ultrastructure of chromatin is of interest. The broad range of adaptability of RGEN-ISL to different temperatures and combinations of methods has the potential to advance the field of chromosome biology. However, like for other imaging methods using fixed cells, the information regarding the chromatin dynamic in labelled regions is missing after application of RGEN-ISL.

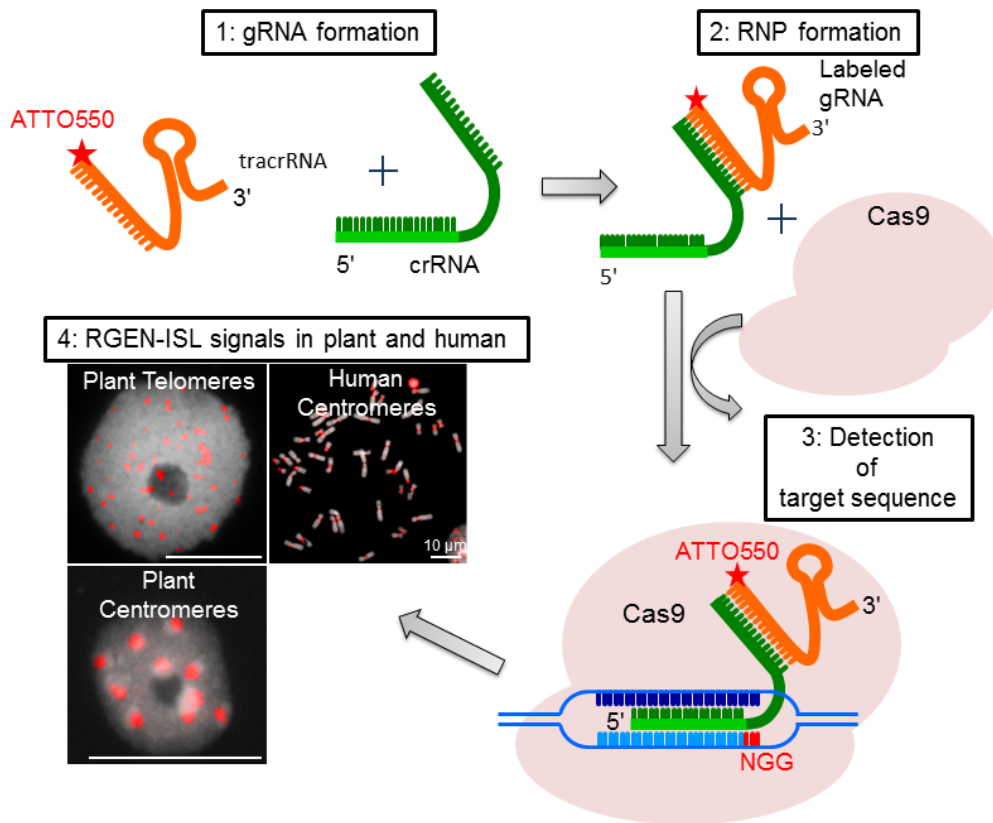


Fig. 2. RNA-guided endonuclease - *in situ* labelling (RGEN-ISL), a CRISPR/Cas9-based method to label genomic sequences in fixed cells. a) *In vitro* assembly of crRNA plus 5' labelled tracrRNA with Cas9 protein forms the RNP complex which can label different genomic regions. b) RGEN-ISL-based labelling of the telomere (*N. benthamiana* nucleus) and centromere (*A. thaliana* nucleus, *H. sapiens* chromosomes) repeats (picture is taken from Ishii et al., 2019).

1.3. Live imaging methods

1.3.1. Labelling of chromatin proteins in living cells

One of the early methods of live-cell imaging was based on the application of chromatin proteins including histones and condensins fused to fluorescent reporter proteins like green fluorescent protein (GFP) (Fujimoto et al., 2005; Kanda et al., 1998). The first application of histone H2B fused to yellow fluorescent protein (H2B:YFP) in *A. thaliana* showed that this live imaging technique does not interfere with the morphogenesis, cell cycle and fertility of the plant (Boisnard-Lorig et al., 2001). With this method, mitosis was observed in root tips and during endosperm development. With the production of transgenic *A. thaliana* lines expressing pWOX2-CENH3-GFP or p35S-CENH3-GFP fusion proteins, *in vivo* monitoring of ploidy levels in gametophytic and somatic cells was performed (De Storme, 2016). Although this method could be used to monitor the dynamics of chromatin, it does not label a defined

genomic sequence (Hihara et al., 2012) . To enable live-cell imaging in thicker tissues like meiocytes, anthers were cultured *in vitro* and treated with DNA interacting dyes, including DAPI. The behaviour of chromosomes during prophase I, anaphase I and II was analysed by multiphoton excitation microscopy. This method is capable of reaching signals up to 200 μm in depth. Accordingly, it was shown that meiotic chromosomes in maize exhibit short-range movements and sweeping motions during zygotene and pachytene, respectively (Sheehan and Pawlowski, 2009). In another method, the DNA dye Syto12 combined with the expression of β -tubulin fused to cyan fluorescent protein (CFP) was used to observe the movement of chromosomes and microtubulin fibres in maize meiocytes (Nannas and Dawe, 2016). Recently, live-cell imaging of male meiocytes of *A. thaliana* based on concomitant visualization of microtubules fused to red fluorescent protein (RFP) and a meiotic cohesin subunit fused to GFP enabled live-cell imaging of meiocytes. Five different cellular parameters including meiocyte cell shape, microtubule array shape, nucleus position, nucleolus position, and chromatin condensation were recorded. Accordingly, 11 different landmarks were identified during meiotic progression (Prusicki et al., 2019).

1.3.2. Application of repressor/operator systems to visualize genomic regions

Later, the fluorescent repressor-operator system (FROS) was developed to label chromatin more specifically. In this regard, specific sequences which can be later recognized by trans elements fused with fluorescent protein are inserted into the genome. The FROS method is taken from the bacterial lac operator/repressor system. In this system, 5 to 10 kb arrays of lac operator are integrated into the genome which can be detected by lacI fused with a fluorescent protein (Lassadi I. et al., 2015; Saad et al., 2014) (Fig. 3). The FROS system based on lac operator repeats was first used in mammalian cells and yeast to trace the chromatin organization (Robinett et al., 1996). Using this approach, the dynamics of chromatin in different cell types during various developmental times in *A. thaliana* could be observed (Kato, 2001). Later, a dual-colour imaging system was established by the application of a YFP-Tet repressor fusion protein bound to a *tet* operator, and a GFP or RFP-Lac repressor fusion protein bound to a *lac* operator (Matzke et al., 2005). Accordingly, a random static arrangement of interphase chromatin was demonstrated. The correlation between chromatin dynamics and gene expression as well as DNA damage was tested in *A. thaliana* (Hirakawa et al., 2015; Rosin et al., 2008). Tagging of two homologues loci in *A. thaliana* with lacO/LacI-EGFP showed that the inter-allelic distances of these loci were constant using time-lapse

microscopy in both elongated and meristemic cells, while the nuclear morphology changed a lot. Additionally, a correlation was found between the inter-allelic distance and the size of root nuclei (Hirakawa et al., 2015). Inter-allelic distances in nuclei are shortened significantly after γ -irradiation and treatment of lacO/LacI tagged plants with the radiomimetic reagent zeocin. Likely the inter-allelic distance of homologous loci is decreasing as part of the repair mechanism mediated by RAD54 (Hirakawa et al., 2015).

Since the FROS method needs the insertion of long tandem operator repeats into the genome of interest, *de novo* methylation of operator repeats and subsequent alteration of chromatin dynamics were observed (Jovtchev et al., 2011). Additionally, FROS may cause changes in the spatial organization of chromatin and tagged loci paired more often with each other than expected (Jovtchev et al., 2008; Pecinka et al., 2005; Schubert and Shaw, 2011). Taken together, FROS enabled to visualize ectopically inserted DNA sequences in live cells, but any observations made need to be interpreted with caution due to *de novo* DNA methylation and biased locus pairing at insertion sites.

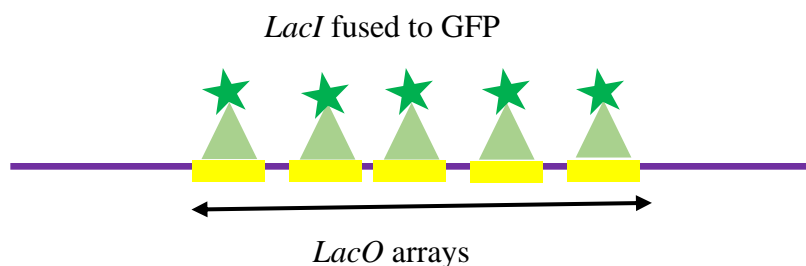


Fig. 3. FROS. LacO arrays (yellow lines) are inserted into the genome randomly and then are detected by LacI proteins (light green triangle) which are fused to a fluorescent protein (green stars).

1.3.4. ANCHOR for imaging of untargeted single-copy sequences in living cells

The ANCHOR system represents an alternative method to label single-copy sequences (Fig. 4). This system is composed of the ParB protein (OR) that specifically binds to a short *parS* non-repetitive DNA target sequence (ANCH) and spreads onto neighbouring sequences by protein oligomerization. When the OR protein is fused to GFP, its accumulation results in a site-specific fluorescent focus. This method includes 0.4 - 1 kb unique sequences called *parS* which can be recognized by ParB proteins. The *parS* is inserted upstream of the target sequence, and once ParB is attached to *parS*, it recruits many other ParB dimers which bind non-specifically to

adjacent DNA (Germier et al., 2018). This method was used to capture the dynamics of human cytomegalovirus (HCMV) infection and replication in human living cells (Mariamé et al., 2018). At present, the drawback of the ANCHOR method similar to FROS is untargeted labelling of the genome. Therefore, the future application of ANCHOR in combination with site-specific integration of *parS* could result in a tool suitable to label single-copy sequences in plants and other species.

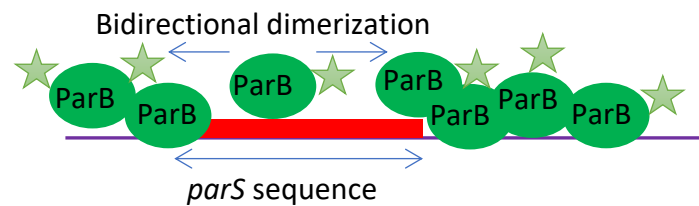


Fig 4. ANCHOR. The *parS* sequence (red line) is inserted into the genome randomly and is then detected by ParB proteins fused to a fluorescent protein. Once ParB is loaded on *parS*, it causes dimerization of other ParB proteins (green ovals) into the location to the adjacent DNA.

1.3.5. Application of zinc finger proteins to visualize high copy repeats in living cells

The Cys₂-His₂ zinc finger motif is the most commonly used DNA binding motif in eukaryotes which was identified from the DNA and RNA binding transcription factor TFIIIA (Miller et al., 1985). Zinc finger proteins (ZFP) consist of 30 amino acids with a $\beta\beta\alpha$ structure (Fig. 5). The α -helix domain of the ZFP is responsible for interacting with three nucleic acids within the major DNA groove. The recognition specificity is based on the position of responsible amino acids at the position of -1, +1, +2, +3, +4, +5 and +6 relative to the start point of the α -helix. Any change in these amino acids alters the recognition site of the ZFP (Liu et al., 1997). To specifically recognize 18 base pairs of DNA, six linked ZFPs are required. In plants, ZFPs fused with GFP under the control of the ribosomal protein 5SA promoter (RPS5Ap) were used to recognize centromeric tandem repeats in the root meristems of *A. thaliana* (Lindhout et al., 2007). Although ZFP-GFP could be used for detection of highly repetitive sequences in mouse and *A. thaliana*, it was not successful for labelling of moderate and low copy sequences. Later the centromere-specific ZFP-GFP reporter was used to identify meiosis-specific promoters in *A. thaliana* (van Tol et al., 2019). For this purpose, the centromere-specific ZFP-GFP reporter was tested with 14 different candidate promoters which were isolated upstream of genes active in meiocytes. Visualization of fluorescent foci in meiocytes revealed which of the selected promoters could be used for the expression of the desired protein in meiocytes.

Since the sequence and chromatin content around the target sequence along with the context-dependent interactions with neighbouring zinc fingers (ZFs) affects the recognition ability of ZFPs (Sanjana et al., 2012); (Gaj et al., 2013), there are limitations regarding which DNA sequence can be visualized with the help of ZFP-GFP reporters.



Fig 5. Zink finger proteins (ZFPs, green circles) fused to a fluorescent protein (green star). Each ZF can detect three bp nucleotides in the DNA.

1.3.6. Transcription activator-like effector (TALE) for live-cell imaging

The transcription activator-like effector (TALE) was discovered in the plant pathogenic bacteria genus *Xanthomonas*. When *Xanthomonas* attacks the plant, TALE proteins are secreted into the plant cell via the type III secretion pathway. By playing the role of plant transcription factors, TALE proteins manipulate the expression of their target genes. Each TALE contains a central repeat domain, which includes 33-35 conserved amino acids. However, amino acid number 12 and 13 within the repeat are variable and called repeat variable di-residue (RVD) (Boch et al., 2009). Each RVD is responsible for recognizing one nucleotide in DNA. The most frequently used RVDs are NI (asparagine, isoleucine), HD (histidine, aspartic acid), NN (asparagine, asparagine) and NG (asparagine, glycine) which can detect the bases A, C, G and T, respectively (Mak et al., 2012) (Fig. 6). Each TALE is capable of binding with a single nucleotide, and the mechanism of attachment is that each repeat of TALE is wound around the DNA in a helical structure (Stella et al., 2013).

Similar to ZFPs, TALEs can be programmed to detect specific DNA sequences (Ma et al., 2013; Miyanari et al., 2013). Using this feature, telomeric sequences, 180-bp centromeric sequences and 18S ribosomal DNA (rDNA) repetitive sequences in different tissues of *A. thaliana* including roots, hypocotyls, leaves, and flowers were successfully used to be visualized by GFP-tagged TALEs (Fujimoto et al., 2016). TALE signals for telomeres were enriched around the nucleolus, while centromere signals were peripherally distributed in the nucleus during interphase. TALE-based imaging demonstrated the mobility of centromeres and telomeres in nuclei of different plant organs. However, the intensity of TALE signals varied among different

tissues. For 18S rDNA, one to four strong signals and regarding 5S rDNA, three to six weak signals were detected. The maximum number of telomere signals recorded by this method was up to 13 signals out of a potential maximum of 20 signals in 2C nuclei. The specificity of TALE signals coming from centromeres and telomeres was confirmed either by CENH3 immunostaining or sequence-specific FISH probes. However, being a time consuming and laborious method due to re-engineering of TALE proteins for the targeting of each new genomic region, the live-cell imaging techniques were improved to use a more user-friendly method called CRISPR/Cas9.



Fig. 6. TALE protein fused to a fluorescent protein (green star). Each RVD (NI, HD, NN and NG) in TALE can recognize one base pair of DNA.

1.3.7. CRISPR/Cas9 for live-cell imaging in plants

The discovery of type II clustered regularly CRISPR/ Cas9 system derived from *Streptococcus pyogenes* has revolutionized the field of chromatin imaging (Fig. 7) (Chen et al., 2013). The system consists of a Cas9 protein and a guide RNA (gRNA) scaffold. The gRNA complex is formed by the fusion of CRISPR RNA (crRNA) and tracrRNA. The crRNA is composed of 20 nucleotides and complementary to the genomic DNA upstream of protospacer adjacent motif (PAM) sequence which is recognized by Cas9, while the tracrRNA has a loop structure required for the stability of the whole complex. Cas9 contains two HNH and RuvC-like domains. The HNH domain cuts the complementary strand of crRNA, and the RuvC-like domain cleaves the opposite strand of the double-stranded DNA (Chen et al., 2014). The induction of two point mutations in the HNH and RuvC domains resulted in the generation of a catalytically inactive, so-called, dead Cas9 variant (dCas9) (Qi et al., 2013). dCas9 has lost its nuclease activity and can be conjugated to fluorescent proteins to be programmed for DNA imaging. CRISPR-based imaging was used for targeting telomere repeats in human cells, pericentric and centric sequences in mouse cells and even a single chromosomal locus in *Xenopus* egg extracts (Anton et al., 2014; Chen et al., 2013; Lane et al., 2015) (Table 1).

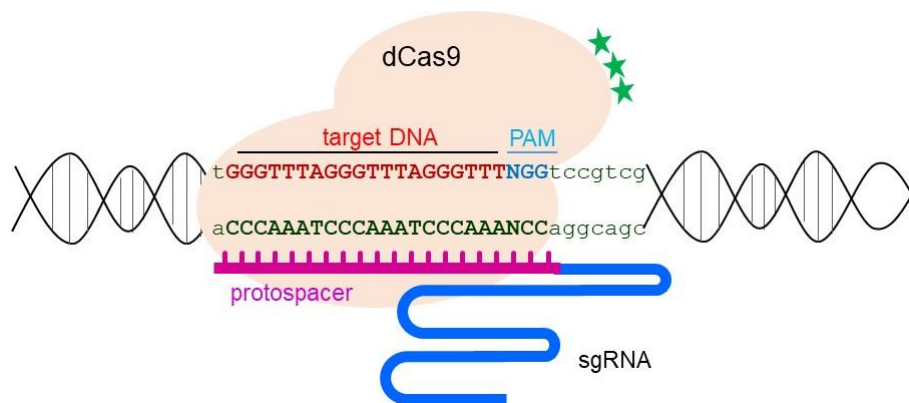


Fig. 7. dCas9 directly labelled with a fluorescent protein (green stars). The PAM region is recognized by the dCas protein, and then the DNA is unwound, allowing the protospacer (pink) of the gRNA to bind the target region in the template strand.

In plants, the successful application of different Cas9 orthologues from *Streptococcus pyogenes* and *Staphylococcus aureus* for imaging of telomeric sequences was reported for *N. benthamiana* (Dreissig et al., 2017; Fujimoto and Matsunaga, 2017). These experiments demonstrated that telomeres are localized in the periphery of interphase nuclei. Furthermore, tracking of individual telomere positions for 30 minutes revealed the dynamic positional changes of telomeres up to $\pm 2 \mu\text{m}$. The observed interphase telomere dynamics could be involved in regulating transcriptional changes due to the silencing effect of telomeric heterochromatin (Cryderman et al., 1999; Gottschling et al., 1990; Nimmo et al., 1994), telomerase activity (Schrumppfova et al., 2016), or transcription of telomeric tandem repeats (Koo et al., 2016). Furthermore, both Cas orthologues of *S. pyogenes* and *S. aureus* could be used for this purpose with comparable efficiency. However, the efficiency of dCas9 was 70% of a telomere labelling by standard FISH. Additionally, *N. benthamiana* plants were co-transformed with Cas9 targeting telomers and a telomeric repeat binding protein (TRB1) (Dvořáčková et al., 2015). Successful colocalization of CRISPR-derived telomeric signals and signals arising from TRB1 showed that this technique can be used for DNA/protein interaction studies (Dreissig et al., 2017). However, the same method was not successful for labelling of telomeric regions in stably transformed *A. thaliana*, suggesting that the CRISPR Cas9-based reporter might interfere with the progression of the cell cycle (Fujimoto and Matsunaga, 2017).

Table 1. Applications of different CRISPR live-cell imaging methods.

| Species | Target | Method | Reference |
|----------------------------------|---|--|---|
| Yeast | rDNA condensation | Directly labelled dCas9 | (Xue and Murat, 2018) |
| <i>N. benthamiana</i> | Dynamic of telomeres | Directly labelled dCas9 variants (Sp, Nm, St1) | (Dreissig et al., 2017) |
| <i>Xenopus</i> egg extracts | Dynamics of pericentric regions | Directly labelled SpdCas9 | Lane et al. 2015 |
| Mouse cell culture | Dynamic of telomeres | Aio-Casilio | (Zhang and Song, 2017) |
| Mouse cell culture | Allele-specific live- cell imaging | SNP-CILING | (Maass et al., 2018) |
| Mouse cell culture | Mobility of <i>cis</i> - elements including promoter and enhancer | Directly labelled SpdCas9 | (Gu et al., 2018) |
| Living mice and cell cultures | Dynamic of telomeres | Directly labelled SpdCas9 | (Duan et al., 2018) |
| Human cell lines | Telomere dynamic and subnuclear localization of nonrepetitive loci | Directly labelled SpdCas9 | (Chen et al., 2013) |
| Human cell lines | Dynamic of telomeres | SunTag | (Tanenbaum et al., 2014; Ye et al., 2017) |

| | | | |
|------------------------------|--|--|--|
| Human cell lines | Dynamic of intranuclear distance between pericentromeric and sub-telomeric regions | Directly labelled dCas9 variants (Sp, Nm, St1) | (Ma et al., 2015) |
| Human cell lines | Dynamic of telomeres and centromeres during mitosis | Indirectly labelled dCas9 with aptamers | (Shao et al., 2016; Wang et al., 2016) |
| Human and mouse cell culture | Dynamic of pericentromeric regions | Indirectly labelled dCas9 with aptamers | (Fu et al., 2016) |
| Human cell lines | Dynamic of single copy loci during cell cycle | Indirectly labelled dCas9 with aptamers | (Qin et al., 2017) |
| Human cell lines | Multiple targeting of repetitive regions | CRISPRainbow | (Ma et al., 2016a) |
| Human cell lines | Dynamic of telomeres and of single copy loci | BiFC | (Hong et al., 2018) |
| Human cell lines | Visualization of chromosome rearrangements | LiveFISH | (Wang et al., 2019) |

To increase the signal intensity of CRISPR-based reporters suitable for the detection of low and single-copy sequences different approaches were developed in the non-plant field. The first CRISPR imaging methods were based on direct labelling of dCas (Chen et al., 2013). Accordingly, the dynamic of chromatin was tracked during mitosis by labelling of telomeres and nonrepetitive genes (*Muc*). To enrich the intensity of signals in the nuclei, SpdCas9 directly

labelled by EGFP was fused with nuclear localization signal (NLS) sequences. Additionally, implementation of some changes in the gRNA scaffold, including induction of A-U flip and insertion of 5'UGCUG3' increased the number of signals rising from telomeres and signal/background noise ratio. Being able to show the minimum required numbers of sgRNAs (at least 36) for labelling of a single copy gene, the genes *Muc4* and *Muc1* were successfully labelled simultaneously (Chen et al., 2013).

Later it was shown that indirect labelling of dCas could produce higher quality signals with more reliability. In this regard, different methods, including SunTag, aptamer-based methods, and biomolecular fluorescence complementation (BiFC) were developed. However, in a comprehensive study, it was shown that the reliability of each labelling method could be different from the other one (Hong et al., 2018).

The SunTag, which is a protein tagging method for enhancement of signals, was combined with CRISPR imaging. For this purpose, the C terminal of dCas9 was linked to 24 copies of a GCN4 peptide which could be recognized by GCN4 peptide-binding single-chain variable fragment antibody (scFv-GCN4) fused to GFP (Fig. 8).

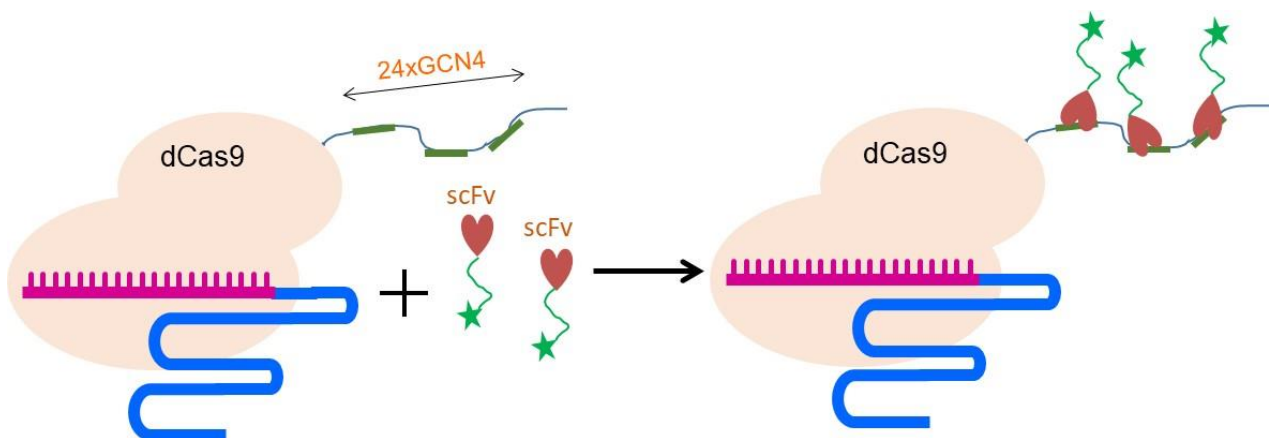


Fig. 8. Indirect labelling of dCas9 with a SunTag. dCas9 is fused to repetitive arrays of GCN4 which can be detected by a specific ScFv antibody. The ScFv is fused to a fluorescent protein (green star).

The telomeric regions were targeted by co-expression of dCas9-SunTag24x_v4 and scFv-GCN4-GFP (Tanenbaum et al., 2014). Notably, the indirect labelling of dCas9 through SunTag method did not affect the mobility of telomeres, though resulted in 19-fold brighter signals in comparison to the application of directed labelled Cas9 to GFP.

The fact that each Cas variant from different bacterial strains pairs only with its cognate sgRNA widened the capacity of CRISPR for multi-colour live-cell imaging (Esvelt et al., 2013). In this

regard, pericentromeric and subtelomeric repeats in human cell line were co-labelled with different orthologues of *S. pyogenes* (Sp), *Neisseria meningitides* (Nm), and *Streptococcus thermophilus* (St1) fused with various fluorescent proteins (Ma et al., 2015). More importantly, orthologues of SpCas9, such as St1Cas9 and SaCas9 have been confirmed to be functional in plants (Dreissig et al., 2017). Although multi-colour labelling of chromatin through the recruitment of various Cas orthologues made great progress. The second generation of CRISPR live-cell imaging vectors was developed due to the complicated required PAM sequences for Cas9 from *N. meningitidis* and *S. thermophilus* compared to *S. pyogenes*. Additionally, dCas9 of *N. meningitidis* and *S. thermophilus* showed lower labelling efficiency in comparison to *S. pyogenes* (Esvelt et al., 2013; Shao et al., 2016). These vectors consist of a “dead” SpCas9 (SpdCas9) protein and structurally modified sgRNAs with RNA aptamer MS2/PP7 insertions that bind to fluorescent coat protein-tagged tdMCP and tdPCP (Fu et al., 2016; Shao et al., 2016) (Fig. 9). According to the position of insertion of aptamers into sgRNA scaffold, various labelling efficiency results were obtained. Subsequently, the dynamics of telomeres and centromeres in human cell culture during mitosis were observed, and the condensation process of these regions during the cell cycle did not affect the binding ability of the new vectors (Shao et al., 2016). Increasing the copy number of MS2 or PP7 aptamers up to 6 increased the signal to background noise ratio while targeting telomeric and centromeric sequences. Co-targeting of these regions with MS2 or PP7 aptamers at the same time resulted in non-overlapping fluorescence signals demonstrating the orthogonality of these aptamers, which is important for multi-colour labelling (Wang et al., 2016).

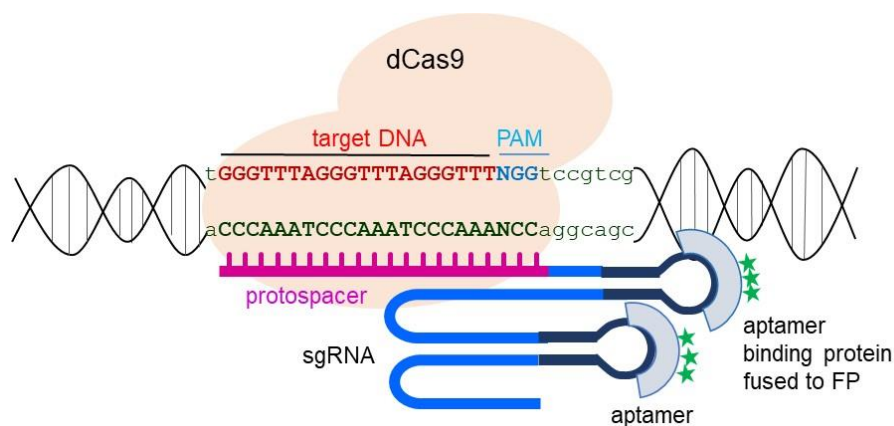


Fig. 9. Indirect labelling of dCas9 with aptamers. In the sgRNA scaffold, a stem-loop structure called aptamer is integrated, which can be recognized with the aptamer binding protein fused to a fluorescent protein (FP, green star).

To optimize the efficiency of this method for labelling of non-repetitive sequences, 16 copies of the MS2 aptamer were integrated into the sgRNA scaffold. Application of only four sgRNAs was enough to label the nonrepetitive Muc4 gene in human cell culture (Qin et al., 2017). In a similar method called Aio-Casilio, 25 copies of a particular eight nucleotides RNA sequence named PUF binding site was inserted in the sgRNA scaffold (Zhang and Song, 2017). PUF binding sites could be recognized by the Pumilio/fem-3 mRNA binding factor proteins and FBF proteins RNA-binding domain (PUF domain) which were fused with mClover. The Aio-Casilio system was used to label telomeric and some major repetitive sequences in a mouse cell culture (Zhang and Song, 2017). Another hairpin structure (boxB) along with MS2 and PP7 was combined with sgRNA scaffold to expand the multiple labelling capacity of aptamer-based imaging vectors (Ma et al., 2016a). Therefore, having the possibility of using three different fluorescent proteins, seven colours could be produced to construct the CRISPRainbow system for the labelling of multiple regions at targets located on human chromosomes 1, 3, 7, 13, 14, and X. Application of short sgRNA sequences, close to the length of the seed region eased the multiple targeting with CRISPRainbow (Ma et al., 2016a).

To increase the specificity of the indirectly labelled dCas9 for imaging of genomic regions, the bimolecular fluorescence complementation (BiFC) assay was employed in combination with the SunTag (Fig. 10) or aptamer-based imaging methods. BiFC is based on the association of fluorescent protein fragments that are attached to components of the same macromolecular complex. To recruit BiFC for the SunTag method, the splitted fluorescent protein Venus was fused with a single-chain variable fragment antibody (scFv). The attachment of scFv to GCN4 peptides in Cas9 brings the splitted parts of the Venus fluorescent protein together and therefore leads to fluorescent signals in the labelled region. Additionally, BiFC was combined with the MS2 aptamer-based live-cell imaging method. In this regard, the divided fluorescent protein Venus was fused to dCas9 and tdMCP. Subsequently, binding of tdMCP to MS2 aptamers bring one part of the split fluorescent protein Venus near to the part which is fused to dCas9, causing the fluorescent signal. In the combination of BiFC with both the SunTag and aptamer-based imaging method, which is called SunTag-dCas9-MCP-BiFC, split parts of Venus were fused to tdMCP and SunTag. Comparison of the BiFC based labelling method with other CRISPR imaging methods showed that the intensity of signals was increased and no non-specific signals were observed (Hong et al., 2018).

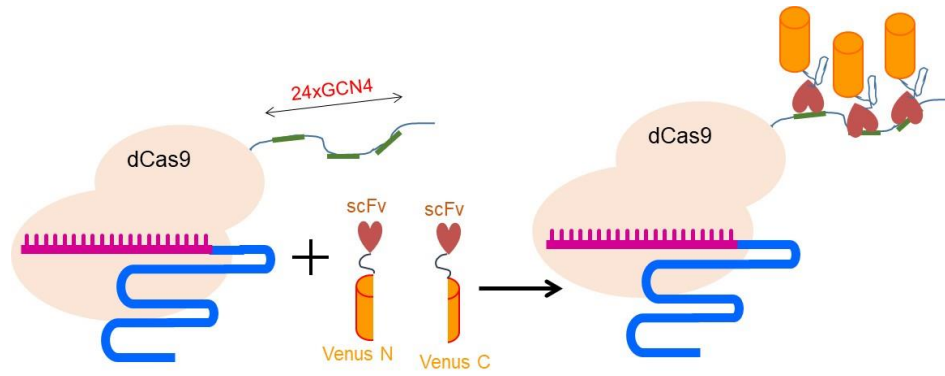


Fig. 10. Indirect labelling of dCas9 with BiFC. dCas9 is tagged with 24 copies of GCN4 which is recognizable by an ScFv antibody. ScFv antibody is fused to divided parts of the Venus fluorescent protein (VN and CN). Once ScFv attaches to GCN4, Venus fluorescent proteins can come in the vicinity and complete each other.

2. Aims

Chromatin is highly dynamic in living cells and has a regulatory role in several biological mechanisms including transcription, replication and DNA repair mechanisms. A live imaging method to study the spatio-temporal organization of chromatin is instrumental in deciphering how these biological processes are regulated in time and space.

Among different live-cell imaging methods, the most convenient and specific labelling method of defined genomic loci in living cells is based on the application of CRISPR/Cas9. CRISPR live-cell imaging was established first for the visualization of repetitive sequences in mammalian cell culture. Afterwards, the method was improved and applied for studying the dynamic of repetitive and non-repetitive loci in mammalian cell culture. However, our knowledge about using this method for live-cell imaging for plants is limited. This study is the continuation of the work of Dreissig et al. (2017) about the application of CRISPR/Cas9 for live-cell imaging in plants with a special focus on:

- I. Improvement of CRISPR live imaging constructs to increase the labelling efficiency in plant cells;
- II. CRISPR-based labelling of different genomic regions like telomeres, 45S rDNA and centromeres;
- III. Establishment of a stable live-cell imaging method in plants;
- IV. Application of Cas12a (Cpf1) for live-cell imaging;
- V. RNA targeting with Cas13.

3. Materials and Methods

3.1. Plant material and transformation

3.1.1. *Arabidopsis thaliana* plant material and stable transformation

Arabidopsis thaliana (L.) var. Columbia-0 (Col-0) was used for transformation in all experiments. Seeds were sown in soil and germinated under short-day conditions (16h dark/8h light, 18-20 °C) and then transferred to long-day conditions (16h light/ 8h dark, 18-20°C) before bolting. *A. thaliana* stable transformation was performed by the floral dip method (Clough and Bent, 1998). For the selection of primary transformants, the seeds were sterilized and plated on ½ Murashige, and Skoog (Lieberman-Aiden et al., 2009) basal medium (Sigma) supplemented with the adequate antibiotics when required and grown in a growth chamber under long-day conditions.

3.1.2. *Nicotiana benthamiana* plant material for transient and stable transformation

Nicotiana benthamiana seeds were grown in a greenhouse under 16/8 hours light/dark conditions and 22°C temperature for 2-4 weeks. Then, the plants were transformed transiently by the syringe infiltration method (Phan and Conrad, 2016) and then the infiltrated plants were kept back in a greenhouse under 16/8 hours light/dark conditions and 22°C temperature for 3 days. Some of the plants which were infiltrated with Cpf1 imaging vectors were kept in a growth chamber under 16/8 hours light/dark conditions and 30°C temperature for 3 days. Stable transformation of *N. benthamiana* leaf samples was done according to (Clemente, 2006). Additionally, *N. benthamiana* line expressing CFP-histone H2B was used for transient expression experiments (Martin et al., 2009).

3.1.3. *Daucus carota* plant material and stable transformation

Three different cultivars of *Daucus carota*, including Blanche, Yellowstone and Rotin were used. *Agrobacterium rhizogenes*-based hairy root transformation was performed according to (Dunemann et al., 2019). The transformation of *D. carota* was performed in the laboratory of Dr. Frank Dunemann (JKI, Quedlinburg).

3.2. Induction of transgene expression with β -estradiol

β -Estradiol was used for gene induction in *N. benthamiana* plants which were transiently transformed with constructs under the control of the inducible XVE promoter. The induction was performed by 'painting' of the injected leaf area with 100 μ M β -Estradiol (Sigma) one day

after injection. One day after 'painting', samples were taken from the painted area for further analysis.

For *A. thaliana* plants which were stably transformed with constructs under the control of the inducible XVE promoter, the induction was performed by transferring three-week-old plants from gentamycin selection medium to MS medium containing 5 μ M β -estradiol. For further analysis, leaf samples were collected 24-48 h after induction. As a control, *A. thaliana* plants which were transformed with the pER8:mCherry plasmid (provided by Dr. David Zalabák) were used. These plants show continuous expression of GFP. However, expression of mCherry can be observed only after transgene induction with β -estradiol.

3.3. Cloning and construct generation

Four types of cloning strategies were used to generate the CRISPR imaging constructs, including traditional cloning with restriction enzymes, Golden Gate Assembly, Gibson (NEB) and Gateway cloning (Invitrogen). For ligation of DNA, the Quick ligation Kit (NEB) was used following the instructions of the manufacturer. Sequencing of constructs was performed by the sequencing platform of IPK, Gatersleben and Eurofins, Germany.

3.3.1. CRISPR live-cell imaging vectors

In collaboration with the research laboratory of Prof. Holger Puchta (KIT, Karlsruhe) we used two different variants of Cas proteins for live-cell imaging including dCas9 from *S. pyogenes* and Cas12 (Cpf1) from *Francisella novicida* (dFnCpf1) and *Acidaminococcus* sp., (dAsCpf1). Both Cas variants were deactivated by induction of mutations in the nuclease domains to produce dCas. RuvC1 and HNH nuclease domains (D10A and H841A), RuvC (E993A) and RuvC (D917A and E1006A) were mutated via site-directed mutagenesis for the Cas9, AsCpf1 and FnCpf1, respectively (Fauser et al., 2014; Yamano et al., 2016; Zetsche et al., 2015).

For RNA targeting, two variants of deactivated Cas13, including dLwCas13a from *Leptotrichia wadeii* (Abudayyeh et al., 2016) and drfxCas13d from *Ruminococcus flavefaciens* (Konermann et al., 2018) were used. Both dCas13 vectors were fused with GFP. dLwCas13a and drfxCas13d were additionally fused to a nuclear export signal (NES) and nuclear export signal (NLS), respectively.

3.3.2. Cloning of entry vector to destiny dCas9 vector

For aptamer-mediated imaging, sgRNA expression vectors were created either harbouring one MS2 aptamer sequence each in the tetraloop and stem-loop 2 of the *S. pyogenes* sgRNA backbone (Koneremann et al. 2015). Besides, three PP7 aptamer sequences only in the tetraloop of the *S. pyogenes* sgRNA backbone additionally comprising an A-U pair flip and stem extension were generated (Shechner et al. 2015). In the case of MS2, vector pDS2.0-MS2 was synthesized comprising the respective sgRNA under control of the AtU6-26 promoter together with the codon-optimized MS2 binding protein CDS joined to a 3' SV40 NLS by a 3x GGGGS linker under control of the ZmUbi-1 promoter. In the case of PP7, the respective sgRNA and codon-optimized PP7 binding protein CDS also harbouring a 3' SV40 NLS were synthesized and subcloned via restriction digestion and ligation into pDS2.0-MS2 creating pDS2.0-PP7. *BsmBI* restriction sites downstream of the aptamer binding protein CDS were used for in-frame cloning of a 3-fold fusion of either eGFP or mRuby2. For this purpose, the respective CDS were amplified from pSIM24-eGFP and pcDNA3-mRuby2 (www.addgene.com) with primers (MS2(NLS)-GFP#1-f, GFP#1-linker1-r, linker1-GFP#2-f, GFP#2-linker2-r, linker2-GFP#3-f, GFP#3-nos_ter-r or MS2(NLS)-mRuby#1-f, mRuby#1-linker1-r, linker1-mRuby#2-f, mRuby#2-linker2-r, linker2-mRuby#3-f, mRuby#3-nos_ter-r) adding homologous flanks for subsequent Gibson Assembly into the linearized pDS2.0-MS2 or pDS2.0-PP7 similar as previously described (Dreissig et al. 2017) creating pDS2.0-MS2/PP7-3xeGFP/3xmRuby2 as entry vectors (primers are listed in Appendix I). The entry vector was digested with *BsmBI* and ligated with annealed primers which include the protospacer sequence for targeting a particular genomic region. The primers hold the *BsmBI* overhangs at 5' ends. The selection marker used for this vector is ampicillin. The DNA fragments of the entry vector required for live-cell imaging were shuttled into the destiny vector by Gateway cloning with LR Clonase II.

The destiny vector pDe-SpydCas9-GentR carries the dCas9 from *S. pyogenes* and the gentamycin selection marker for plant material and spectinomycin resistant gene for bacterial selection. The dCas9 is driven by the ubiquitin promoter from parsley.

The entry vectors pEn-RZ_As-Chimera and pEn-RZ_Fn-Chimera were used as gRNA expression vectors for AsCpf1 and FnCpf1. The gRNA scaffold is driven by the AtU6-26 promoter. The integration of protospacer sequence into entry vectors was performed by digestion of the vector with *BbsI* and the following ligation with the annealed primers which carry the

sequence of target region based on complementary flanks to *BbsI* overhangs. The vector includes an ampicillin-resistant gene. The DNA fragments of vectors required for live-cell imaging were cloned into the destiny vector by Gateway cloning with LR Clonase II.

The destiny vectors pDe-dAsCpf1:3xeGFP-PPT and pDe-dFnCpf1:3xeGFP-PPT were used as expression vectors for ASCpf1 and FnCpf1, respectively. Both vectors include a spectinomycin resistant gene for bacterial selection and phosphinothricin resistance for plant material selection.

The entry vectors pENLwaCas13a and pENCasRX were used as gRNA expression vectors for dLwCas13a and dRfxCas13d. The gRNA scaffold is driven by the AtU6-26 promoter. The integration of protospacer sequence into entry vectors was performed by digestion of the vector with *BbsI*. Ligation was performed with the annealed primers which carry the sequence of the target region based on complementary flanks to *BbsI* overhangs. The vectors include an ampicillin-resistant gene. The DNA fragments of vectors required for live-cell imaging were cloned into the destiny vector by Gateway cloning with LR Clonase II.

The destiny vectors pDe-LwdCas13a-GFP-PPT-NF-NES and pDe-dCas13d-GFP-PPT-NLS/NES were used as expression vectors for dLwCas13a and dRfxCas13d, respectively. Both vectors include a spectinomycin resistant gene for bacterial selection and phosphinothricin resistance gene for plant material selection.

3.3.3. Control vectors

According to previous work, pChimera expression gRNA vector in combination with dCas9:GFP expression vector was used as a control vector to target telomeric regions (Dreissig et al., 2017). As negative controls, infiltration of *N. benthamiana* with constructs carrying pSpdCas9GFP without telomere-specific gRNA or pMS2mRuby targeting telomers without dCas9 was performed. pMS2mRuby contains a gRNA scaffold for *S. pyogenes* fused to the MS2 aptamer sequence and tdMCP fused to mRuby.

3.4. Protospacer design

The protospacer design was performed with the help of on-line software DeskGen (<https://www.deskgen.com/>).

3.4.1. Targeting telomeric regions in *N. benthamiana* and *A. thaliana*

The telomere protospacer sequence was selected based on the PAM sequence of Cas9 and Cpf1 and synthesized as primer oligos (Eurofins) with appropriate overhangs at 5' ends for cloning into the pDS2.0-MS2:3xeGFP/mRuby for dCas9 and respective pChimera vector for dCpf1 (Table 2). The telomere protospacer was designed based on *Arabidopsis*-type telomere repeat sequence 5'-(TTTAGGG)(n)-3'.

Table 2 Different telomeric protospacers for dCas9, dCpf1 and dLwCas13a. Overhangs at 5' end are shown in lowercase.

| dCas variant | PAM | Telomere specific protospacer oligos |
|--------------|------|---|
| dCas9 | NGG | Forward : 5'-attgGGGTTTAGGGTTTAGGGTTT-3' Reverse: 5'-aaacAAACCCTAAACCCTAAACCC-3' |
| dAsCpf1 | TTTA | Forward : 5'-agatGGGTTTAGGGTTTGGGTTTAG-3' Reverse: 5'-ggccCTAAACCCAAACCCTAAACCC-3' |
| dAsCpf1 | TTTA | Forward : 5'-agatGGGTTTAGGGTTTGGGTTTAGGG-3' Reverse: 5'-ggccCCCTAAACCCAAACCCTAAACCC-3' |
| dFnCpf1 | TTTG | Forward : 5'-agatGGTTTAGGGTTTAGGGTTTGGGTT-3' Reverse: 5'-ggccCAACCCAAACCCTAAACCCTAAACC-3' |
| dFnCpf1 | TTT | Forward : 5'-agatAGGGTTTAGGGTTTGGGTTTAGG-3' Reverse: 5'-ggccCCTAAACCCAAACCCTAAACCCT-3' |
| dLwCas13a | --- | Forward: 5'-aaacGTTTAGGGTTTAGGGTTTGGTTTAGGGT-3' Reverse: 5'-aaaaACCCTAAACCCAAACCCTAAACCCTAAAC-3' |

3.4.2. Targeting centromeric regions in *A. thaliana*

The centromere-specific protospacer was designed based on the centromeric pAL repeat of *A. thaliana* (Martinez-Zapater et al., 1986). Different PAM sequences were considered to

select the protospacer sequences (Table 3). Similar to telomere protospacers, each pair of protospacers was synthesized as oligo primers with appropriate overhangs at 5' ends for cloning into the pDS2.0-MS2:3xeGFP vector.

Table 3. Different centromeric protospacers for dCas9. Overhangs at 5' end are shown in lowercase.

| PAM | Centromere specific protospacer oligos |
|-----|---|
| TGG | Forward: 5'-attgACCTTCTTCTTGCTTCTCAA -3' Reverse: 5'-aacTTGAGAAGCAAGAAGAAGGT -3' |
| AGG | Forward : 5'-attgTCTTCTTGCTTCTCAAAGCT-3' Reverse: 5'-aacAGCTTTGAGAAGCAAGAAGA-3' |
| GGG | Forward: 5'-attgATATGAGTCTTTGGCTTTGT-3' Reverse: 5'-aacACAAAGCCAAAGACTCATAT-3' |

3.4.3. Targeting 5S rDNA, 45S rDNA and ITS regions in *N. benthamiana*

The 45S rDNA sequence of *N. benthamiana* with accession number KP824745.1 was used to design protospacer for 25S and 18S rDNA plus ITS1 and ITS2 regions (Table 4). The protospacer sequence was synthesized as oligo primers and cloned into pDS2.0-MS2:3xeGFP. To target 5S rDNA, the CDS of 5S rDNA from *A. thaliana* with the accession number M65137 was selected and blasted against the 5S rDNA sequence from *N. benthamiana* with the accession number KP824744.1. Sequence identical regions were selected to design FISH probes (Table 5) and protospacers (Table 4). The 5srDNA protospacers were also cloned into pDS2.0-MS2:3xeGFP.

Table 4. Different 45S rDNA and 5S rDNA protospacers for dCas9 and dRfxCas13d. Overhangs at 5' end are shown in lowercase.

| dCas variant | Target region | PAM | Protospacer sequence |
|--------------|--------------------------|-----|--|
| dCas9 | 25S rDNA | GGG | Forward : 5'-attgGACGACTTAAATACGCGACG-3' Reverse: 5'- aaacCGTCGCGTATTTAAGTCGTC-3' |
| dCas9 | 25S rDNA | GGG | Forward : 5'- attgGATGGTGAACACTATGCCTGAG-3' Reverse: 5'- aaacCTCAGGCATAGTTCACCATC-3' |
| dCas9 | 18S rDNA | TGG | Forward: 5'- attgCGAGGCGCTGTCTACGAGTC-3' Reverse: 5'- aaacGACTCGTAGACAGCGCCTCG-3' |
| dCas9 | 5S rDNA | TGG | Forward: 5'-attgGGGCGAGAGTAGTACTAGGA-3' Reverse: 5'-aaacTCCTAGTACTACTCTCGCCC-3' |
| dCas9 | 5S rDNA | GGG | Forward: 5'-attgGGCGAGAGTAGTACTAGGAT-3' Reverse: 5'-aaacATCCTAGTACTACTCTCGCC-3' |
| dCas9 | ITS1-non template strand | CGG | Forward: 5'- attgGGTGATTAACGAACCCCGGC-3' Reverse: 5'- aaacGCCGGGGTTCGTTAATCACC-3' |
| dCas9 | ITS1- template strand | CGG | Forward: 5'- attgGTGATTAACGAACCCCGGCG-3' Reverse: 5'- aaacCGCCGGGGTTCGTTAATCAC-3' |
| dCas9 | ITS2 | TGG | Forward: 5'- attgGCGACGGACGTACGACAAG-3' Reverse: 5'- aaacCTTGTCGTGACGTCCGTCGC-3' |
| dRfxCas13d | 25S rDNA | --- | Forward:5'- aaacTTTAAGCATATCAATAAGCGGAGGAAAA-3' Reverse: 5'- aaaaTTTTCTCCGCTTATTGATATGCTTAAA-3' |

3.5. Preparation of dCas9 constructs under the control of different promoters

3.5.1. Isolation and cloning of the 35s promoter

The 35S promoter was amplified with *EcoRI*-35S-f1 and r1 primers flanking with *EcoRI* recognition site from pCCNCEN (Appendix I). Then it was digested with *EcoRI* and cloned to linearized pDe-SpydCas9-GentR with *EcoRI* from which the *EcoRI* site in the backbone was removed by a site-directed mutation in advance.

3.5.2. Isolation and cloning of the RPS5a promoter

The same procedure that was used for cloning of 35s promoter was used for RPS5a promoter (Weijers *et al.*, 2001). The isolation of RPS5A was done by RPS5A-FWD and REV primers from the pGPTV-BAR (Appendix I).

3.5.3. Isolation and cloning of XVE inducible promoter

The XVE inducible promoter was generated with primers (Cas9-XVE-F, XVE-Lexa-A-R, XVE-Lexa-A-F and LexA-Cas9-R) containing homologous flanks for further Gibson Assembly into the pDe-Sp-dCas9 GentR (Appendix I). The pER8-v3 plasmid was used for the preparation of the XVE inducible promoter (Zuo *et al.*, 2000)

3.6. Improving the gRNA scaffold

3.6.1. Insertion of aptamer sequences into the sgRNA scaffold

For aptamer-mediated imaging, sgRNA expression vectors were created either harbouring one MS2 aptamer sequence each in the tetraloop and stem-loop 2 of the *S. pyogenes* sgRNA backbone (Konermann *et al.*, 2015) or three PP7 aptamer sequences only in the tetraloop of the *S. pyogenes* sgRNA backbone additionally comprising an A-U pair flip and stem extension (Shechner *et al.*, 2015). In case of MS2, the vector pDS2.0-MS2 was synthesized comprising the respective sgRNA under control of the AtU6-26 promoter together with the codon-optimized MS2 binding protein CDS joined to a 3' SV40 NLS by a 3x GGGGS linker under control of the ZmUbi-1 promoter. In case of PP7, the respective sgRNA and codon-optimized PP7 binding protein CDS also harbouring a 3' SV40 NLS were synthesized and subcloned via restriction digestion and ligation into pDS2.0-MS2 creating pDS2.0-PP7. *BsmBI* restriction sites downstream of the aptamer binding protein CDS were used for in-frame cloning of a 3-fold fusion of either eGFP or mRuby2. For this purpose, the respective CDS were amplified from pSIM24-eGFP and pcDNA3-mRuby2 (www.addgene.com) with primers (MS2(NLS)-GFP#1-f, GFP#1-linker1-r, linker1-GFP#2-f, GFP#2-linker2-r, linker2-GFP#3-f, GFP#3-nos_ter-r or

MS2(NLS)-mRuby#1-f, mRuby#1-linker1-r, linker1-mRuby#2-f, mRuby#2-linker2-r, linker2-mRuby#3-f, mRuby#3-nos_ter-r) adding homologous flanks for subsequent Gibson Assembly into the linearized pDS2.0-MS2 or pDS2.0-PP7 similar as previously described (Dreissig et al. 2017) creating pDS2.0-MS2/PP7-3xeGFP/3xmRuby2 (Appendix I).

3.6.2. Changing the sgRNA scaffold

A MS2 aptamer-harboring sgRNA additionally comprising an A-U flip and stem extension (Chen et al., 2013) was synthesized and subcloned into pDS2.0-MS2-eGFP/mRuby2. For this purpose, pDS2.0-MS2-eGFP/mRuby2 was amplified with primers (pDS2.0- Δ sgRNA-r, pDS2.0- Δ sgRNA-f) deleting the sgRNA and the synthesized sgRNA was amplified with primers (sgRNA2.0-MS2-flip/ext-f, sgRNA2.0-MS2-flip/ext-r) adding overhangs for subsequent Gibson Assembly into the linearized backbone (Appendix I).

3.6.3. Altering the copy number of aptamers

To change the copy number of aptamers, the pDS.2.0-MS2:3xeGFP expression vector was used. To delete one of MS2 copies, pDS.2.0-MS2:3xeGFP was double digested with *AgeI* and *MscI* restriction enzymes and then was ligated to annealed primers Apta2-FWD and Apta2-Rev flanked by *AgeI* overhang (Appendix I). Annealing of primers was done by mixing 2 μ l of each primer (100 pM) in a total volume of 50 μ l double distilled water and incubation at 95 °C. Colony PCR was performed by SS42 and Apta2-Rev2 primers under following conditions: 95°C for 5 min, 30x (95°C for 30 sec, 58°C for 30 sec, 72°C for 30 sec.), 72°C 5 min. Positive clones were confirmed by sequencing with the SS42 primer (Appendix I). To increase the copy number of aptamer sequences, a sgRNA harbouring 16 MS2 aptamers was synthesized and subcloned into pDS2.0-MS2-eGFP/mRuby2. For this purpose, pDS2.0-MS2-eGFP/mRuby2 was digested with *BsmBI* and *AgeI* for sgRNA deletion, and the synthesized sgRNA was digested with *BsaI* and *AgeI* for subsequent ligation into the linearized pDS2.0-MS2-eGFP/mRuby2 creating pDS2.0-16xMS2-eGFP/mRuby2.

3.7. Immunostaining and fluorescence *in situ* hybridization (FISH)

For immunostaining, the plant material was fixed in 4% paraformaldehyde (freshly made from a 37% solution) in 1x phosphate buffer solution, pH 7.4 (PBS) (137 mM NaCl, 2.7 mM KCl, 10 mM Na₂HPO₄, 1.8 mM KH₂PO₄) on ice for 5 min under vacuum condition in a Concentrator (5301, Eppendorf) following 25 min without vacuum condition. Then, it was washed twice with 1xPBS. After, the plant material was chopped in a droplet of chromosome isolation buffer (15

mM Tris, 2 mM Na₂EDTA, 0.5 mM spermine tetrahydrochloride, 80 mM KCL, 20 mM NaCl, 15 mM β-mercaptoethanol, 0.1% (vol/vol) Triton X-100, adjusted pH to 7.5 with 1 M NaOH) in a petri dish with a sharp razor blade. Subsequently, 450 µL of chromosome isolation buffer was added to the homogenate, and then it was filtrated through a 35 µm cell suspension filter tube. Then, 200 µl of the homogenate was applied to a cytology funnel and centrifuged for 5 min at 450 rpm in a Cyto centrifuge (Cytospin3, Shandon). The slides were washed two times in PBS for 5 min. Then, 60 µl of 4% bovine serum albumin (BSA) was applied, followed by incubation at room temperature for 45 min in a high humidity plastic box. The slides were carefully covered with parafilm tape. The slides were washed two times in PBS for 5 min. Afterwards, 60 µl of GFP antibody solution was applied (2% (vol/vol) BSA in PBS, GFP antibody in 1:2500 dilution) (directly labelled GFP mouse antibody Dylight 488; Rockland, cat. 200-341-215) followed by incubation at room temperature for 1 hour in a high humidity plastic box. The slides were carefully covered with parafilm tape.

For combining immunostaining with FISH, the slides were washed two times in PBS for 5 min and then fixed in acetic acid solution (1:3 mixture of acetic acid glacial:100% ethanol) for 24 hours in darkness. Later, sequential dehydration was performed in ethanol solutions starting with lower to higher concentration (70, 90, and 100 %) for 2 min each and let the slides to dry for some minutes. Afterwards, pre-hybridization at 37 °C was performed overnight by adding 15 µl FISH hybridization solution (50% (vol/vol) formamide, 10% (vol/vol) dextran sulfate in 2xSSC). The slides were covered with coverslips and stored in a high humidity plastic box. Following, they were washed twice in 2x saline sodium citrate (SSC: 0.30 M sodium citrate, 0.030 M NaCl, pH 7.0.) for 5 min and sequential dehydration was performed in 70, 90, and 100 % ethanol for 2 min each. The slides left to dry for some minutes.

For DNA denaturation, the slides were kept in a denaturation solution (0.2 M NaOH in 70% ethanol) at room temperature for 10 min followed by sequential dehydration in 70, 90, and 100 % ethanol for 2 min each. The slides left to dry for some minutes. Meanwhile, the FISH hybridization solution was prepared by mixing 0.5 µl of the 5'-labelled oligonucleotide probe (10 µM) (Table 5) with 14.5 µl of FISH hybridization solution per slide. Therefore, the mixture was incubated at 95 °C for 5 min, followed by rapid transfer onto the ice for 5 minutes. Later, 15 µl of the mixture was applied per slide and hybridized at 37 °C overnight. Slides were covered with coverslips and stored in a high-humidity plastic box.

Subsequently, the slides were washed two times in 2x SSC for 5 min, followed by sequential dehydration in 70, 90, and 100 % ethanol for 2 min each and left to dry for some minutes. Finally, 10 µl VECTASHIELD solution containing DAPI (1:1000) was applied on each slide. Slides were analyzed by fluorescence microscopy.

Table 5. 5'-labelled oligonucleotide FISH probes used for labelling of different genomic regions.

| Probe name | Probe sequence |
|-----------------|---|
| Telomere | 5'-Cy5-GGGTTTAGGGTTTAGGGTTT-3' |
| Centromere | 5'- Cy3- ATACGTTCTTCTTGCTTCTCAAAGCGTTCATGGTGTACCCAAAGCCCATATGAGTCT TTGGCTTTGTGTCTTCTAACAAGGAACTTAAGTCTTTAAGATCCGGTTGCG GTTAAGTTCTTATACTCAATCATATCACATGCGATCAAGTCATATTCGACTCCAAA ACACTAACC-3' (Martinez-Zapater et al., 1986) |
| 5s rDNA probe 1 | 5'-Cy3-CTTGGGCGAGAGTAGTACTAGGATGGGTG-3' |
| 5s rDNA probe 2 | 5'-Cy3-CACCGGATCCCATCAGAACTCCG-3' |

3.8. Microscopy

Micrographs were captured using an epifluorescence microscope (Olympus BX61) equipped with a cooled charge-coupled device (CCD) camera (Orca ER; Hamamastu). Images were collected from at least 10 nuclei per experiment and then analyzed with IMAGEJ. For live-cell imaging, a confocal laser scanning microscope (LSM780, Carl Zeiss) was used. To detect fluorescence signals *in vivo*, a piece of infiltrated leaf was cut, and with the use of 40x NA 1.2 water objective nuclei with clear signals were tracked for 20 minutes. 488-nm laser line was used for excitation of GFP, and emission was detected over a range of 490-540 nm.

3.9. Protease inhibitor test

MG-132 (Serva) stock solution in DMSO was prepared (42 mM). Then, the stably transformed *A. thaliana* plants were treated with MS medium plus MG-132 with a concentration of 50, 100 or 150 µM was prepared. The plants were kept in this medium under the dark condition at room temperature for 16 h.

3.10. Analysis of telomere signals

3.10.1. Labelling efficiency and signal/background noise

To estimate and compare the labelling efficiency of different constructs, the observed number of signals from 20 nuclei for each experiment was counted, and the mean value was calculated.

To measure the signal/background noise ratio, images were acquired with an epifluorescence microscope (BX61; Olympus) using a cooled charge-coupled device (CCD) camera. The ImageJ software was used for analyzing the signal/background noise ratio by dividing the signal intensity to minimum signal intensity rising from the background. The mean value was calculated from three measurements in each nucleus, and 10 nuclei were considered in total for each construct.

3.10.2. Dynamics of telomeres

To study the movement of telomeres, *N. benthamiana* leaves were transiently transformed with dCas9:2xMS2:GFP (dCas9 derived by different promoters) and dCas9:GFP for targeting telomeres. Telomere tracking was performed for 5 nuclei per applied construct and was based on time-laps z stacks from IMARIS 8.0 (Bitplane). The adjustments to calculate the coordinates (x, y, z) of each telomere and also measuring the inter-telomere distances were based on Dreissig et al. 2017. To assess true displacements of telomeres over time, global movements of nuclei have to be computationally eliminated. For this purpose, 3D point clouds of telomere mass centres for all subsequent time steps ($t>0$) were rigidly registered to the reference system of coordinates defined by the first time step ($t=0$) using absolute orientation quaternions (Horn, 1987). To quantify the intranuclear telomere motion, the mean square distance (MSD) of telomeres relatively to their initial position ($t=0$) was calculated as

$$MSD(t) = \frac{1}{N} \sum_{i=1}^N (R_i(t) - R_i(0))^2, \quad \text{Eq. 1}$$

where $R_i(t)$ is the radius vector of the i -th registered telomere in the reference system of coordinates at the time point $t>0$.

3.11. Analysis of stably transformed plants

N. benthamiana and *A. thaliana* plants and *D. carota* roots were stably transformed with telomere imaging construct pDS2.0-MS2:3xeGFP:dCas9-Gent. The plants and roots from *N. benthamiana*, *A. thaliana* and *D. carota* growing on selection medium were analyzed by fluorescence microscopy, respectively. Later, DNA and RNA were extracted from *N. benthamiana*, *A. thaliana* and *D. carota* leaves and roots, respectively.

3.11.1. DNA extraction

DNA was extracted from 100 mg of grounded plant materials. The extraction buffer (1.2 ml) was mixed with RNase (5 µl/10ml from 100 mg stock) and added to the plant material and incubated at 65°C for 15 min. Then, it was cooled down at room temperature (RT) for 1 min. Later, 600 µl of chloroform:isoamyl alcohol (1:24) was added and gently mixed for 5 min. Afterwards, the samples were centrifuged for 2 min at RT. The top layer was transferred into a clean tube, and 700 µl of isopropanol was added and well mixed. The mixture was kept for 2 min at RT and then centrifuged 10 min at RT. The pellet was washed with 70% ethanol and finally was dissolved in 50 µl of distilled water.

3.11.2. PCR

The extracted DNA from selected plants was used to perform PCR to confirm the presence of T-DNA. Therefore, primers amplifying GFP and dCas9 were designed and used for PCR (Appendix I). PCR was done in the following condition: 95°C for 5 min, 30x (95°C for 30 sec, 60°C for 30 sec, 72°C for 30 sec.), 72°C 5 min.

3.11.3. RNA extraction

RNA was extracted from 100 mg of the grounded leaf of *N. benthamiana* and *A. thaliana* and root of *D. carota* with the Spectrum plant total RNA isolation kit (Sigma). Then, the quantity and quality of extracted RNAs were measured using a NanoDrop spectral photometer.

3.11.4. cDNA synthesis

cDNA was synthesized from 1 µg of isolated RNA with the RevertAid H minus reverse Transcriptas kit (Thermo Scientific). Then, 1 µl of each synthesized cDNA was used to perform PCR with PP2A-F and PP2A-R primers for PP2A endogenous gene of *N. benthamiana*, Helicase-F and Helicase-R for the endogenous gene in *A. thaliana* and Actin-F and Actin-R for the endogenous gene in *D. carota* (Appendix I) with following conditions: 95°C for 5 min, 30x (95°C

for 30 sec, 60°C for 30 sec, 72°C for 30 sec.), 72°C 5 min. RNA samples were used as the negative control.

3.11.5. real-time PCR

The relative quantification method ($2^{-\Delta CT}$) was used to evaluate the quantitative variation of dCas9 and GFP expression between stable and transient transformed plants with the telomere targeting construct pDS2.0-MS2:3xeGFP:dCas9-Gent (Schmittgen and Livak, 2008). First, the efficiency of all primers including PP2A, helicase, actin, GFP and dCas9 (Appendix I) were measured by performing real-time PCR with the serial dilution of synthesized cDNAs (1:10, 1:50, 1:100, 1:200, 1:500, and 1:1000) with following conditions: 95°C for 10 min, 40x (95°C for 15 sec, 60°C for 1 min) and program of 95 °C for 15 s, 60 °C for 1 min, and 95 °C for 30 s, 60 °C for 15 s (melt curve stage) in Applied Biosystems® QuantStudio™ 6 Flex Real-Time PCR.

In the next step, all real-time PCR experiments were performed under the same condition and 1:10 diluted cDNA samples. To prepare the master mix for real-time reactions, Power SYBR Green PCR master mix (ThermoFisher Scientific, Cat. 436759) was used with the following mixture: 5 µl of Cyber green, 1 µl of each forward and reverse primers (3 µmol) and 3 µl of diluted cDNA in final 10 µl. To load the samples, 348-well plates (Applied Biosystems, Cat. 4483320), and ThermalSeal sealing films (Sigma, cat. Z734438-100EA) was used.

3.11.6. Immunostaining of dCas9

Nuclei were isolated from stably transformed *A. thaliana* encoding a centromere-specific CRISPR imaging construct. Immunostaining of dCas9 was performed as described in section 3.7 with a mouse monoclonal antibody against SpCas9 (0.67 mg/ µl, Novus Biologicals, cat. NBP2-52398R) with different concentrations 5, 10 and 20 µg. Isolated nuclei from wild type plants were used as a negative control. The Cy3 channel was used for microscopy.

3.12. Comparison of XVE and ubiquitin promoter activity by real-time PCR

N. benthamiana leaves were separately infiltrated with the telomere imaging constructs pDS2.0-MS2:3xeGFP:dCas9-Gent in which dCas9 was driven by XVE or ubiquitin promoters. DNA and RNA were extracted as described in section 3.11.1 and 3.11.3, respectively. Then, cDNA was synthesized and controlled, as explained in section 3.11.4. Real-time experiments were performed with three biological samples for each transformation plus three technical

replicates (described in section 3.11.5) to compare the expression level of dCas9 when it is driven with an inducible or constitutive promoter.

4. Results

4.1. Improving live-cell imaging of telomeres with aptamer-based CRISPR/dCas9 vectors

4.1.1. Aptamer-based labelled SpdCas9 (dCas9:2xMS/3xPP7:FP) vs. directly fused dCas9 to FP (dCas9:FP) for targeting the telomeric regions in *N. benthamiana*

Previously, the application of directly fused dCas9 to FPs resulted in the labelling of ~27 telomeres of 72 expected signals in 2C nuclei of *N. benthamiana* (Dreissig et al., 2017). To improve the labelling efficiency, RNA aptamer-based CRISPR/dCas9 imaging constructs were established for plants. The three-component constructs (called dCas9:2xMS2:FP and dCas9:3xPP7:FP) encode dCas9 of *S. pyogenes*, an *Arabidopsis* telomere-specific sgRNA with integrated aptamer sequences (2x MS2 or 3x PP7) and aptamer coat proteins fused to three copies of fluorescent proteins (tdMCP:GFP/mRuby or tdPCP:GFP/mRuby for binding to MS2 or PP7 aptamers, respectively) (Fig. 11a,b).

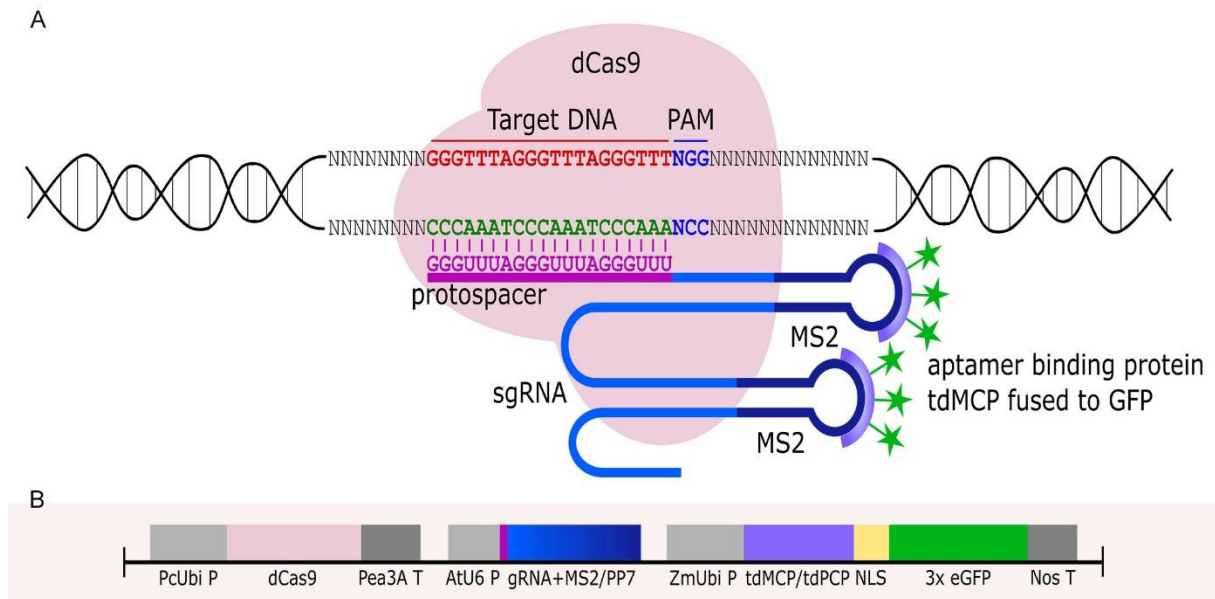


Fig. 11. RNA aptamer-based CRISPR/dCas9 imaging of telomere repeats. (a) Schemata depicting the components of the aptamer-based CRISPR labelling method: 1) dCas9 from *S. pyogenes*, 2) MS2 or PP7 aptamers (here only MS2 is shown) which are integrated into the sgRNA scaffold. 3) RNA binding protein (tdMCP or tdPCP) fused to fluorescent protein (3x eGFP) which recognizes aptamers. Protospacer designed to target *Arabidopsis*-type telomere DNA sequence. (b) Structure of the aptamer-based CRISPR imaging construct. dCas9 is driven by a ubiquitin promoter from parsley (PcUbi P), chimeric gRNA including aptamers (M4S2/PP7) are driven by the AtU6 promoter (AtU6 P), aptamer binding proteins fused to a fluorescent protein (tdMCP/tdPCP) with the help of nuclear localization signal (NLS) are driven by a ubiquitin promoter from maize (ZmUbi P). Pea RBCS3A (Pea3A) T and Nopaline synthetase (Nos) T were used as terminators.

To compare the labelling efficiency of the newly designed constructs, *N. benthamiana* leaves were separately infiltrated with both types of *Arabidopsis*-type telomere-specific dCas9-aptamer constructs (dCas9:2xMS2:GFP and dCas9:3xPP7:GFP) and the previously employed dCas9:GFP reporter (Dreissig et al., 2017). Both types of aptamer-based constructs successfully labelled telomeres in nuclei (Fig. 12b, c). In average, 48 and 37 signals were recognized by dCas9-2xMS2:GFP and dCas9-3xPP7:GFP, respectively (Figure 12d). In contrast, the application of dCas9:GFP resulted in ~28 CRISPR-based signals which is consistent with earlier research (Dreissig et al., 2017) (Fig. 1 2a, d).

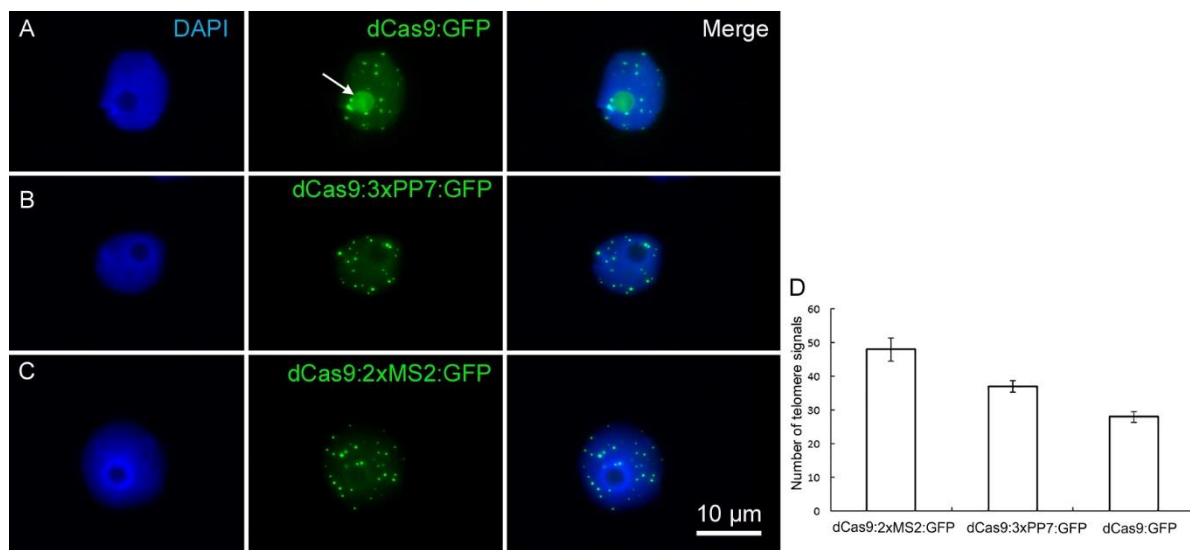


Fig. 12. Live imaging of telomeres in *N. benthamiana* leaf cells during interphase by CRISPR/dCas9. The distribution of telomeres recognized by (a) dCas9:GFP (b) dCas9:3xPP7:GFP and (c) dCas9:2xMS2:GFP. Note, aptamer-based imaging constructs (dCas9:3xPP7:GFP and dCas9:2xMS2:GFP) did not label nucleoli, while the application of dCas9:GFP does (nucleolus is shown with white arrow). Nuclei are counterstained with DAPI. (d) Diagram showing the efficiency of indirectly and directly labelled dCas9 for targeting telomeric regions. The number of telomere signals was determined based on 20 nuclei per construct. dCas9 indirectly labelled either with MS2 or PP7 aptamers shows more telomeres ($p < 0.05$).

As a negative control, the transformation of *N. benthamiana* with partial constructs carrying dCas9:GFP without target-specific gRNA or pMS2:mRuby targeting telomeres without the dCas9 component was performed. For both, nonspecific labelling of nuclei was found (Fig. 13a, b). After co-transformation with both partial constructs, overlapping telomere-like signals of green and red fluorescence were found due to the presence of all components required for CRISPR imaging of telomeres (Fig. 13c).

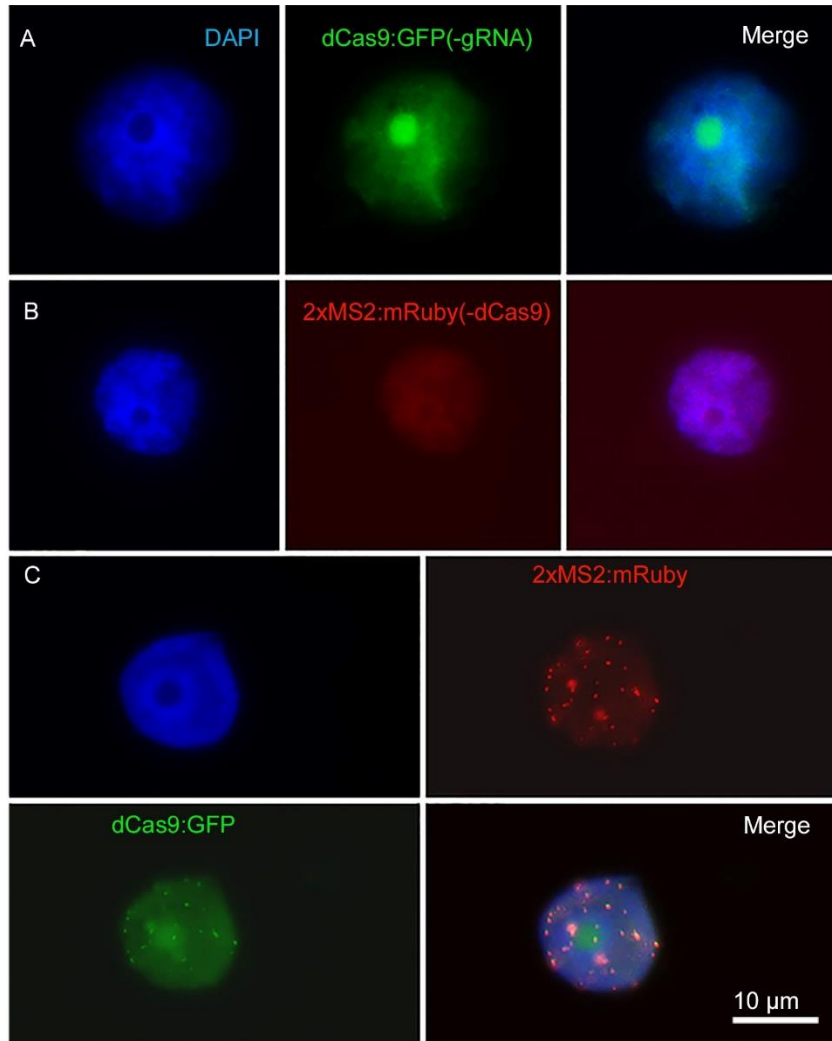


Fig. 13. Negative control with partial constructs carrying (a) dCas9:GFP without gRNA or (b) 2xMS2:3xmRuby targeting telomeres without dCas9. (c) Co-transformation of *N. benthamiana* leaves with both partial dCas9:GFP and 2xMS2:3xmRuby constructs resulted in labelling of telomeres, while no telomere-like signals were found after transformation with either partial construct (a, b). Nuclei are counterstained with DAPI.

To confirm the target specificity of the observed telomere-like signals, FISH with a labelled telomere-specific probe was performed after CRISPR imaging. All dCas9:2xMS2/PP7:GFP signals co-localized with FISH signals, demonstrating the target specificity of the aptamer-based imaging approach (Fig. 14a). However, the labelling efficiency of CRISPR was less than FISH as only 78% and 75% of FISH signals colocalized with dCas9:2xMS2:GFP and dCas9:3xPP7:GFP signals, respectively (Fig. 14b).

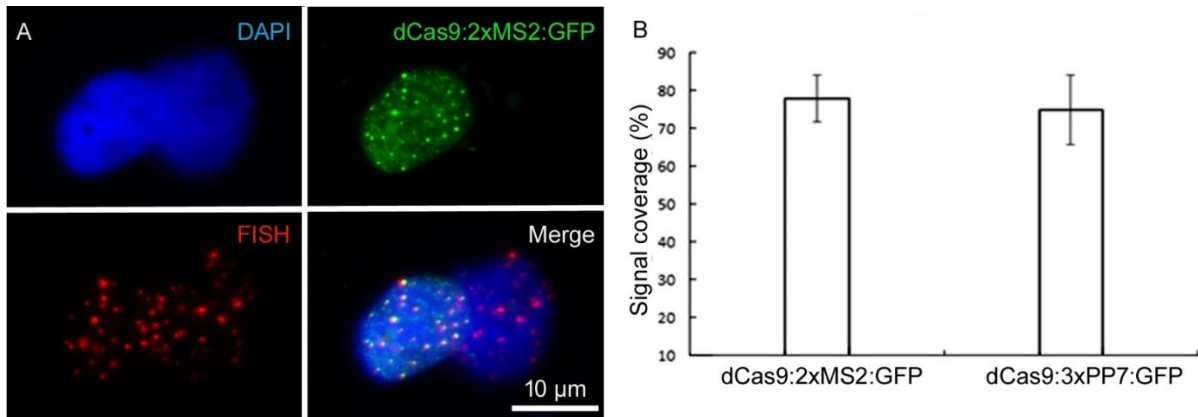


Fig. 14. Confirming the target specificity of aptamer-based CRISPR imaging. (a) Immunofluorescence staining against dCas9:2xMS2:GFP combined with telomere-specific FISH. Nuclei are counterstained with DAPI (in blue). (b) Comparing the efficiency of both types of aptamer-based CRISPR imaging with FISH. Telomeric signals based on 20 isolated nuclei per each construct after ImmunoFISH. dCas9:2xMs2:GFP and dCas9:3xPP7:GFP recognized 78% and 75% of telomere signals identified by FISH, respectively ($p < 0.05$).

4.1.2. Changing the sgRNA scaffold

Since four sequential U nucleotides in the sgRNA stem-loop could be recognized as a transcription termination signal for the *A. thaliana* derived U6 pol-III promoter, a U to A substitution was performed and also the structure of sgRNA was changed by the insertion of an extension to improve the stability of sgRNA and its assembly with dCas9 (Fig. 15).

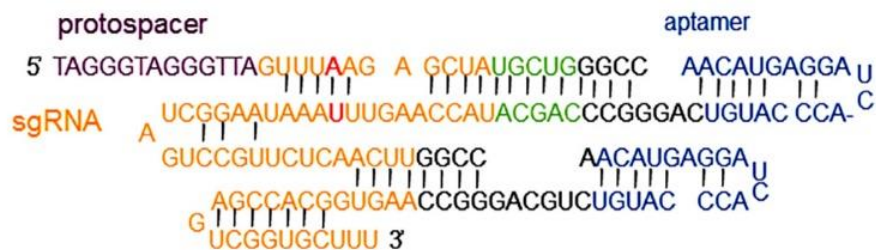


Fig. 15. Changing the sgRNA scaffold with A/U flip (in red) and insertion of an extension (UGCUG) (in green).

The U/A flip along with increasing the length of the sgRNA stem size did not result in a significant increase of telomere signal intensity and did not improve the signal/background noise ratio of telomere signals in *N. benthamiana* (Fig. 16a, b, c).

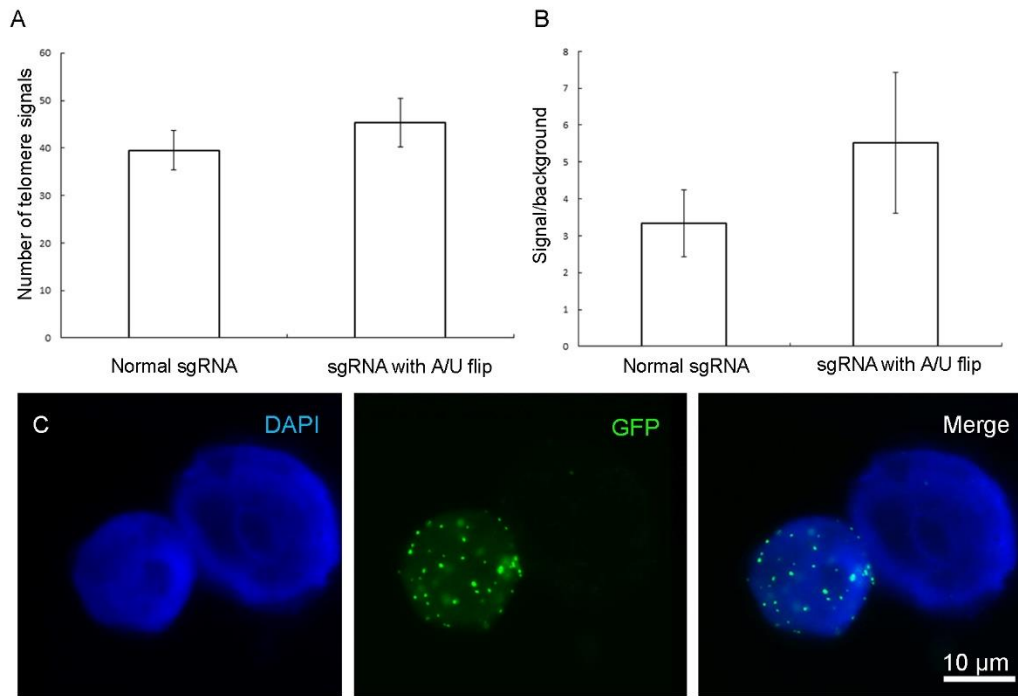


Fig. 16. Effect of changing the sgRNA scaffold with a U/A flip and extension on quantity and quality of observed telomere signals. No significant change was observed in the terms of a) telomere number or b) signal/background noise ratio ($p < 0.05$). c) Labelled telomeres by the vector which has the change in sgRNA scaffold. Measurements were performed based on data from 10 isolated nuclei.

4.1.3. Effect of aptamer copy numbers on labelling efficiency of telomeres

To test whether the copy number of aptamers affects the labelling efficiency, dCas9:MS2:GFP carrying 1, 2 or 16 copies of the MS2 aptamer was constructed. By reducing the aptamer copy number to 1, the number of observed signals reduced (Fig. 17a). 16 copies of MS2 did not result in enhanced telomere signals, instead strong background signals were produced (Fig. 17c).

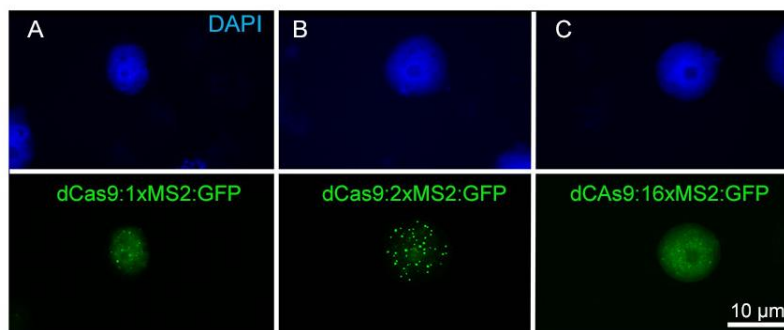


Fig. 17. Effect of MS2 aptamer copy number of aptamer-based CRISPR imaging constructs on signal intensity. (a) dCas9:1xMS2, (b) dCas9:2xMS2 and (c) dCas9:16xMS2. The construct with two copies of MS2 revealed the best labelling of telomeres. Nuclei are counterstained with DAPI.

4.1.4. Comparing the effect of different promoters to express dCas9

Beside the ubiquitin promoter from parsley to drive the expression of dCas9 in *N. benthamiana*, we tested the Cauliflower mosaic virus (CaMV) 35S (Tepfer et al., 2004), RPS5A (Weijers et al., 2001) and the β -estradiol inducible promoter XVE (Zuo et al., 2000). Changing the promoter in dCas9:2xMS2:GFP construct did not increase the number of observed telomere signals in comparison to the ubiquitin promoter (Fig. 18a). The 35S promoter led to a better signal/background noise ratio (Fig. 18b). After induction of the β -estradiol inducible XVE promoter, the same number of telomere signals was observed which was recognized by the construct driven by the ubiquitin promoter (Fig. 18e). The specificity of signals was approved by subsequent FISH with a telomere-specific probe (Fig. 19a). Without induction, no telomere-specific signal was observed (Fig. 19b).

Comparison of dCas9 transcription driven by the XVE or ubiquitin promoter revealed that even weak dCas9 expression by XVE is sufficient to produce telomere-specific CRISPR-based signals (Fig. 20).

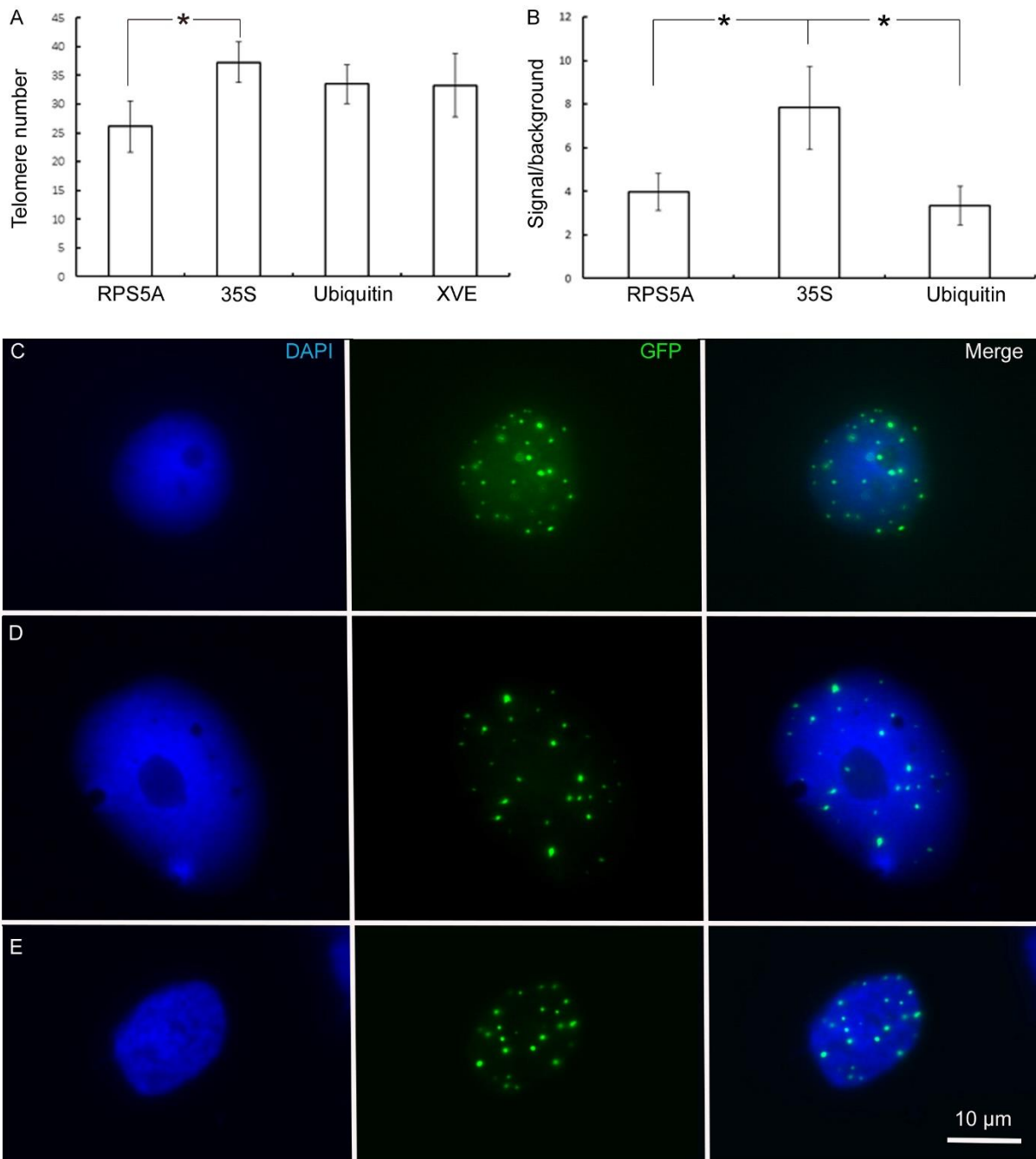


Fig. 18. Effect of different promoters used for expression of dCas9 on the efficiency of telomere labelling. a) The expression of dCas9 by PRS5A promoter resulted in the recognition of a smaller number of telomeres compared to 35S and ubiquitin promoters. Using XVE inducible promoter was as efficient as ubiquitin promoter regarding the number of labelled telomeres ($p < 0.05$). b) 35S promoter caused the better signal to background noise ratio. c) Regardless of promoter type, dCas9 driven by c) RPS5A, d) 35S, e) XVE could label telomeric regions in *N. benthamiana*. Data obtained from 10 isolated nuclei per construct.

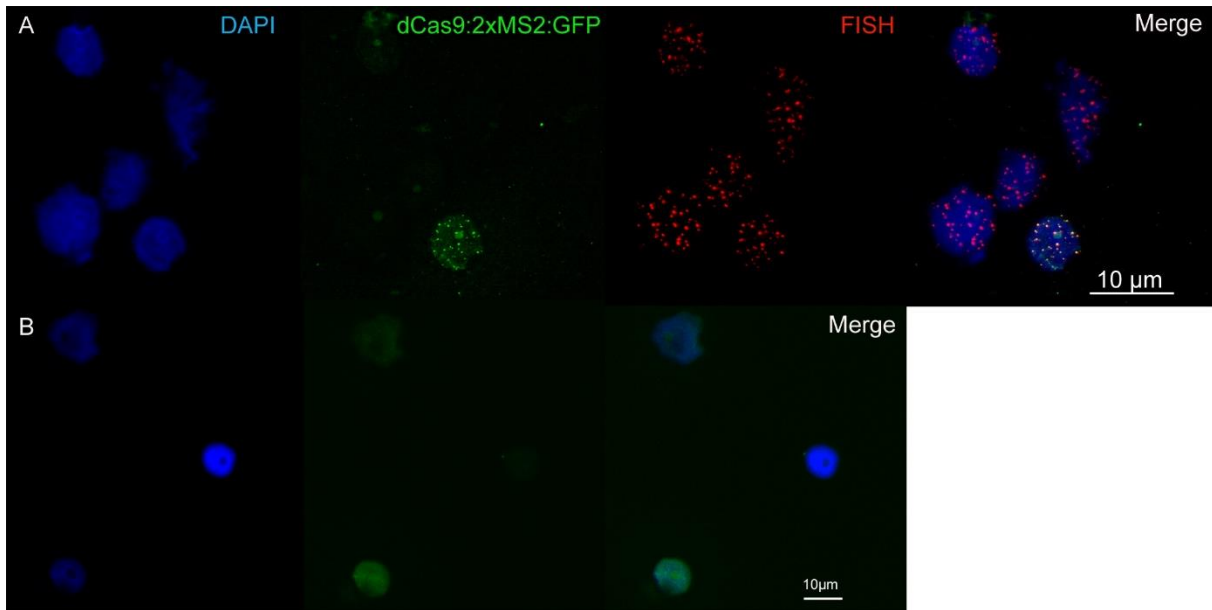


Fig. 19. Specificity control test by ImmunoFISH for the activity of the inducible XVE promoter. a) Isolated nuclei after treatment of leaves with β -estradiol show telomeric signals. Co-localization of dCas9:2xMS2:GFP and FISH signals show that the observed signals are telomeric specific. b) Nuclei isolated from β -estradiol-untreated leaves show uniform labelling of nuclei.

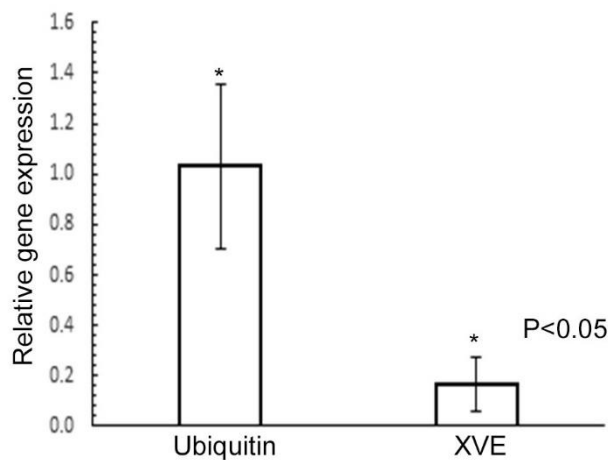


Fig. 20. Real-time expression of dCas9 expressed by ubiquitin and XVE promoters. dCas9 expression is much lower when it is driven by inducible XVE promoter compared to ubiquitin from parsley. Error bars are standard deviation.

4.1.5. Analysis of telomere signals

Regardless of the promoter type, telomeres showed similar dynamic and random movements (Fig. 21). To quantify these movements the mean square displacement (MSD) of telomeres was measured over a period of time. Calculating the changes of intratelomeric distance

showed the minimum $\pm 1 \mu\text{m}$ to maximum $\pm 4 \mu\text{m}$ of changes for each type of promoter (Fig. 22). In summary, application of RNA-aptamers for CRISPR-based live-cell imaging increases the efficiency of telomere labelling in plant cells.

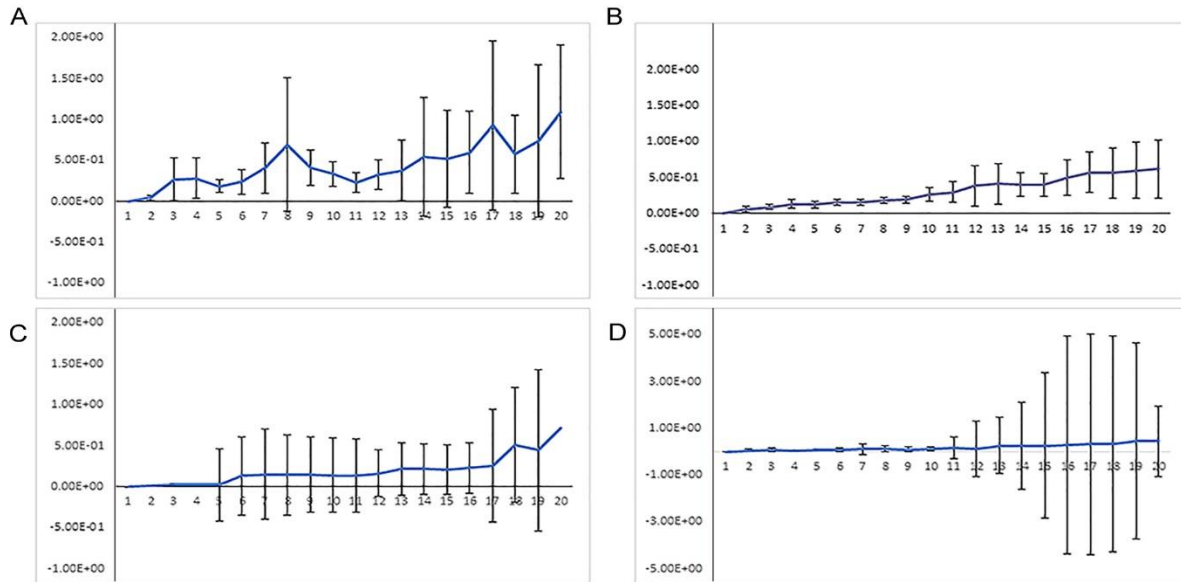


Fig. 21. Comparing mean square distance (MSD in μm) of telomeres labelled by indirectly labelled aptamer-dCas9 which were under the control of a) 35S, b) RPS5a or c) ubiquitin promoters. d) Directly labelled dCas9, which was under the control of a ubiquitin promoter. Telomeres showed random movements regardless of promoter type and how dCas9 was labelled.

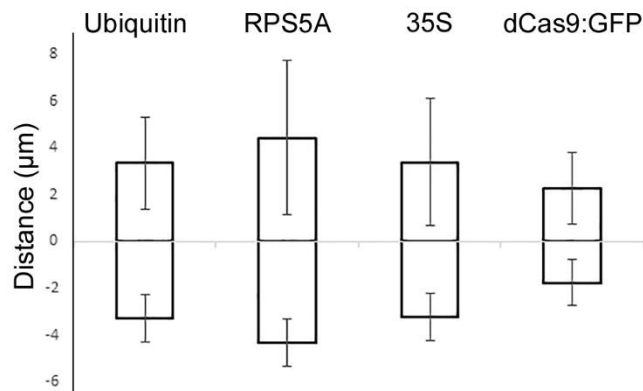


Fig. 22. Measurement of inter-telomeric distance changes in nuclei transformed with three different indirectly labelled aptamer-dCas9 which were under the control of ubiquitin, RPS5a or 35S promoters and directly labelled dCas9 which was under the control of the ubiquitin promoter. Intra-telomeric distance changes vary between minimum $\pm 1 \mu\text{m}$ to maximum $\pm 4 \mu\text{m}$.

4.2. Targeting 5S rDNA, 45S rDNA and ITS regions in *N. benthamiana*

After improving live-cell imaging of telomeres in *N. benthamiana* with aptamer-based CRISPR imaging vectors, other repetitive sequences including 5S rDNA, 45S rDNA and ITS regions were

selected as next targets for live-cell imaging. The dCas9:2xMS2:GFP construct was used to label the selected sequences.

4.2.1. Labelling of 5S rDNA

To confirm whether the selected 5S rDNA sequence is appropriate for live-cell imaging in *N. benthamiana*, first two 5S rDNA FISH probes (Table 5) specific for a region that is identical in *A. thaliana* and *N. benthamiana* were designed. The number and position of 5S rDNA signals in *A. thaliana*, *N. benthamiana* and *N. tabacum* were determined (Fig. 23). In *A. thaliana*, 5 interphase signals were seen for the 5S rDNA probe 1. Most signals co-localised with chromocenters. For probe 2 a variable number of signals could be counted. The signals for probe 2 were like big foci containing two to three smaller signals. The variability of 5S rDNA FISH signals (six to ten signals) and the co-localisation with some chromocenters in *A. thaliana* were shown before (Municio et al., 2019). In *N. benthamiana*, the number of signals for 5S rDNA probe 1 varied between different nuclei, and at least 5 signals per nucleus were observed. 8 to 10 signals were identified for probe 2. For *N. tabacum*, three and four 5S rDNA signals were recognized for probe 1 and 2, respectively. In accordance with our observation Sýkorová et al. (2012) reported four 5S rDNA hybridization signals on mitotic chromosomes of *N. tabacum*. The 5S rDNA signals in all three tested species located outside the nucleolus. Accordingly, the same selected regions used as both FISH probes were selected to design protospacers for subcloning into dCas9:2xMS2:GFP. However, no 5S rDNA-specific signal was observed after transient transformation of *N. benthamiana* and *N. tabacum*. The 5S rDNA labelling attempt using dCas9:2xMS2:GFP was performed only once.

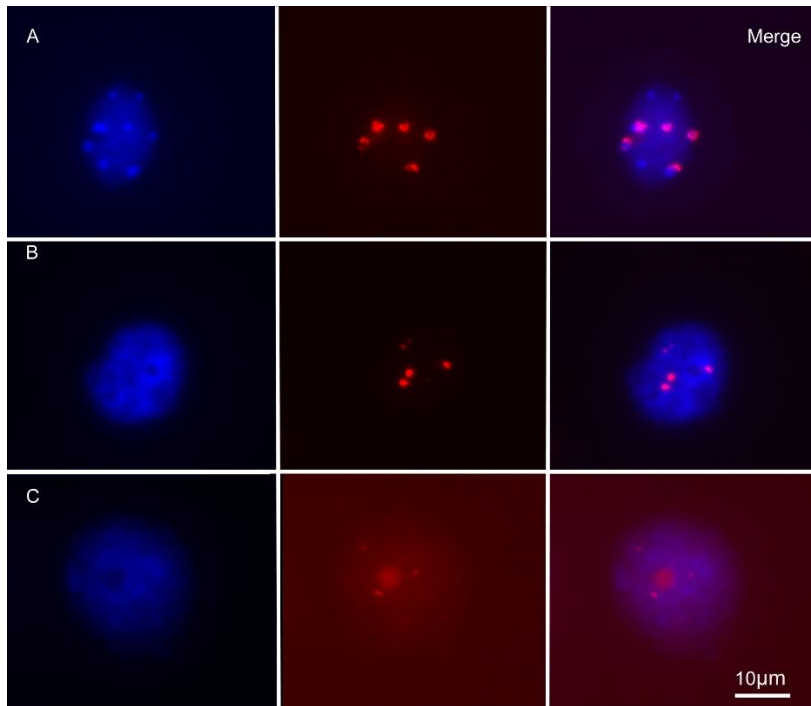


Fig. 23. Nuclei of (a) *A. thaliana*, (b) *N. benthamiana* and (c) *N. tabacum* after FISH with labelled 5S rDNA. The number of 5S rDNA signals (in red) varied between different species. In (a - c), FISH signals obtained from probe 1 are shown.

4.2.2. Labelling of 45S rDNA

Targeting of the 45S rDNA with the help of the dCas9:2xMS2:GFP construct resulted in dot-like GFP signals in the nucleus. However, the location of GFP signals, which were expected to be in the periphery of the nucleolus, were dispersed in the nucleus (Fig. 24).

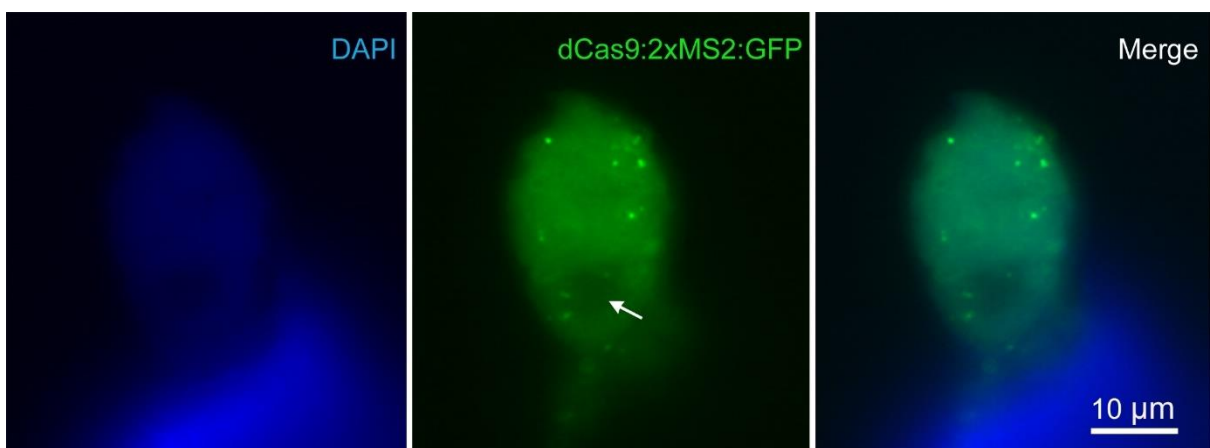


Fig. 24. Isolated leaf nuclei from transiently transformed *N. benthamiana* with dCas9:2xMS2:GFP vector for targeting 45S rDNA. Unlike expected, no GFP signal was found in the nucleolus. The nucleolus is indicated with a white arrow.

4.2.3. Labelling of 45S rDNA ITS regions

All attempts to label different ITS regions (ITS1 and ITS2) and different ITS strands including coding and non-coding strands of the 45S rDNA resulted only in a uniform labelling of *N. benthamiana* nuclei. No dot-like GFP signals were found in transiently transformed plants (Fig. 25).

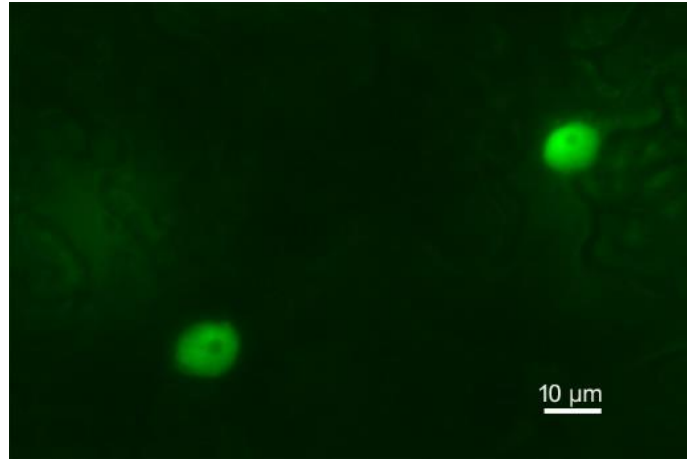


Fig. 25. Living leaf nuclei of *N. benthamiana* which were transformed with the dCas9:2xMS2:GFP vector for targeting the ITS1 coding region of the 45S rDNA. Only an uniform labelling of nuclei was observed.

4.3. Application of CRISPR-imaging in stably transformed plants

Stable transformation of *N. benthamiana*, *A. thaliana* plants and *D. carota* roots with the telomere-specific dCas9:2xMS2:GFP construct did not result in transgenic plants exhibiting GFP-labelled telomeres in living leaf or root cells. However, the presence and expression of dCas9 and GFP genes were confirmed by PCR and real-time RT-PCR (Fig. 26 and 17, Table 6). For this purpose, RNA was isolated from selected plants or roots. cDNA was prepared and tested with Cas9 and GFP-specific primers to confirm the presence of the transgenes in selected plants and roots. From 7 selected *N. benthamiana* plants, 5 showed the presence of dCas9. 4 of 5 selected root lines of *D. carota* were transgenic (Fig. 26). Two samples from *N. benthamiana* leaves, transiently transformed with dCas9:2xMS2:GFP for targeting telomeres were used as the positive control. Then, the relative expression of dCas9 and GFP was measured using real-time PCR (Fig. 27). Accordingly, selected plants and roots which did not show any GFP-telomere signal showed the expression of GFP and dCas9. However, the expression was lower compared to transiently transformed plants.

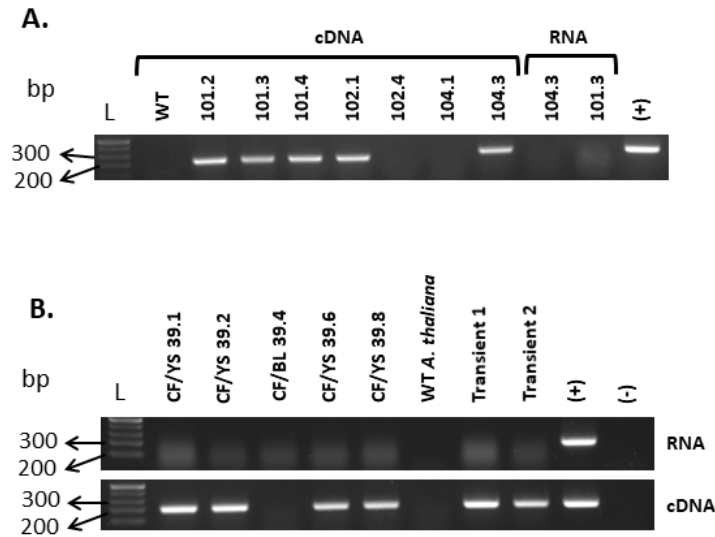


Fig. 26. Agarose gel electrophoresis of PCR amplicons for cDNAs obtained from A) *N. benthamiana* and B) *D. carota* which were stably transformed with telomere-specific dCas9:2xMS2:GFP construct. A) from left to right, first lane: 1 kb plus ladder, second: wild type cDNA sample, third to ninth lane: cDNA from transgenic *N. benthamiana* plants, tenth and eleventh: RNA from two transgenic *N. benthamiana* plants as the negative control, twelfth lane: plasmid from dCas9:2xMS2:GFP construct positive control. B) The top gel picture from left to right, first lane: 1 kb plus ladder, second to sixth: RNA samples from transgenic *D. carota* root lines, seventh lane: RNA from wild type *A. thaliana* as the negative control, eighth and ninth lane: RNA transiently transformed *N. benthamiana*, tenth lane: plasmid from dCas9:2xMS2:GFP construct positive control. The results shown in the lower gel picture are from PCR on cDNA samples in the same order as in the top gel picture. PCR on RNA samples did not show any amplification which shows that the RNA is not contaminated with genomic DNA.

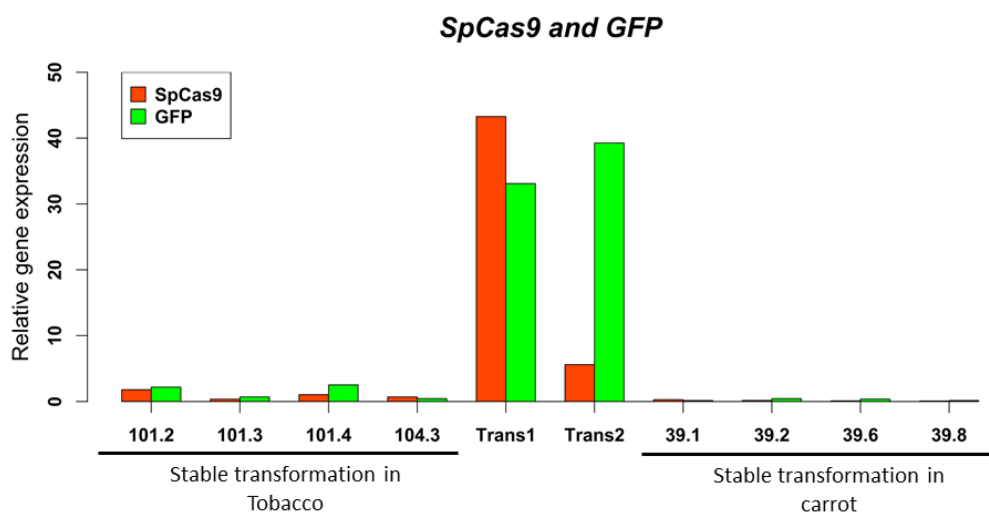


Fig. 27. Real-time expression of dCas9 and GFP in stably transformed *N. benthamiana* and *D. carota* compared to transiently transformed *N. benthamiana* (Trans1 and 2). Transcription of dCas9 and GFP occurred in stably transformed *N. benthamiana* and *D. carota*, however, the rate of transcription is much lower compared to transiently transformed *N. benthamiana*.

Only transformation of *A. thaliana* with dCas9:2xMS2:GFP targeting centromeric regions resulted in few plants that showed some dot-like GFP signals. However, the number and pattern of signals were atypical for interphase centromeres (Fig. 28).

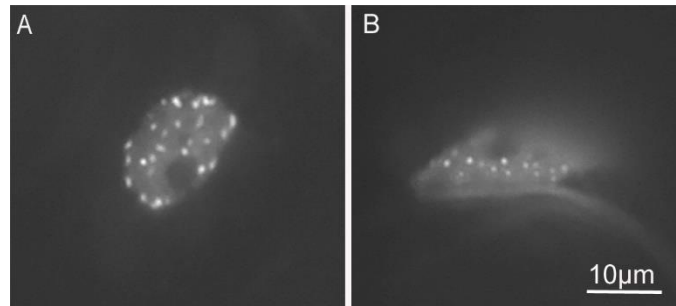


Fig. 28. Selected nuclei of *A. thaliana* stably transformed with a centromere-specific dCas9:2xMS2:GFP construct exhibiting dot-like signals. Application of the a) centromere-specific protospacer 1 and b) 2, respectively. The number of GFP signals was higher than expected.

In total, 141 selection marker resistant *A. thaliana* plants were screened for three different centromere imaging constructs by microscopy. Among them, 27 plants showed uniform labelling of nuclei and 9 plants showed dot-like signals. The dot-like signals were unstable and could not be detected in seedlings older than three weeks or subsequent generations (T3). However, some nuclei with GFP dot-like signals could still be observed in the generative tissue. ImmunoFISH was performed to determine the centromere-specificity of the CRISPR imaging signals. No colocalization between GFP and FISH centromere signals was found (Fig. 29). Phenotype and seed setting of plants exhibiting dot-like signals were wild-type like. Among the three different protospacers used, only protospacer 1 and 2 produced signals. The same protospacer 1 was successfully used to label centromeres in fixed nuclei of *A. thaliana* with the help of CRISPR-FISH (Ishii et al., 2019).

Plants that were transformed with dCas9:2xMS2:GFP under the control of an inducible promoter with a centromere- or telomere-specific protospacer revealed no target sequence-specific signals after induction with β -estradiol (Table 6).

Table 6. Summary of CRISPR live-cell imaging in stably transformed plants.

| Species | Construct used for transformation | dCas9 promoter | Target region | No. of gentamycin resistant plants and root lines analyzed by microscopy | No. of plants with signals | Signal description |
|-----------------------|-----------------------------------|----------------|---------------|--|----------------------------|---|
| <i>N. benthamiana</i> | dCas9:2xMS2:GFP | ubiquitin | Telomere | 30 plants | 7 | weak uniform labelling of nuclei |
| <i>N. benthamiana</i> | dCas9:2xMS2:GFP | CaMV 35S | Telomere | 33 plants | 5 | uniform labelling of nuclei |
| <i>A. thaliana</i> | dCas9:2xMS2:GFP | ubiquitin | Centromere | 141 plants | 27 | dot-like and uniform labeling of nuclei |
| <i>A. thaliana</i> | dCas9:2xMS2:GFP | ubiquitin | Telomere | - | 3 | no signal or one signal only |
| <i>A. thaliana</i> | dCas9:2xMS2:GFP | CaMV 35S | Telomere | 18 plants | 4 | uniform labeling of leaf nuclei and stomata |
| <i>A. thaliana</i> | dCas9:2xMS2:GFP | XVE | Centromere | 7 plants | 7 | uniform labelling |
| <i>A. thaliana</i> | dCas9:2xMS2:GFP | XVE | Telomere | 6 plants | 6 | some nuclei with many dot-like signals |
| <i>D. carota</i> | dCas9:2xMS2:GFP | ubiquitin | Telomere | 15 root lines | 4 | weak uniform labelling of nuclei |
| <i>D. carota</i> | dCas9:2xMS2:GFP | CaMV 35S | Telomere | 12 root lines | 1 | weak uniform labelling of nuclei |

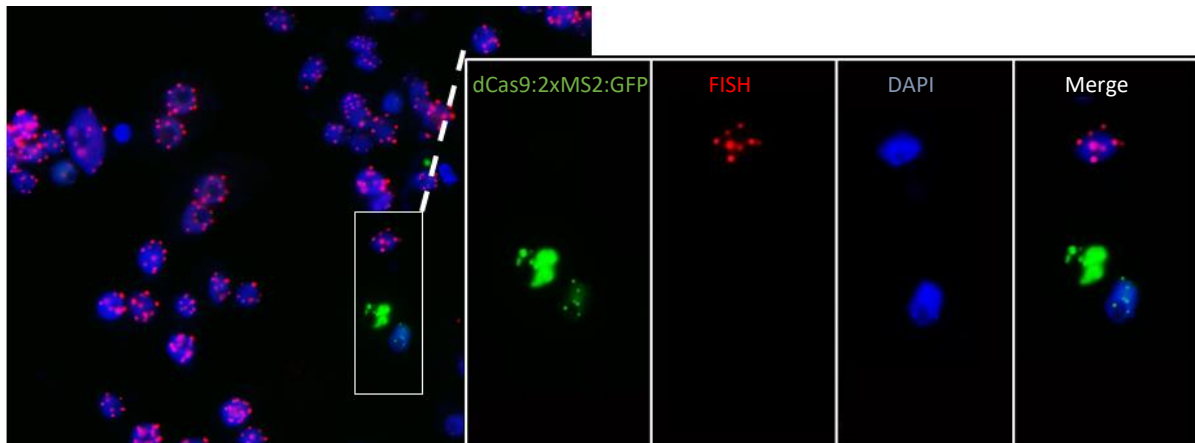


Fig. 29. Isolated nuclei from generative tissue of dCas9:2xMS2:GFP stably transformed *A. thaliana* after anti-GFP immunostaining and FISH with a telomere-specific probe. No colocalization of GFP signals and centromeric FISH signals occurred.

To test whether the absence of dot-like GFP signals is caused by the degradation of the dCas9 protein, transgenic plants were treated with different concentrations of the proteasome inhibitor MG-132. However, no dot-like signals were recovered. Additionally, the presence of the dCas9 protein was confirmed by immunostaining using a dCas9-specific antibody (Fig. 30a, b). Accordingly, leaf nuclei which were isolated from stably transformed *A. thaliana* showed the presence of dCas9 protein by a weak uniform labelling after immunostaining of dCas9 (Fig. 30a). In contrast, leaf nuclei isolated from wild type plants did not show uniform labelling of nuclei after immunostaining of dCas9 (Fig. 30b).

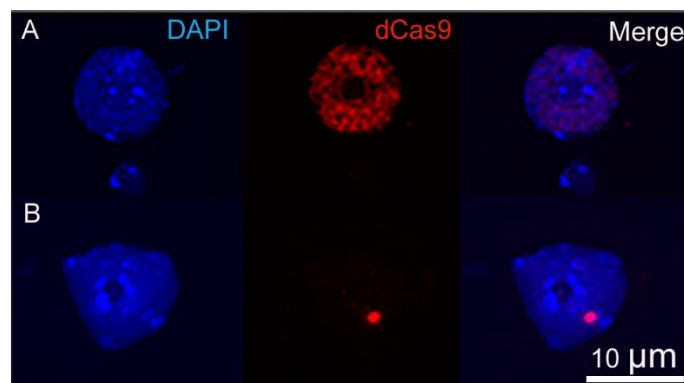


Fig. 30. Immunostaining of dCas9 protein in isolated nuclei from *A. thaliana* leaf material. a) Uniform immunostaining of dCas9 (in red) of a nucleus isolated from a stably transformed *A. thaliana* plants with the dCas9:2xMS2:GFP construct targeting centromeric sequences. b) Immunostaining of an isolated nucleus from a wild type *A. thaliana* leaf did not result in uniform signals. Absence of immunosignals demonstrates the specificity of the applied dCas9 antibody. The red dot-like signal in (b) is unspecific signal.

4.4. Application of Cas12 (Cpf1) for live-cell imaging of telomeres in *N. benthamiana*

To increase the capacity of CRISPR/Cas for multi-color imaging, different orthologues of dCas9 proteins fused with various fluorescent proteins were used to label pericentromeric and subtelomeric repeats in human cells (Ma et al., 2015). Among different Cas9 variants, St1-Cas9 and Sa-Cas9 have been confirmed to be functional in plants (Dreissig et al., 2017). Two dead variants of Cas12 including Cpf1 of *Francisella novicida* (dFnCpf1) and Cpf1 of *Acidaminococcus* sp. (dAsCpf1) were used for live-cell imaging of telomeres in *N. benthamiana* to test the functionality of another CRISPR/Cas system for live-cell imaging in plants. Cpf1 belongs to class II type V endonucleases. From the gene-editing perspective, Cpf1 has the advantage of producing sticky end overhangs compared to Cas9. However, for live-cell imaging, this would not be considered because the deactivated Cpf1 is used. Nevertheless, the preference of Cpf1 for binding to genomic A/T-rich regions made it an interesting candidate for imaging. Additionally, Cpf1 contains RNaseIII activity which can be exploited for multiple labelling via tandemly arrayed pre-crRNA-expressing constructs that produce multiple mature crRNAs processed by Cpf1 (Zaidi et al., 2017).

Therefore, suitable protospacers for labelling telomeres were designed based on the Cas12-specific PAM preferences. Regardless of the selected PAM sequence and the length of the designed protospacer, transiently transformed *N. benthamiana* with telomere-specific dFnCpf1 and dAsCpf1 constructs did not show telomeric signals in interphase nuclei (Fig. 31). Also, the treatment of infiltrated plants with a higher temperature (30 °C) did not improve the result.

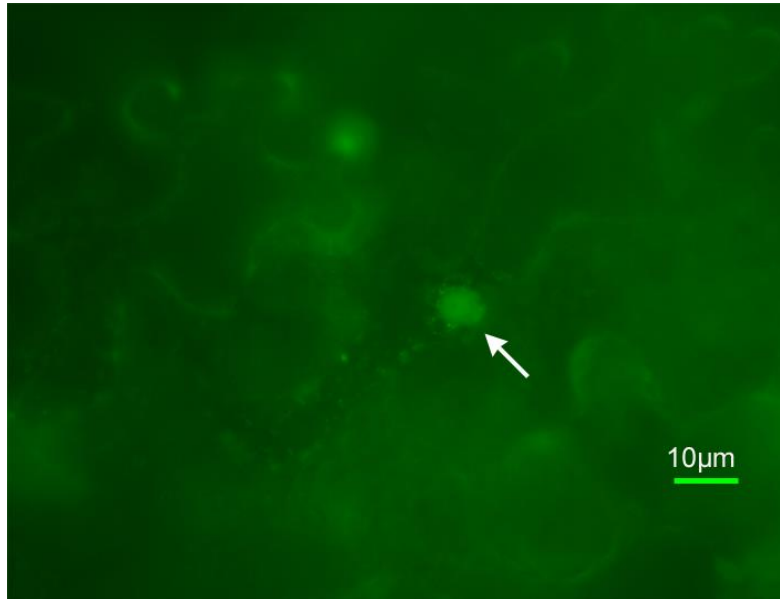


Fig. 31. Living leaf nucleus of *N. benthamiana* transformed with dAsCpf1:GFP vector for targeting telomeres. Uniform labelling of the nucleus (indicated with white arrow) was observed without any telomere-specific signals.

4.5. RNA targeting with dCas13

Among the CRISPR enzymes, Cas9 and Cas12a have DNA targeting ability. In contrast, Cas13 has been used for RNA tagging in non-plant species (Abudayyeh et al., 2017; Yang et al., 2019). Similar to Cas9, Cas13 complexes with a guide RNA. Cas13 proteins are guided to their target RNAs by a single CRISPR RNA (crRNA) composed of a direct repeat stem-loop and a spacer sequence (gRNA) that mediates target recognition by RNA–RNA hybridization (Abudayyeh et al., 2017). Protospacers for targeting telomeric RNA and 25S rRNA were selected for two different variants of dCas13 including dLwCas13a and dRfxCas13d. pDe-dRfxCas13d-GFP-PPT-NES and pDe-dRfxCas13d-GFP-PPT-NLS vectors were used to target 25S rDNA. pDe-LwdCas13a-GFP-PPT-NF-NES vector was applied for targeting telomeric RNAs. Then, *N. benthamiana* was transiently transformed. Application of pDe-dRfxCas13d-GFP-PPT-NES to target 25S rRNA resulted in cytoplasmic tubulin-like signals (Fig. 32).

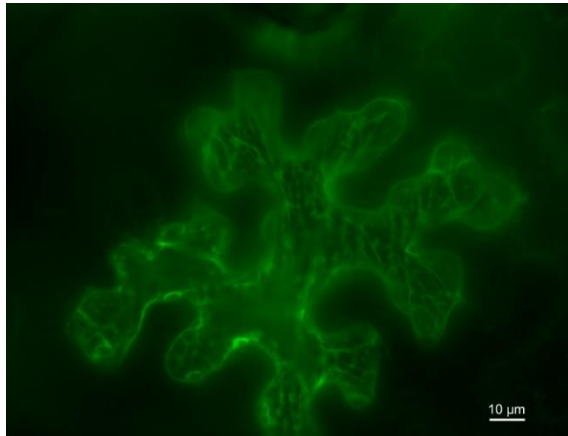


Fig. 32. Living leaf cell of *N. benthamiana* transformed with pDe-dRfxCas13d-GFP-PPT-NES vector for visualizing 25S rRNA. Tubulin structure-like signals were observed without any 25S rRNA -specific signals.

Application of pDe-dRfxCas13d-GFP-PPT-NLS to target 25S rRNA resulted in GFP signals decorating the nucleoplasm and nucleoli (Fig. 33). Uniform labelling of nucleoli looks promising compared to RNA-FISH of 18S and 5S transcripts in *Zea mays* (Koo et al., 2016).

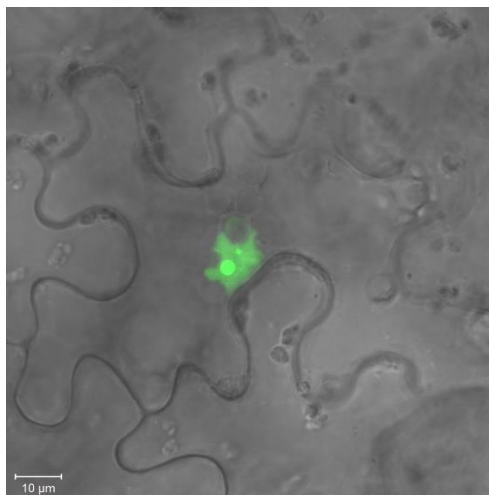


Fig. 33. Living leaf nucleus of *N. benthamiana* transformed with pDe-dRfxCas13d-GFP-PPT-NLS vector for targeting 25S rRNA. Uniform labelling of the nucleoplasm and nucleoli was observed.

The telomere RNA-specific pDe-LwdCas13a-GFP-PPT-NF-NES construct resulted after the transient transformation of *N. benthamiana* in cytoplasmic signals (Fig. 34). Comparing the RNA-FISH results of telomere transcripts in *N. benthamiana* (Koo et al., 2016), the obtained results from this experiment should be confirmed with RNA-FISH.

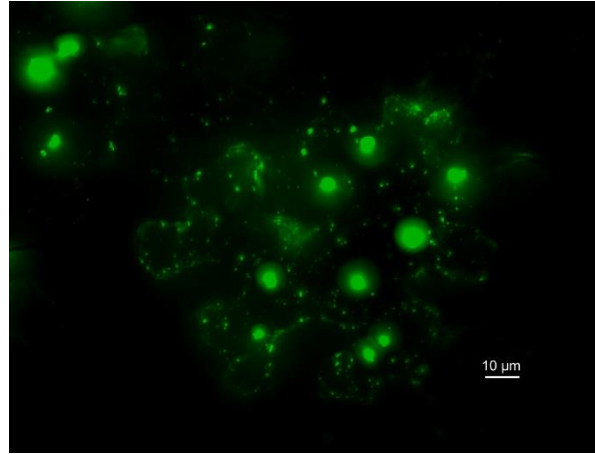


Fig. 34. Living leaf cell of *N. benthamiana* transformed with pDe-LwdCas13a-GFP-PPT-NF-NES vector for targeting telomeric RNA. GFP signals localized in the cytoplasm.

5. Discussion

5.1. Improving live imaging of telomeres with aptamer-based CRISPR/dCas9 vectors

The application of MS2 and PP7 aptamers resulted in improved CRISPR imaging constructs instrumental to trace telomeres in transiently transformed *N. benthamiana*. Labelling efficiency, based on the mean value of signal numbers per nucleus, was increased up to 1.7 fold in comparison to dCas9:GFP. The number of individual telomere signals per nucleus was lower than expected though, which may be due to clustering of individual telomeres or, our reporter could not occupy all telomeres. Clustering of telomeres has been also observed in other organisms like *A. thaliana* (Fransz et al., 2002), yeast and *Drosophila melanogaster* (Hozé et al., 2013; Wesolowska et al., 2013).

Despite the improved labelling of telomeres, the aptamer-based CRISPR imaging in *N. benthamiana* resulted in a labelling efficiency of 73 - 75% compared with FISH. In contrast, in human cell cultures, the number of telomeric signals obtained by CRISPR imaging was almost equal to the number of FISH signals (Chen et al., 2013). The copy number difference of telomere repeats is unlikely the reason for this discrepancy because human telomeres are 5 to 15 kb (Moyzis et al., 1988) while the telomeres in *N. benthamiana* are 60 to 160 kb long (Fajkus et al., 1995). Since the temperature of 37°C is required for optimal Cas9 activity (Xiang et al., 2017), the temperature difference between plant (22°C) and mammalian cell cultures (37°C) might contribute to the observed labelling difference between mammalian and plant species.

While dCas9:GFP expressing cells showed background signals in nucleoli (Dreissig et al., 2017), such background was absent from leaves expressing aptamer-containing reporter constructs. Nucleolar accumulation of dCas9 has been noted in other species like human cell cultures (Chen et al., 2013). Likely, unspecific labelling of nucleoli was reduced because fluorescent proteins were not directly fused to dCas9.

One of the approaches that has been applied to improve the gene-editing efficiency is manipulating the Cas9 expression by using developmental and constitutive gene promoter (Feng et al., 2018; Hu et al., 2018; Ma et al., 2016b; Wang et al., 2015). It is shown that strong expression of sgRNA:Cas9 could result in off-target mutagenesis. More off-targets occurred when a higher dosage of sgRNA:Cas9 was applied in human cells. In maize and rice,

off-targets were up to 100× higher after application of a constitutive-Cas9 as compared to transient-Cas9 (Hsu et al., 2013; Hu et al., 2018; Pattanayak et al., 2013; Svitashv et al., 2015). Therefore, one criterion that affects targeting efficacy is the dosage of the sgRNA:Cas9 complex. In our case, the substitution of the ubiquitin promoter with the inducible XVE promoter caused a 5-fold expression decrease of dCas9. However, changing the expression of dCas9 gene by application of XVE promoter did not result in a significant change in the number of telomere signals. In contrast, in mammalian cell cultures, a low dosage of sgRNA affects the quality of CRISPR imaging signals (Chen et al., 2013). The PRS5A promoter resulted in a lower number of telomere signals. This could be because PRS5A is more active in meristematic tissues rather than leaves, the tissue which was used for transient transformation (Winter et al., 2007).

Increasing the number of MS2 aptamers to 16 copies did not enhance the efficiency of telomere labelling in *N. benthamiana*, although in human cell cultures increment of aptamer numbers up to 16 improved the labelling (Qin et al., 2017). Additionally, changing the sgRNA scaffold did not increase the quantity and quality of observed signals. In human cell cultures, though, similar modifications increased the number of CRISPR-labelled telomeres and improved the signal/background noise (Chen et al., 2013). Fujimoto and Matsunaga (2017) used sgRNA scaffold modifications (T to G change and A/U flip combined with UGCUG extension) within a CRISPR imaging construct to improve the signal to noise ratio of telomere labelling in transiently transformed *N. tabacum*. The different outcome reported here might be due to the different constructs used.

5.2. Targeting 5S rDNA, 45S rDNA and ITS regions in *N. benthamiana*

While the application of aptamer-based CRISPR reporters showed a significant improvement for telomere imaging in transiently transformed *N. benthamiana*, they could not successfully label other target regions including 45S rDNA, 5S rDNA and ITS regions in the same species. Early studies found that chromatin accessibility or DNA methylation affects the binding of dCas9 (Knight et al., 2015; Kuscu et al., 2014; Wu et al., 2014). Also, the literature suggests that the genomic context influences Cas9 binding and cleavage efficiency (Gisler et al., 2019).

Most telomeres possess a single-stranded DNA overhang formed by a G-rich strand that is required to form a specific structure termed a telomeric loop (t-loop) (Griffith et al., 1999). Another specific local DNA structure that may be formed by the G-rich strand of telomeres is

a four-stranded structure (G quadruplex, G4) (Burge et al., 2006). Importantly, rDNA in many organisms, including budding yeast and human, shows a number of G-rich elements with high quadruplex-forming potential (Hershman et al., 2007). Thus, enrichment in quadruplex-forming potential is an interesting feature common to telomeres and rDNA. Therefore, it is assumed that the structure of the 45S rDNA might not interfere with the binding ability of dCas9 for live-cell imaging.

However, the organization of ribosomal chromatin is different from that of telomeres. 45S rDNA of *A. thaliana* is composed of tandemly repeated 10 kb long units, of which approximately 5.5 kb is the coding region for 18S, 5.8S and 25S rRNAs separated from each other by the short internal transcribed spacers ITS1 and ITS2. These gene clusters are joined to neighbouring clusters by a 4.5 kb intergenic spacer (IGS) (Dvořáčková et al., 2015). Although, rDNA units are usually repeated hundreds to thousands of times, the chromatin state of individual rDNA units varies significantly, and only approximately 10% of copies are transcriptionally active and decondense inside in the nucleus. While the inactive rDNA is more compact and locates outside the nucleolus. 5S rDNA is also organized differently from telomeres, for example, the *A. thaliana* genome contains approximately 1000 copies of 5S genes per haploid genome, which are arranged in tandem arrays located within the pericentromeric heterochromatin of some chromosomes (Campbell et al., 1992). A typical 5S rDNA unit is 500 bp long and consists of a 120 bp transcribed sequence, with an internal promoter and an approximately 380 bp intergenic spacer (IGS) (Cloix et al., 2000). In the *A. thaliana* Columbia accession, only two 5S rDNA arrays out of 3 loci are transcribed (Douet and Tourmente, 2007).

Altogether, for both rDNA types, some rDNA units are selectively activated while others are repressed. Considering the fact that the chromatin inaccessibility decreases the DNA binding ability of dCas9 (Wu et al., 2014), one possibility why CRISPR-based imaging reporters could not label rDNAs can be that the accessibility of rDNAs regions for dCas9 differs from telomeres because of the differently organized chromatin.

Another potential reason might be the fact that the formation of RNA:DNA hybrids are affecting the stability of the genome. RNA:DNA hybrids are associated with DNA double-strand break formation, which could result in chromosomal rearrangements (Wahba et al., 2011). Although, accumulation of RNA:DNA hybrids have been detected at rDNA, telomeres,

transposons or transcribed loci (Huertas and Aguilera, 2003; Lin et al., 2014; Wahba et al., 2011), the 45S rDNA regions are considered as fragile sites in the genome (Rocha et al., 2015; Ruiz-Herrera et al., 2008; Steinert et al., 2015). Therefore, the persistent formation of RNA:DNA hybrids followed by dCas9 attachment to these fragile regions might disorder the natural balance of R-Loops at 45S rDNA sites and cause genome instability.

5.3. Why does CRISPR imaging not work in stably transformed plants?

Our CRISPR imaging constructs which were successfully applied in transiently transformed *N. benthamiana* leaves could not be used to label defined sequences in stably transformed *N. benthamiana*, *A. thaliana* or *D. carota*. The same observation was made by Fujimoto and Matsunaga (2017) for GFP-fused dCas9 imaging constructs. Intriguingly, CRISPR-imaging of centromeric and telomeric repeats works-fine on fixed nuclei and chromosomes of different plant and animal species (Deng et al., 2015; Ishii et al., 2019; Němečková et al., 2019; Potlapalli et al., 2020). The *in situ* imaging method CRISPR-FISH (also called REGEN-ISL) is based on a fluorescence-labelled two-part guide RNA with a recombinant Cas9 endonuclease complex. For both imaging methods, we used telomere- and centromere-specific gRNA and *A. thaliana* and *N. benthamiana*, subsequently (Ishii et al., 2019), this work). Hence, we expected that the selected gRNA in combination with dCas9 should also work in stably transformed plants.

Why then did-CRISPR imaging fail in stably transformed plants? In contrast to CRISPR-based editing, for CRISPR imaging a constant interaction of the RNP complex with the target DNA is a functional prerequisite. It is tempting to speculate that a permanent binding of the RNP complex with its target DNA interferes with processes required for plant development. The formation of R-loops, which is underlying the CRISPR/Cas mechanism, might hamper cellular processes. R-loops are three-stranded nucleic acid structures composed of a DNA-RNA hybrid and a displaced single-stranded DNA. R-loops have a role in transcription, chromatin modification, DNA damage response. Once the R-loop homeostasis is perturbed, it can lead to genome instability (Crossley et al., 2019; Palmer, 2020). The R-loop distribution atlas of *A. thaliana* has shown that R-loop distribution patterns are relatively preserved during different developmental and environmental conditions (Xu et al., 2020). Therefore, by imposing consistent formation of R-loops in targeted regions, CRISPR imaging constructs might change R-loop dynamics in defined genomic regions of stably transformed plants. Alternatively, the selected Cas9 variant of *S. pyogenes* is not suitable and further optimized Cas variants with

higher efficiency could overcome this problem. A negative selection against CRISPR-imaging constructs in stably transformed plants at the transcript level is less likely because corresponding transcripts exist. Besides, uniform labelling of anti-Cas9 immunosignals was detected in transformed plants. Overcoming the discussed problem will also help to increase the efficiency of CRISPR-based editing in plants.

Taking advantage of the intrinsic stability of CRISPR guide RNA, (Wang et al., 2019) used fluorescent ribonucleoproteins consisting of chemically synthesized fluorescent gRNAs and recombinant dCas9 protein for imaging in transfected living human lymphocytes. Live-cell fluorescent *in situ* hybridization (LiveFISH) allowed tracking of multiple chromosomal loci in lymphocytes. Whether the transient transformation of cells with fluorescent RNP complexes could become another option to label defined sequences in living plant cells remains to be demonstrated.

5.4. Application of Cas12a (Cpf1) for live-cell imaging of telomeres in *N. benthamiana*

A variety of Cas12a orthologues have been identified which show solid genome editing activity in mammalian systems. For plants, Cas12a from *Lachnospiraceae* bacterium ND2006 (*LbCas12a*), *Francisella novicida* (FnCas12a) and *Acidaminococcus* sp. BV3L6 (*AsCas12a*) have been used for genome editing (Endo et al., 2016; Lee et al., 2019; Malzahn et al., 2019). However, different studies showed that the Cas12a variants need a higher temperature for DNA binding and efficient genome editing than Cas9 (Malzahn et al., 2019). However, regardless of the application of higher temperature (30°C) for live-cell imaging of telomeres in transiently transformed *N. benthamiana*, the application of dFnCas12a and AsCas12a did not result in fluorescence labelled telomeres. Since the transient transformation with *A. tumefaciens* can be affected by temperature, the application of higher temperatures could cause problems. Thus, the application of tested Cas12a variants is not possible for live-cell imaging in plants.

5.5. RNA targeting with Cas13 in plants

The first successful application of LwaCas13 for RNA knockdown and RNA targeting in living cells was shown in mammalian cell cultures and an *Oryza sativa* protoplast culture by Abudayyeh et al., (2017). In this study to reduce background noise, negative feedback (NF)

based on zinc finger self-targeting and KRAB domain repression was used. The application of NF resulted in the effective translocation of dLwaCas13:NF from the nucleus to cytoplasm compared to dLwaCas13 without NF element when targeting ACTB transcripts in mammalian cell cultures. In the *O. sativa* protoplast cell culture, LwaCas13 was used for knocking down three different target transcripts including EPSPS, HTC and PDS (Abudayyeh et al., 2017). In our experiment, the visualization of telomeric RNA with dLwCas13a and of 25S rRNA with dRfxCas13d was not successful, though we used NF in our RNA imaging vectors.

The secondary structure of targeted RNA can affect the binding ability of Cas13. In our experiment, the secondary structures of our target RNAs were analysed, and the protospacers were designed for regions that do not form a secondary structure which are inaccessible for dCas13 vectors. Therefore, the unspecific labelling of the target RNAs cannot be caused by this reason. Nonetheless, the reason might be that the dCas13 variants that we selected are not suitable for RNA targeting in plants. Previously, it was shown that among eight Cas13 proteins, including *Lachnospiraceae bacterium* (Lba)Cas13a, *Leptotrichia wadei* (Lwa)Cas13a, *Prevotella* sp. P5-125 (Psp)Cas13b, *Porphyromonas gulae* (Pgu)Cas13b, *Porphyromonas gulae* (Ran)Cas13b, *Eubacterium siraeum* DSM15702 (Es)Cas13d, *Anaerobic digester* metagenome 15706 (Adm)Cas13d, and *Ruminococcus flavefaciens* XPD3002 (Rfx)Cas13d, only three Cas13 proteins including dPspCas13b, dPguCas13b, and dRfxCas13d showed GFP signals when targeting the structural RNA *NEAT1* in human HeLa cells (Yang et al., 2019). Besides, dPspCas13b out of these three Cas13 variants was the only variant that showed specific labelling of *Neat1* RNA and the other two variants had an only non-specific accumulation of GFP. Hence, all available Cas13 variants should be checked regarding their ability to bind plant RNA for imaging in future.

6. Outlook

Following questions should be addressed in the future:

- I. The application of live-cell imaging vectors with an inducible promoter for targeting 45S or 5S rDNA repeats in transiently transformed *N. benthamiana* should be tested for temporary expression of the reporter construct. Temporarily restricted expression of live imaging vectors could result in the observation of rDNA specific signals in living cells.
- II. Transformation of a *Nicotiana* cell suspension culture with telomere-specific imaging vectors to investigate the functionality of vectors in single plant cells compared to stably transformed plants.
- III. Transformation of plants with a high-copy repeat-specific RNP complex instead of using live-cell imaging plasmids. A RNP complex is obtained by *in vitro* assembly of the dCas9 protein with a fluorophore-tagged gRNA which carries (Wang et al., 2019). The RNP complex in comparison to a live-cell imaging vector does not need to be integrated into the genome and then expressed. Therefore, the off-target problem which could be caused by continuous expression of the CRISPR/Cas9 plasmid can be avoided. However, to transfer the RNP complex into the plant cell is challenging. Besides, the lifetime of RNP complex in transformed cells is limited compared to stably transformed cells with a CRISPR vector which express RNPs continuously. Despite, the different expression levels of gRNA and Cas9 enzyme which can happen via CRISPR vector transformation and affect the live imaging quality, might be avoided when RNP transformation is performed.
- IV. Stable transformation of *A. thaliana* chromatin mutants including DDM1, DRD1, RDR6 or MOM1 with centromere-specific live imaging vectors. These genotypes which have been mutated in one of the genes involved in silencing pathways can be used to decipher whether the live-cell imaging vectors are not functional in stably transformed plants due to the silencing of transgene expression which can be tested by RT-PCR analysis or methylation-specific PCR.
- V. For CRISPR/Cas-based imaging of RNA, screening of other dCas13 variants is suggested.
- VI. For targeting of telomere RNA and 25S rRNA, performing RNA-FISH is needed to confirm the specificity of observed signals by dCas13 imaging vector.

- VII. Live imaging of medium level abundant RNAs or inducible genes is recommended. Group IX ERF genes are regulated by methyl jasmonate in a number of plant species including *Arabidopsis* and tobacco (NtORC1). They are expressed in leaf tissue and only in presences of methyl jasmonate (Rushton et al., 2008)
- VIII. Establishment of CRISPR imaging vectors with various copy number of aptamers between 2 and 16.

7. Summary

In this work we present new findings of CRISPR live-cell imaging in plants:

- I. Indirect labelling of dCas9 with integrated aptamer sequences in the sgRNA scaffold including MS2 and PP7 (dCas9:2xMS2/3xPP7:FP) increased the efficiency of CRISPR live-cell imaging in transiently transformed *N. benthamiana* plants up to 75% compared to the application of directly labelled dCas9 (dCas9:GFP). When the dead Cas9 (dCas9) is co-expressed with chimeric sgRNA, the aptamer-binding proteins fused to a fluorescent protein (MCP-FP and PCP-FP) are recruited to the targeted sequence. Besides, the use of the aptamer-based method reduced the unspecific labelling of nucleoli.
- II. The labelling efficiency of the aptamer-based live-cell imaging method is still less than FISH. The reason might be that the optimum temperature for Cas9 protein functionality is different from the temperatures applied in this experiment.
- III. Application of different promoters including RPS5a, 35S and the inducible XVE promoter for dCas9 expression, did not affect the efficiency of telomere labelling using the aptamer-based labelling method.
- IV. Increasing the copy number of MS2 aptamers to 16 for the telomere-specific aptamer construct (dCas9:16xMS2:GFP) resulted in uniform labelling of the *N. benthamiana* nuclei. In contrast, the application of only one MS2 aptamer (dCas9:1xMS2:GFP) reduced the number of labelled telomeres.
- V. Transient transformation of *N. benthamiana* with 5S and 45S rDNA-specific CRISPR live-cell imaging vectors did not result in a specific labelling rDNA. The reason can be chromatin inaccessibility in these regions or because they are considered as fragile sites in the genome. Therefore, the formation of DNA:RNA hybrids in these regions might cause genome instability.
- VI. Stable transformation of *N. benthamiana*, *A. thaliana* and *D. carota* with optimized telomere-, rDNA- and centromere-specific CRISPR live-cell dCas9 imaging vectors did not result in specific labelling of the target sequences. This can be caused by continuous formation of DNA:RNA hybrids via CRISPR/Cas9 which triggers genome instability.

- VII. Application of Cpf1 (dCas12) was not suitable for CRISPR live-cell imaging of genomic sequences.
- VIII. Application of LwdCas13a and dRfxCas13d for the transient detection of 25S rRNA and telomere RNA was not successful. Functional screening of additional dCas13 variants will be required.

8. Zusammenfassung

In dieser Arbeit stellen wir neue Erkenntnisse der CRISPR/Cas-basierten Lebendzellfärbung von DNA und RNA bei Pflanzen vor:

I. Die indirekte Markierung von dCas9 mit Hilfe der Integration von Aptamersequenzen wie MS2 und PP7 im sgRNA-Gerüst (dCas9:2xMS2/3xPP7:FP) konnte die Effizienz der CRISPR-Lebendzellfärbung um bis zu 75% im Vergleich zur Anwendung des direkt markierten dCas9 Proteins (dCas9:GFP) erhöhen. Die Signalqualität bei der Aptamer-basierten Methode wurde durch die Eliminierung des Hintergrundsignals im Nukleolus verbessert.

II. Die Effizienz der Aptamer-basierten Methode zur DNA-Markierung in lebenden Zellen ist geringer als bei der FISH Methode. Der Grund könnte darin liegen, dass die optimale Temperatur für die Funktionalität des Cas9-Proteins von den Temperaturbedingungen abweicht, die in den beschriebenen Experimenten angewendet wurden.

III. Die Anwendung verschiedener Promotoren einschließlich RPS5a, 35S und dem induzierbaren Promotoren XVE für die Expression von dCas9 hatte keinen Einfluss auf die Effizienz der DNA Markierung.

IV. Die Erhöhung der Kopienzahl des MS2-Aptamers im Telomer-spezifischen dCas9:2xMS2:GFP Konstrukt auf 16 Kopien (dCas9:16xMS2:GFP) führte zu einer einheitlichen Markierung des Zellkerns, während die Anwendung einer einzelnen MS2 Kopie (dCas9:1xMS2:GFP), die Anzahl der markierten Telomere im Zellkern reduzierte.

V. Trotz der Verbesserung der für die CRISPR-Lebendzellfärbung verwendeten Vektoren mittels Anwendung von Aptameren, konnten keine anderen genomischen Sequenzen, ausser Telomere in transient oder stabil transformierten Pflanzen erfolgreich in lebenden Zellen markiert werden. Der Grund dafür kann in der Unzugänglichkeit des Chromatins in diesen Regionen liegen. Es kann auch davon ausgegangen werden, dass die Bildung von DNA:RNA-Hybriden in diesen Regionen zu einer Instabilität des Genoms führt.

VI. Cpf1 (dCas12) konnten nicht erfolgreich für die CRISPR-Lebendzellfärbung in Pflanzen eingesetzt werden.

VII. Die Anwendung von dCas13 (LwdCas13a und dRfxCas13d) zur Markierung von 25s rRNA und Telomer-RNA in Pflanzen war nicht erfolgreich. Weitere dCas13-Varianten sollten für die RNA Markierung in lebenden Zellen Zweck getestet werden.

9. References

- Abranches, R., Beven, A.F., Aragón-Alcaide, L., and Shaw, P.J. (1998). Transcription sites are not correlated with chromosome territories in wheat nuclei. *Journal of Cell Biology* 143, 5-12.
- Abudayyeh, O.O., Gootenberg, J.S., Essletzbichler, P., Han, S., Joung, J., Belanto, J.J., Verdine, V., Cox, D.B.T., Kellner, M.J., Regev, A., *et al.* (2017). RNA targeting with CRISPR–Cas13. *Nature* 550, 280-284.
- Abudayyeh, O.O., Gootenberg, J.S., Konermann, S., Joung, J., Slaymaker, I.M., Cox, D.B.T., and Shmakov, S. (2016). C2c2 is a single-component programmable RNA-guided RNA-targeting CRISPR effector. *Science* 353, aaf5573.
- Alleman, M., and Doctor, J. (2000). Genomic imprinting in plants: observations and evolutionary implications. *Plant Molecular Biology* 43, 147-161.
- Anton, T., Bultmann, S., Leonhardt, H., and Markaki, Y. (2014). Visualization of specific DNA sequences in living mouse embryonic stem cells with a programmable fluorescent CRISPR/Cas system. *Nucleus-Austin* 5, 163-172.
- Boch, J., Scholze, H., Schornack, S., Landgraf, A., Hahn, S., Kay, S., Lahaye, T., Nickstadt, A., and Bonas, U. (2009). Breaking the code of DNA binding specificity of TAL-type III effectors. *Science* 326, 1509-1512.
- Boisnard-Lorig, C., Colon-Carmona, A., Bauch, M., Hodge, S., Doerner, P., Bancharel, E., Dumas, C., Haseloff, J., and Berger, F. (2001). Dynamic analyses of the expression of the histone: YFP fusion protein in *Arabidopsis* show that syncytial endosperm is divided in mitotic domains. *The Plant Cell* 13, 495-509.
- Boverly, T. (1909). Die Blastomerenkerne von *Ascaris megalocephala* und die Theorie der Chromosomenindividualität. *Arch. Zellforsch* 3, 181-286.
- Bridger, J., and Volpi, E. (2010). Fluorescence *in situ* hybridization (FISH): protocols and applications (Totowa: Humana Press).
- Burge, S., Parkinson, G.N., Hazel, P., Todd, A.K., and Neidle, S. (2006). Quadruplex DNA: sequence, topology and structure. *Nucleic Acids Research* 34, 5402-5415.
- Bystricky, K. (2015). Chromosome dynamics and folding in eukaryotes: Insights from live cell microscopy. *FEBS Lett* 589, 3014-3022.
- Campell, B.R., Song, Y., Posch, T.E., Cullis, C.A., and Town, C.D. (1992). Sequence and organization of 5S ribosomal RNA-encoding genes of *Arabidopsis thaliana*. *Gene* 112, 225-228.
- Chaumeil, J., Augui, S., Chow, J.C., and Heard, E. (2008). Combined immunofluorescence, RNA fluorescent *in situ* hybridization, and DNA fluorescent *in situ* hybridization to study chromatin changes, transcriptional activity, nuclear organization, and x-chromosome inactivation. In *The Nucleus: Volume 1: Nuclei and Subnuclear Components*, R. Hancock, ed. (Totowa, NJ: Humana Press), pp. 297-308.
- Chen, B., Gilbert, L.A., Cimini, B.A., Schnitzbauer, J., Zhang, W., Li, G.W., Park, J., Blackburn, E.H., Weissman, J.S., Qi, L.S., *et al.* (2013). Dynamic imaging of genomic loci in living human cells by an optimized CRISPR/Cas system. *Cell* 155, 1479-1491.
- Chen, H., Choi, J., and Bailey, S. (2014). Cut site selection by the two nuclease domains of the Cas9 RNA-guided endonuclease. *Journal of Biological Chemistry* 289, 13284-13294.
- Clemente, T. (2006). *Nicotiana (Nicotiana tobaccum, Nicotiana benthamiana)*. In *Agrobacterium Protocols*, K. Wang, ed. (Totowa, NJ: Humana Press), pp. 153-154.
- Cloix, C., Tutois, S., Mathieu, O., Cuvillier, C., Espagnol, M.C., Picard, G., and Tourmente, S. (2000). Analysis of 5S rDNA Arrays in *Arabidopsis thaliana*: Physical Mapping and Chromosome-Specific Polymorphisms. *Genome Research* 10, 679-690.
- Clough, S.J., and Bent, A.F. (1998). Floral dip: A simplified method for *Agrobacterium*-mediated transformation of *Arabidopsis thaliana*. *The Plant Journal* 16, 735–743.
- Cremer, M., Müller, S., Köhler, D., Brero, A., and Solovei, I. (2007). Cell Preparation and Multicolor FISH in 3D Preserved Cultured Mammalian Cells. *Cold Spring Harbor Protocols* 2007, pdb.prot4723.
- Crossley, M.P., Bocek, M., and Cimprich, K.A. (2019). R-Loops as cellular regulators and genomic threats. *Molecular Cell* 73, 398-411.

Cryderman, D.E., Morris, E.J., Biessmann, H., Elgin, S.C.R., and Wallrath, L.L. (1999). Silencing at *Drosophila* telomeres: nuclear organization and chromatin structure play critical roles. *EMBO J* *18*, 3724-3735.

de Nooijer, S., Wellink, J., Mulder, B., and Bisseling, T. (2009). Non-specific interactions are sufficient to explain the position of heterochromatic chromocenters and nucleoli in interphase nuclei. *Nucleic Acids Research* *37*, 3558-3568.

de Storme N, Keçeli BN, Zamariola L, Angenon G, and Daneey, G. (2016). CENH3-GFP: a visual marker for gametophytic and somatic ploidy determination in *Arabidopsis thaliana*. *BMC Plant Biology* *16*, DOI 10.1186/s12870-015-0700-5.

de Wit, E., and de Laat, W. (2012). A decade of 3C technologies: insights into nuclear organization. *Genes and Development* *26*, 11-24.

Del Prete, S., Arpón, J., Sakai, K., Andrey, P., and Gaudin, V. (2014). Nuclear architecture and chromatin dynamics in interphase nuclei of *Arabidopsis thaliana*. *Cytogenetic and Genome Research* *143*, 28–50.

Deng, W.L., Shi, X.H., Tjian, R., Lionnet, T., and Singer, R.H. (2015). CASFISH: CRISPR/Cas9-mediated *in situ* labeling of genomic loci in fixed cells. *Proceedings of the National Academy of Sciences of the United States of America* *112*, 11870-11875.

Dreissig, S., Schiml, S., Schindele, P., Weiss, O., Rutten, T., Schubert, V., Gladilin, E., Mette, M.F., Puchta, H., and Houben, A. (2017). Live-cell CRISPR imaging in plants reveals dynamic telomere movements. *The Plant Journal* *91*, 565-573.

Duan, J., Lu, G., Hong, Y., Hu, Q., Mai, X., Guo, J., Si, X., Wang, F., and Zhang, Y. (2018). Live imaging and tracking of genome regions in CRISPR/dCas9 knock-in mice. *Genome Biology* *19*, 192.

Dunemann, F., Unkel, K., and Sprink, T. (2019). Using CRISPR/Cas9 to produce haploid inducers of carrot through targeted mutations of centromeric histone H3 (CENH3). *Acta Hort.* *1264*, 211 -219, ISHS 2019. Proc. II Int. Symp. on Carrot and Other *Apiaceae*. Eds. D. Grzebelus and R. Barański, DOI 10.17660/ActaHortic.2019.1264.2

Douet, J., and Tourmente, S. (2007). Transcription of the 5S rRNA heterochromatic genes is epigenetically controlled in *Arabidopsis thaliana* and *Xenopus laevis*. *Heredity* *99*, 5–13.

Dvořáčková, M., Fojtová, M., and Fajkus, J. (2015). Chromatin dynamics of plant telomeres and ribosomal genes. *The Plant Journal* *83*, 18-37.

Endo, A., Masafumi, M., Kaya, H., and Toki, S. (2016). Efficient targeted mutagenesis of rice and tobacco genomes using Cpf1 from *Francisella novicida*. *Scientific Reports* *6*, 38169.

Esvelt, K.M., Mali, P., Braff, J.L., Moosburner, M., Yaung, S.J., and Church, G.M. (2013). Orthogonal Cas9 proteins for RNA-guided gene regulation and editing. *Nature Methods* *10*, 1116.

Fajkus, J., Kovařík, A., mKrálovics, R., and Bezděk, M. (1995). Organization of telomeric and subtelomeric chromatin in the higher plant *Nicotiana tabacum*. *Molecular Genetics and Genomics* *247*, 633-638.

Fauser, F., Schiml, S., and Puchta, H. (2014). Both CRISPR/Cas-based nucleases and nickases can be used efficiently for genome engineering in *Arabidopsis thaliana*. *The Plant journal* *79*, 348-359.

Feng, C., Su, H., Bai, H., Wang, R., Liu, Y., Guo, X., Liu, C., Zhang, J., Yuan, J., Birchler, J.A., *et al.* (2018). High-efficiency genome editing using a dmc1 promoter-controlled CRISPR /Cas9 system in maize. *Plant Biotechnology Journal* *16*, 1848-1857.

Fransz, P., de Jong, J.H., Lysak, M., Castiglione, M.R., and Schubert, I. (2002). Interphase chromosomes in *Arabidopsis* are organized as well defined chromocenters from which euchromatin loops emanate. *Proceedings of the National Academy of Sciences of the United States of America* *99*, 14584-14589.

Fu, Y., Rocha, P.P., Luo, V.M., Raviram, R., Deng, Y., Mazzoni, E.O., and Skok, J.A. (2016). CRISPR-dCas9 and sgRNA scaffolds enable dual-colour live imaging of satellite sequences and repeat-enriched individual loci. *Nature Communications* *7*, 11707.

Fujimoto, S., and Matsunaga, S. (2017). Visualization of Chromatin Loci with Transiently Expressed CRISPR/Cas9 in Plants. *Cytologia* *82*, 559–562.

Fujimoto, S., Sugano, S.S., Kuwata, K., Osakabe, K., and Matsunaga, S. (2016). Visualization of specific repetitive genomic sequences with fluorescent TALEs in *Arabidopsis thaliana*. *Journal of Experimental Botany* *67*, 6101-6110.

Fujimoto S., Yonemura M., Matsunaga S., Nakagawa T., Uchiyama S., and Fukui, K. (2005). Characterization and dynamic analysis of *Arabidopsis* condensin subunits, AtCAP-H and AtCAP-H2. *Planta* 222, 293–300.

Gaj, T., Gersbach, C.A., and Barbas, C.F. (2013). ZFN, TALEN, and CRISPR/Cas-based methods for genome engineering. *Trends in Biotechnology* 31, 397-405.

Garimberti, E., and Tosi, S. (2010). Fluorescence *in situ* Hybridization (FISH), Basic Principles and Methodology. In *Fluorescence in situ Hybridization (FISH): Protocols and Applications*, J.M. Bridger, and E.V. Volpi, eds. (Totowa, NJ: Humana Press), pp. 3-20.

Germier, T., Sylvain, A., Silvia, K., David, L., and Kerstin, B. (2018). Real-time imaging of specific genomic loci in eukaryotic cells using the ANCHOR DNA labelling system. *Methods in Enzymology* 142, 16-23.

Giorgetti, L., and Heard, E. (2016). Closing the loop: 3C versus DNA FISH. *Genome Biology* 17, 215.

Gisler, S., Gonçalves, J.P., Akhtar, W., de Jong, J., Pindyurin, A.V., Wessels, L.F.A., and van Lohuizen, M. (2019). Multiplexed Cas9 targeting reveals genomic location effects and gRNA-based staggered breaks influencing mutation efficiency. *Nature Communications* 10, 1598.

Gottschling, D.E., Aparicio, O.M., Billington, B.L., and Zakian, V.A. (1990). Position effect at *Saccharomyces cerevisiae* telomeres - Reversible repression of Pol-II transcription. *Cell* 63, 751-762.

Griffith, J.D., Comeau, L., Rosenfield, S., Stansel, R.M., Bianchi, A., Moss, H., and de Lange, T. (1999). Mammalian Telomeres End in a Large Duplex Loop. *Cell* 97, 503-514.

Gu, B., Swigut, T., Spencley, A., Bauer, M.R., Chung, M., Meyer, T., and Wysocka, J. (2018). Transcription-coupled changes in nuclear mobility of mammalian cis-regulatory elements. *Science* 359, 1050-1055.

Han, Y.H., Moon, H.J., You, B.R., and Park, W.H. (2009). The effect of MG132, a proteasome inhibitor on HeLa cells in relation to cell growth, reactive oxygen species and GSH. *Oncology Reports* 22, 215-221.

Heitz, E. (1928). Das Heterochromatin der Moose. *Jahrbücher für wissenschaftliche Botanik* 69, 762–819.

Hershman, S.G., Chen, Q., Lee, J.Y., Kozak, M.L., Yue, P., Wang, L.-S., and Johnson, F.B. (2007). Genomic distribution and functional analyses of potential G-quadruplex-forming sequences in *Saccharomyces cerevisiae*. *Nucleic Acids Research* 36, 144-156.

Hihara S., P.G., Kaizu K., Tani T., Hanafusa T., and Nozaki T. (2012). Local nucleosome dynamics facilitate chromatin accessibility in living mammalian cells. *Cell Report* 2, 1645- 1656.

Hirakawa, T., Katagiri, Y., Ando, T., and Matsunaga, S. (2015). DNA double-strand breaks alter the spatial arrangement of homologous loci in plant cells. *Scientific Reports* 5, 11058.

Hong, Y., Lu, G., Duan, J., Liu, W., and Zhang, Y. (2018). Comparison and optimization of CRISPR/dCas9/gRNA genome-labeling systems for live cell imaging. *Genome Biology* 19, 39.

Horn, B.K.P. (1987). Closed-form solution of absolute orientation using unit quaternions. *Journal of Optical Society of America A* 4, 629-642.

Hoshi, Y., Yagi, K., Matsuda, M., Matoba, H., Tagashira, N., Pląder, W., Malepszy, S., Nagano, K., and Morikawa, A. (2011). A comparative study of the three cucumber cultivars using fluorescent staining and fluorescence *in situ* hybridization. *Cytologia* 76, 3-10

Hozé, N., Ruault, M., Amoruso, C., Taddei, A., and Holcman, D. (2013). Spatial telomere organization and clustering in yeast *Saccharomyces cerevisiae* nucleus is generated by a random dynamics of aggregation–dissociation. *Molecular Biology of the Cell* 24, 1791-1800.

Hsu, P.D., Scott, D.A., Weinstein, J.A., Ran, F.A., Konermann, S., Agarwala, V., Li, Y., Fine, E.J., Wu, X., Shalem, O., *et al.* (2013). DNA targeting specificity of RNA-guided Cas9 nucleases. *Nature biotechnology* 31, 827-832.

Hu, X., Meng, X., Liu, Q., Li, J., and Wang, K. (2018). Increasing the efficiency of CRISPR-Cas9-VQR precise genome editing in rice. *Plant Biotechnology Journal* 16, 292-297.

Huertas, P., and Aguilera, A. (2003). Cotranscriptionally Formed DNA:RNA Hybrids Mediate Transcription Elongation Impairment and Transcription-Associated Recombination. *Molecular Cell* 12, 711-721.

Ishii, T., Schubert, V., Khosravi, S., Dreissig, S., Metje-Sprink, J., Sprink, T., Fuchs, J., Meister, A., and Houben, A. (2019). RNA-guided endonuclease - *in situ* labelling (RGEN-ISL): a fast CRISPR/Cas9-based method to label genomic sequences in various species. *New Phytology* 222, 1652-1661.

Jovtchev, G., Borisova, B., Kuhlmann, M., Fuchs, J., Watanabe, K., Schubert, I., and Mette, M.F. (2011). Pairing of lacO tandem repeats in *Arabidopsis thaliana* nuclei requires the presence of hypermethylated, large arrays at two chromosomal positions, but does not depend on H3-lysine-9-dimethylation. *Chromosoma* 120, 609-619.

Jovtchev, G., Watanabe, K., Pecinka, A., Rosin, F.M., Mette, M.F., Lam, E., and Schubert, I. (2008). Size and number of tandem repeat arrays can determine somatic homologous pairing of transgene loci mediated by epigenetic modifications in *Arabidopsis thaliana* nuclei. *Chromosoma* 117, 267-276.

Kanda, T., Sullivan, K.F., and Wahl, G.M. (1998). Histone-GFP fusion protein enables sensitive analysis of chromosome dynamics in living mammalian cells. *Current Biology* 8, 377-385.

Kato, L. (2001). Detection of chromosomes tagged with green fluorescent protein in live *Arabidopsis thaliana* plants. *Genome Biology* 2.

Knight, S.C., Xie, L., Deng, W., Guglielmi, B., Witkowsky, L.B., Bosanac, L., Zhang, E.T., El Beheiry, M., Masson, J.-B., Dahan, M., *et al.* (2015). Dynamics of CRISPR-Cas9 genome interrogation in living cells. *Science* 350, 823-826.

Konermann, S., Brigham, M.D., Trevino, A.E., Joung, J., Abudayyeh, O.O., Barcena, C., Hsu, P.D., Habib, N., Gootenberg, J.S., Nishimasu, H., *et al.* (2015). Genome-scale transcriptional activation by an engineered CRISPR-Cas9 complex. *Nature* 517, 583-588.

Konermann, S., Lotfy, P., Brideau, N.J., Oki, J., Shokhirev, M.N., and Hsu, P.D. (2018). Transcriptome engineering with rna-targeting type vi-d crispr effectors. *Cell* 173, 665-676.

Koo, D.H., Zhao, H., and Jiang, J. (2016). Chromatin-associated transcripts of tandemly repetitive DNA sequences revealed by RNA-FISH. *Chromosome Research* 24, 467-480.

Kuscu, C., Arslan, S., Singh, R., Thorpe, J., and Adli, M. (2014). Genome-wide analysis reveals characteristics of off-target sites bound by the Cas9 endonuclease. *Nature Biotechnology* 32, 677-683.

Lane, A.B., Strzelecka, M., Ettinger, A., Grenfell, A.W., Wittmann, T., and Heald, R. (2015). Enzymatically Generated CRISPR Libraries for Genome Labeling and Screening. *Developmental Cell* 34, 373-378.

Lassadi I., Kamgoué A., Goiffon I., Tanguy-le-Gac N., and Bystricky K. (2015). Differential chromosome conformations as hallmarks of cellular identity revealed by mathematical polymer modeling. *PLoS Computational Biology*, 1- 21.

Lee, K., Zhang, Y., Kleinstiver, B.P., Guo, J.A., Aryee, M.J., Miller, J., Malzahn, A., Zarecor, S., Lawrence-Dill, C.J., Joung, J.K., *et al.* (2019). Activities and specificities of CRISPR/Cas9 and Cas12a nucleases for targeted mutagenesis in maize. *Plant Biotechnology Journal* 17, 362-372.

Lieberman-Aiden, E., van Berkum, N.L., Williams, L., Imakaev, M., Ragozcy, T., Telling, A., Amit, I., Lajoie, B.R., Sabo, P.J., Dorschner, M.O., *et al.* (2009). Comprehensive mapping of long-range interactions reveals folding principles of the human genome. *Science* 326, 289-293.

Lin, C.-J., Koh, Fong M., Wong, P., Conti, M., and Ramalho-Santos, M. (2014). Hira-mediated h3.3 incorporation is required for DNA replication and ribosomal RNA transcription in the mouse zygote. *Developmental Cell* 30, 268-279.

Lindhout, B.I., Fransz, P., Tessadori, F., Meckel, T., Hooykaas, P.J.J., and Zaal, B.J. (2007). Live cell imaging of repetitive DNA sequences via GFP-tagged polydactyl zinc finger proteins. *Nucleic Acids Research* 35, e107.

Liu Q., Segal D.J., Ghiara, J.B., and Barbaras, C.F. (1997). Design of polydactyl zinc-finger proteins for unique addressing within complex genomes. *Proceedings of the National Academy of Sciences of the United States of America* 94, 5525-5530.

Ma, H., Naserib, A., Reyes-Gutierrez, P., Wolfec, S.A., Zhangb, S., and Pederson, T. (2015). Multicolor CRISPR labeling of chromosomal loci in human cells. *PNAS* 112, 3002-3007.

Ma, H., Reyes-Gutierrez, P., and Pederson, T. (2013). Visualization of repetitive DNA sequences in human chromosomes with transcription activator-like effectors. *Proceedings of the National Academy of Sciences of the United States of America* 110.

Ma, H., Tu, L.C., Naseri, A., Huisman, M., Zhang, S., Grunwald, D., and Pederson, T. (2016a). Multiplexed labeling of genomic loci with dCas9 and engineered sgRNAs using CRISPRainbow. *Nature Biotechnology* **34**, 528-530.

Ma, X., Zhu, Q., Chen, Y., and Liu, Y. (2016b). CRISPR/Cas9 Platforms for Genome Editing in Plants: Developments and Applications. *Molecular Plant* **9**, 961-974.

Maass, P.G., Barutcu, A.R., Shechner, D.M., Weiner, C.L., Melé, M., and Rinn, J.L. (2018). Spatiotemporal allele organization by allele-specific CRISPR live-cell imaging (SNP-CLING). *Nature Structural & Molecular Biology* **25**, 176-184.

Mak, A.N.-S., Bradley, P., Cernadas, R.A., Bogdanove, A.J., and Stoddard, B.L. (2012). The crystal structure of tal effector pthx1 bound to its DNA target. *Science* **335**, 716-719.

Malzahn, A.A., Tang, X., Lee, K., Ren, Q., Sretenovic, S., Zhang, Y., Chen, H., Kang, M., Bao, Y., Zheng, X., *et al.* (2019). Application of CRISPR-Cas12a temperature sensitivity for improved genome editing in rice, maize, and *Arabidopsis*. *BMC Biology* **17**, 9.

Mariamé, B., Kappler-Gratias, S., Kappler, M., Balor, S., Gallardo, F., and Bystricky, K. (2018). Real-time visualization and quantification of human cytomegalovirus replication in living cells using the anchor DNA labeling technology. *Journal of Virology* **92**, e00571-00518.

Martinez-Zapater, J., Estelle, A., Sommerville, C. (1986) A highly repeated DNA sequence in *Arabidopsis thaliana*. *Molecular Genetics and Genomics* **204**, 4417-4423

Martin, K., Kopperud, K., Chakrabarty, R., Banerjee, R., Brooks, R., and Goodin, M.M. (2009). Transient expression in *Nicotiana benthamiana* fluorescent marker lines provides enhanced definition of protein localization, movement and interactions *in planta*. *The Plant Journal* **59**, 150-162.

Matzke, A.J.M., Huettel, B., van der Winden, J., and Matzke, M. (2005). Use of two-color fluorescence-tagged transgenes to study interphase chromosomes in living plants. *Plant Physiol* **139**, 1586-1596.

Miller, J., McLachlan, A.D., and Klug, A. (1985). Repetitive zinc-binding domains in the protein transcription factor IIIA from *Xenopus* oocytes. *EMBO J* **4**, 1609-1614.

Miyinari, Y., Ziegler-Birling, C., and Torres-Padilla, M.-E. (2013). Live visualization of chromatin dynamics with fluorescent TALEs. *Nature Structural and Molecular Biology* **20**, 1321-1324.

Moyzis, R.K., Buckingham, J.M., Cram, L.S., Dani, M., Deaven, L.L., Jones, M.D., Meyne, J., Ratliff, R.L., and Wu, J.R. (1988). A highly conserved repetitive DNA sequence, (TTAGGG)_n, present at the telomeres of human chromosomes. *Proceedings of the National Academy of Sciences of the United States of America* **85**, 6622-6626.

Municio, C., Antosz, W., Grasser, K., Kornobis, E., Van Bel, M., Eguinoa, I., Coppens, F., Bräutigam, A., Lermontova, I., Bruckmann, A., *et al.* (2019). The *Arabidopsis* condensin CAP-D subunits arrange interphase chromatin (bioRxiv).

Nannas, N.J., and Dawe, R.K. (2016). Live-cell imaging of meiotic spindle and chromosome dynamics in Maize (*Zea mays*). *Current Protocols in Plant Biology* **1**, 546-565.

Němečková, A., Wäsch, C., Schubert, V., Ishii, T., Hřibová, E., and Houben, A. (2019). CRISPR/Cas9-based RGEN-ISL allows the simultaneous and specific visualization of proteins, DNA repeats and sites of DNA replication. *Cytogenetic and Genome Research* **159**, 48-53.

Nimmo, E.R., Cranston, G., and Allshire, R.C.E.J., 3801-3811. (1994). Telomere-associated chromosome breakage in fission yeast results in variegated expression of adjacent genes. *EMBO J* **13**, 3801-3811.

Nishibuchi, G., and Déjardin, J. (2017). The molecular basis of the organization of repetitive DNA-containing constitutive heterochromatin in mammals. *Chromosome Research* **25**, 77-87.

Palmer, L. (2020). The R-loop: An additional chromatin feature for gene regulation in *Arabidopsis* *Plant Cell* **32**, 785-786.

Pattanayak, V., Lin, S., Guilinger, J.P., Ma, E., Doudna, J.A., and Liu, D.R. (2013). High-throughput profiling of off-target DNA cleavage reveals RNA-programmed Cas9 nuclease specificity. *Nature Biotechnology* **31**, 839-843.

Pecinka, A., Kato, N., Meister, A., Probst, A.V., Schubert, I., and Lam, E. (2005). Tandem repetitive transgenes and fluorescent chromatin tags alter local interphase chromosome arrangement in *Arabidopsis thaliana*. *Journal of Cell Science* **118**, 3751-3758.

Phan, H.T., and Conrad, U. (2016). Plant-Based Vaccine Antigen Production. In vaccine technologies for veterinary viral diseases: Methods and Protocols, A. Brun, ed. (New York, NY: Springer New York), pp. 35-47.

Potlapalli, B.P., Schubert, V., Metje-Sprink, J., Liehr, T., and Houben, A. (2020). Application of Tris-HCl allows the specific labeling of regularly prepared chromosomes by CRISPR-FISH. *Cytogenetic and Genome Research* *160*, 156-165.

Prusicki, M.A., Keizer, E.M., van Rosmalen, R.P., Komaki, S., Seifert, F., Müller, K., Wijnker, E., Fleck, C., and Schnittger, A. (2019). Live cell imaging of meiosis in *Arabidopsis thaliana*. *eLife* *8*, e42834.

Qi, L.S., Larson, M.H., Gilbert, L.A., Doudna, J.A., Weissman, J.S., Arkin, A.P., and Lim, W.A. (2013). Repurposing crispr as an rna-guided platform for sequence-specific control of gene expression. *Cell* *152*, 1173–1183.

Qin, P., Parlak, M., Kuscü, C., Bandaria, J., Mir, M., Szlachta, K., Singh, R., Darzacq, X., Yildiz, A., and Adli, M. (2017). Live cell imaging of low- and non-repetitive chromosome loci using CRISPR-Cas9. *Nature Communications* *8*, 14725.

Rabl, C. (1885). Über Zelltheilung. *Morphol Jahrb* *10*, 214–330.

Robinett, C.C., Straight, A.F., Li, G.W., Wilhelm, C., Sudlow, G., Murray, A., and Belmont, A.S. (1996). *In vivo* localization of DNA sequences and visualization of large-scale chromatin organization using lac operator/repressor recognition. *Journal of Cell Biology* *135*, 1685–1700.

Rocha, L.C., de Oliveira Bustamante, F., Silveira, R.A.D., Torres, G.A., Mittelman, A., and Techio, V.H. (2015). Functional repetitive sequences and fragile sites in chromosomes of *Lolium perenne* L. *Protoplasma* *252*, 451-460.

Rosa, S., and Shaw, P. (2013). Insights into chromatin structure and dynamics in plants. *Biology (Basel)* *2*, 1378–1410.

Rosin, F.M., Watanabe, N., Cacas, J., Kato, N., Arroyo, J.M., Fang, Y., May, B., Vaughn, M., Simorowski, J., Ramu, U., *et al.* (2008). Genome-wide transposon tagging reveals location-dependent effects on transcription and chromatin organization in *Arabidopsis*. *The Plant Journal* *55*, 514-525.

Ruiz-Herrera, A., Nergadze, S.G., Santagostino, M., and Giulotto, E. (2008). Telomeric repeats far from the ends: mechanisms of origin and role in evolution. *Cytogenetic and Genome Research* *122*, 219-228.

Saad H., Gallardo F., Dalvai M., Tanguy-le-Gac N., Lane D., and Bystricky K. (2014). DNA dynamics during early double-strand break processing revealed by non-intrusive imaging of living cells. *PLoS Genetics* *10*, e1004187.

Sanjana, N.E., Cong, L., Zhou, Y., Cunniff, M.M., Feng, G., and Zhang, F. (2012). A transcription activator-like effector toolbox for genome engineering. *Nature Protocols* *7*, 171-192.

Schmittgen, T.D., and Livak, K.J. (2008). Analyzing real-time PCR data by the comparative C_T method. *Nature Protocols* *6*, 1101-1108.

Schrumpfova, P.P., Schorova, S., and Fajkus, J. (2016). Telomere- and telomerase-associated proteins and their functions in the plant cell. *Frontiers in Plant Science* *7*, 851.

Schubert, I. and Shaw P. (2011). Organization and dynamics of plant interphase chromosomes. *Trends in Plant Science* *16*, 273-281.

Shao, S., Zhang, W., Hu, H., Xue, B., Qin, J., Sun, C., Sun, Y., Wei, W., and Sun, Y. (2016). Long-term dual-color tracking of genomic loci by modified sgRNAs of the CRISPR/Cas9 system. *Nucleic Acids Research* *44*, e86.

Shechner, D.M., Hacısuleyman, E., Younger, S.T., and Rinn, J.L. (2015). Multiplexable, locus-specific targeting of long RNAs with CRISPR-Display. *Nature Methods* *12*, 664-670.

Sheehan, M.J., and Pawlowski, W.P. (2009). Live imaging of rapid chromosome movements in meiotic prophase I in maize. *Proceedings of the National Academy of Sciences of United States of America* *106*, 20989-20994.

Steinert, J., Schiml, S., Fauser, F., and Puchta, H. (2015). Highly efficient heritable plant genome engineering using Cas9 orthologues from *Streptococcus thermophilus* and *Staphylococcus aureus*. *The Plant Journal* *84*, 1295-1305.

Stella, S., Molina, R., Yefimenko, I., Prieto, J., Silva, G., Bertonati, C., Juillerat, A., Duchateau, P., and Montoya, G. (2013). Structure of the AvrBs3-DNA complex provides new insights into the initial thymine-recognition mechanism. *Acta Crystallographica Section D* *69*, 1707-1716.

Svitashev, S., Young, J.K., Schwartz, C., Gao, H., Falco, S.C., and Cigan, A.M. (2015). Targeted mutagenesis, precise gene editing, and site-specific gene insertion in maize using cas9 and guide RNA. *Plant Physiology* *169*, 931-945.

Sýkorová, E., Fulnečková, J., Mokroš, P., Fajkus, J., Fojtová, M., and Peška, V. (2012). Three TERT genes in *Nicotiana tabacum*. *Chromosome Research* *20*, 381-394.

Rushton, P., Bokowiec, M.T., Han, S., Zhang, H., Brannock, J.F., Chen, X., Laudeman, T.W., and Timko, M.P. (2008). Tobacco transcription factors: Novel insights into transcriptional regulation in the solanaceae. *American Society of Plant Biologists* *147*, 280-295.

Tanenbaum, M.E., Gilbert, L.A., Qi, L.S., Weissman, J.S., and Vale, R.D. (2014). A protein tagging system for signal amplification in gene expression and fluorescence imaging. *Cell* *159*, 635.

Tepfer, M., Gaubert, S., Leroux-Coyau, M., Prince, S., and Houdebine, L. (2004). Transient expression in mammalian cells of transgenes transcribed from the Cauliflower mosaic virus 35S promoter. *Environmental Biosafety Research* *3*, 91-97.

van Tol N., Rolloos M., Hooykaas P.J., and van der Zaal B.J. (2019). Two novel strategies to assess meiotic protein *in vivo* expression in *Arabidopsis thaliana*. *F1000Research* *8*, 539.

Wahba, L., Amon, Jeremy D., Koshland, D., and Vuica-Ross, M. (2011). RNase H and multiple RNA biogenesis factors cooperate to prevent RNA:DNA hybrids from generating genome instability. *Molecular Cell* *44*, 978-988.

Wang, H., Nakamura, M., Abbott, T.R., Zhao, D., Luo, K., Yu, C., Nguyen, C.M., Lo, A., Daley, T.P., La Russa, M., *et al.* (2019). CRISPR-mediated live imaging of genome editing and transcription. *Science* *365*, 1301-1305.

Wang, S., Su, J.H., Zhang, F., and Zhuang, X. (2016). An RNA-aptamer-based two-color CRISPR labeling system. *Scientific Reports* *6*, 26857.

Wang, Z.-P., Xing, H.-L., Dong, L., Zhang, H.-Y., Han, C.-Y., Wang, X.-C., and Chen, Q.J. (2015). Egg cell-specific promoter-controlled CRISPR/Cas9 efficiently generates homozygous mutants for multiple target genes in *Arabidopsis* in a single generation. *Genome Biology* *16*, 144.

Wegel, E., Koumproglou, R., Shaw, P., and Osbourn, A. (2009). Cell type-specific chromatin decondensation of a metabolic gene cluster in oats. *The Plant Cell* *21*, 3926-3936.

Weijers, D., Franke-van Dijk, M., Vencken, R.J., Quint, A., Hooykaas, P., and Offringa, R. (2001). An *Arabidopsis* Minute-like phenotype caused by a semi-dominant mutation in a ribosomal protein S5 gene. *Development* *128*, 4289-4299.

Wesolowska, N., Amariei, F.L., and Rong, Y.S. (2013). Clustering and protein dynamics of *Drosophila melanogaster* telomeres. *Genetics* *195*, 381-391.

Winter, D., Vinegar, B., Nahal, H., Ammar, R., Wilson, G.V., and Provart, N.J. (2007). An "Electronic Fluorescent Pictograph" browser for exploring and analyzing large-scale biological data sets. *PLoS ONE* *2*, e718.

Wu, X., Scott, D.A., Kriz, A.J., Chiu, A.C., Hsu, P.D., Dadon, D.B., Cheng, A.W., Trevino, A.E., Konermann, S., Chen, S., *et al.* (2014). Genome-wide binding of the CRISPR endonuclease Cas9 in mammalian cells. *Nature Biotechnology* *32*, 670-676.

Xiang, G., Zhang, X., An, C., Cheng, C., and Wang, H. (2017). Temperature effect on CRISPR-Cas9 mediated genome editing. *Journal of Genetics and Genomics* *44*, 199-205.

Xu, W., Li, K., Li, S., Hou, Q., Zhang, Y., Liu, K., and Sun, Q. (2020). The R-loop atlas of *Arabidopsis* development and responses to environmental stimuli. *The Plant Cell* *32*, 888-903.

Xue, Y., and Murat, A. (2018). Live-cell imaging of chromatin condensation dynamics by CRISPR. *Cell press* *4*, 216-235.

Yamano, T., Nishimasu, H., Zetsche, B., Hirano, H., Slaymaker, I.M., Li, Y., Fedorova, I., Nakane, T., Makarova, K.S., Koonin, E.V., *et al.* (2016). Crystal Structure of Cpf1 in Complex with Guide RNA and Target DNA. *Cell* *165*, 949-962.

Yang, L.-Z., Wang, Y., Li, S.-Q., Yao, R.-W., Luan, P.-F., Wu, H., Carmichael, G.G., and Chen, L.L. (2019). Dynamic imaging of RNA in living cells by crispr-cas13 systems. *Molecular Cell* 76, 981-997.

Ye, H., Rong, Z., and Lin, Y. (2017). Live cell imaging of genomic loci using dCas9-SunTag system and a bright fluorescent protein. *Cell* 8, 853-855.

Zaidi, S.S., Mahfouz, M.M., and Mansoor, S. (2017). CRISPR-Cpf1: A new tool for plant genome editing. *Trends in Plant Science* 22, 550-553.

Zetsche, B., Gootenberg, J.S., Abudayyeh, O.O., Slaymaker, I.M., Makarova, K.S., Essletzbichler, P., Volz, S.E., Joung, J.v., van der Oost, J., Regev, A., *et al.* (2015). Cpf1 is a single RNA-guided endonuclease of a class 2 CRISPR-Cas system. *Cell* 163, 759-771.

Zhang, S., and Song, Z. (2017). Aio-Casilio: a robust CRISPR-Cas9-Pumilio system for chromosome labeling. *Journal of Molecular Histology* 48, 293-299.

Zuo, J., Niu, Q.-W., and Chua, N.-H. (2000). An estrogen receptor-based transactivator XVE mediates highly inducible gene expression in transgenic plants. *The Plant Journal* 24, 265-273.

10. Curriculum vitae

Job experiences

Since 2017 PhD student in the department of breeding research, research group chromosome structure and function, IPK.

Improvement of methods for live cell imaging with CRISPR, microscopy, immunostaining, FISH, Supervising Bachelor and Master students.

2010-2017 Research associate in the department of tissue culture and gene transformation, ABRII, Karaj, Iran.

Method development to quantitatively assess GMO crops; Double haploid production in barley; Genetic transformation of cotton.

2007-2010 Lab manager in department of tissue culture, north-west ABRII, Tabriz, Iran.

Development of *in vitro* culture techniques; Transferring the *in vitro* culture protocols to private companies; Collaboration with physiology lab to establish physio markers for barley resistant to drought; Supervising of students and guest researchers in the lab.

2006-2007 Secretary of bio-safety society of Iran and executive director of biotechnology magazine for biotechnology society of Iran.

Organising conferences; Collecting information about biotech events for journals.

2005-2006 Research assistant in the department of tissue culture, ABRII, Karaj, Iran.

Assessment of GMO crops.

Skills

- Cell and tissue culture
- Molecular techniques: DNA & RNA extraction, Primer designing, PCR, Real-time PCR, Western blot, Southern blot
- Cloning techniques: Gateway, Gibson, Golden Gate and others
- Ballistic and *Agrobacterium*-mediated plant transformation

- Extraction of carbohydrates, carotenoids, hormones, vitamins, antioxidants, enzymes, proteins, chlorophylls, HPLC
- Cytogenetic techniques: Immunostaining, Fluorescent *in situ* hybridization (FISH), Fluorescence microscopy
- Software: Word, PowerPoint, Photoshop, SAS, DNA star, Vector NTI

Education

2017- now PhD in Agricultural sciences

Martin-Luther-University Halle-Wittenberg, Germany

Thesis Development of a CRISPR-imaging toolset for imaging of genomic loci in living plants , financed by DFG

2003-2005 M.Sc. in Agricultural biotechnology

Faculty of Engineering and Technology, Imam Khomeini International University, Qazvin, Iran

Thesis Study on somatic embryogenesis of *Lilium longiflorum* var. Ceb-Dazzle

1998-2002 Bachelor in Horticulture

Department of Horticulture, Gilan University, Rasht, Iran

Thesis Self incompatibility in sweet and sour cherries

AWARDS

- Plant Science Student Conference (PSSC) prize for poster presentation, Halle (Saale), Germany, 2019.
- Awarded best M.Sc. thesis in Imam Khomeini International University, 2005.
- Acknowledged for sincere endeavours in achieving research objectives of ABRII, 2008.
- Acknowledged for sincere endeavours in achieving research objectives of ABRII, 2010.
- Acknowledged for sincere endeavours in achieving research objectives of ABRII, 2011.
- Acknowledged for sincere endeavours in team working at ABRII, 2013.

SCIENTIFIC PUBLICATIONS FROM PhD THESIS

- Khosravi S., Schindele P., Gladilin E., Dunemann F., Rutten T., Puchta H., Houben A. 2020. Application of aptamers improves CRISPR-based live imaging of plant telomeres. *Frontiers in Plant Science*, 11: 1254.
- Khosravi S., Ishii S., Dreissig S., Houben A. 2020. Application and prospects of CRISPR/Cas9-based methods to trace defined genomic sequences in living and fixed plant cells. *Chromosome Res.* 28: 7-17.
- Adamusova K., Khosravi S., Fujimoto S., Houben A., Matsunaga S., Fajkus J., Fojtova M. 2020. Two combinatorial patterns of telomere histone marks in plants with canonical and non-canonical telomere repeats. *Plant J.* 102: 678-687.

- Ishii T., Schubert V., Khosravi S., Dreissig S., Sprink J.M., Sprink T., Fuchs J., Meister A., Houben A. 2019. RNA-guided endonuclease – *in situ* labelling (RGEN-ISL): a fast CRISPR/Cas9-based method to label genomic sequences in various species. *New Phytologist* 222(3): 1652-1661.

PRESENTATIONS FROM PhD THESIS

- Khosravi S., Dreissig S., Schindele P., Puchta H., Houben A. 2019. Live imaging of chromatin in plant cells: A challenging task for CRISPR. 03-04, July, Plant Transformation and Biotechnology V, Vienna, Austria.
- Khosravi S., Dreissig S., Schindele P., Puchta H., Houben A. 2019. Live imaging of chromatin in plant cells: A challenging task for CRISPR. 05-06, July, Plant Genome Editing and Genome Engineering II, Vienna, Austria.
- Khosravi S., Dreissig S., Schindele P., Puchta H., Houben A. 2019. Live imaging of chromatin in plant cells: A challenging task for CRISPR. 18-21, Jun, 15th Plant Science Student Conference (PSSC), Halle (Saale), Germany.
- Khosravi S., Dreissig S., Schindele P., Puchta H., Houben A. 2018. Live imaging of chromatin by CRISPR in plant cells. 22nd International Chromosome Conference (ICC). 2-5, Sep., 2018. Prague, Czech Republic.

Book Publication FROM PhD THESIS

- Khosravi S., Dreissig S., Schindele P., Wolter F., Puchta H., Houben A. 2020. Live-cell CRISPR imaging in plant cells with a telomere-specific guide RNA. In Book: RNA tagging methods and protocols, Editors: Heinlein M. (Ed.) Springer, ISBN 978-1-0716-0711-4.

OTHER SCIENTIFIC PUBLICATIONS

ORCHID NUMBER: <https://orcid.org/0000-0002-7781-1085>

- Bakhshaie M., Khosravi S., Azadi P., Bagheri H., van Tuyl JM. 2016. Biotechnological advances in *Lilium*. *Plant Cell Rep.* 2016 35(9):1799-826.
- Tohidfar M., Khosravi S. 2015. Transgenic crops with an improved resistance to biotic stresses. *Biotechnologie, Agronomie, Société et Environnement* 19(1): 62-71.
- Mojtahedi N., Koobaz P., Fathi M., Dabirashrafi O., Azadi P., Khosravi S. 2014. Maturation, enlargement and breaking dormancy of *in vitro Lilium* bulblets. *International Journal of Horticultural Science and Technology* 1(2): 101-109.
- Mojtahedi N., Koobaz P., Khosravi S. 2013. Applications, factors and responsible genes in somatic embryogenesis of plants. *Journal of Agricultural Biotechnology* 3(5): 99-118. In Farsi.
- Khosravi S., Tohidfar M. 2012. Transgenic crops meeting the sustainable development goals. *Journal of Biosafety Society* 4(4): 87-102, In Farsi.
- Khosravi S., Eyha F., Tohidfar M. 2011. The economic aspects of GM crops. *Journal of biosafety society* 4(3): 105-120. In Farsi.

- Dejampour J., Majidi I., Khosravi S. Farhadi S., Shadmehr A. 2011. *In vitro* propagation of HS314 Rootstock (*Prunus amygdalus* × *P. persica*). HortScience 46(6): 928-931.
- Khosravi S., Azghandi Vatanpour A., Mojtahedi N., Haddad R. 2007. *In vitro* propagation of *Lilium longiflorum* var. Ceb-Dazzle through somatic embryogenesis. Pakistan Journal of Biological Sciences 10(15): 2517-2521.

Other Scientific Presentations

- Mojtahedi N., Khosravi S., Azghandi Vatanpour A. 2013. Recent progresses in micropropagation of horticultural, herbal, woody and ornamental plants. 8th national biotechnology congress and 4th national biosafety congress, Tehran, Iran.
- Sheykhrezai S., Enayati Shariatpanahi M., Janatabadi A.A., Khosravi S. and Nikkhah H.R. 2013. Effect of culture media, cold and hunger treatments on callus induction and regeneration of anther cultures in *Hordeum vulgare*. 8th national biotechnology congress and 4th national biosafety congress, Tehran, Iran.
- Sheykhrezai S., Enayati Shariatpanahi M., Janatabadi A.A., Khosravi S. and Nikkhah H.R. 2012. Factors effecting embryogenesis of isolated microspores from *Hordeum vulgare*. 3rd congress on agricultural biotechnology, Ferdowsi University of Mashhad, Iran.
- Khosravi S., Ehya F. And Tohidfar M. 2012. The economic aspects of GM crops. 3rd congress on agricultural biotechnology, Ferdowsi University of Mashhad, Iran.
- Mazloomi R., Savari S., Khosravi S. and Hejazi M.A. 2012. Identification of physio-morphological markers associated with drought tolerance in barley cultivars. 15th European congress on biotechnology, Istanbul, Turkey.
- Hejazi M.A., Hosseinzadeh N., Mazloomi R., Khosravi S. 2011. Optimum salinity and carotenoids determination in *Dunaliella* isolates from Gavkhuni lagoon in Iran. The national congress of biotechnology applications in food industry, Gilan, Iran.
- Nasiri, Z., Mousavizadeh S.A., Rashidi V., Razban A., Khosravi S. 2011. Callogenesis of *Allium sativum* through root meristem culture. The 5th regional congress on advances of agricultural researches, Kurdistan, Iran.
- Dejampour J., Majidi I., Khosravi S., Farhadi S. 2010. A reliable approach for micropropagation of HS314 rootstock (*Prunus amygdalus* × *P. persica*). The 16th national and 4th international conference of biology, FUM, Iran.
- Khosravi S. Tohidfar M. 2006. Detection and identifying of imported GM corn. 1th congress on agricultural biotechnology, Razi University, Iran.
- Khosravi S., Mojtahedi N., Azghandi Vatanpour A., Haddad R. 2005. Induction of somatic embryogenesis in *Lilium longiflorum* var. Ceb-Dazzle. International congress on plant genomics & biotechnology: challenges and opportunities, Raipur, India.

Other Book Publications

- Kahrizi D., Esfehani K., Ashraf Mehrabi A., Ghaheri M., Azizi Aram Z., Khosravi S., Eslamian S. 2017. "Biotechnology for Drought Improvement" in Eslamian S, Eslamian F. (ed.) *Handbook of Drought and Water Scarcity: Environmental Impacts and Analysis of Drought and Water Scarcity*. CRC press Taylor and Francis group, pp.446-459
- Tohidfar M., Mohsenpour M., Khosravi S. 2014. Production of recombinant proteins in plants. Hagshenas Press, Gilan, Iran.

Stay in other research groups

May-August 2017 Plant reproductive biology group, IPK, Germany. Supervisor: Dr. Jochen Kumlen

January 2018 Botanical institute, Karlsruhe, Institute of Technology, Karlsruhe, Germany. Supervisor: Prof. Holger Puchta

Language Skills

Persian: Native

English: IELTS 7

German: **B1**.

References

Prof. Dr. Andreas Houben

Address: Leibniz Institute of Plant Genetics and Crop Plant Research (IPK), Gatersleben, Corrensstraße 3, 06466 Stadt Seeland, Germany

Phone: (0049) (0)39482 5486

E-mail: houben@ipk-gatersleben.de

Prof. Dr. Holger Puchta

Address: Botanical Institute, Karlsruhe Institute of Technology, Karlsruhe, Germany

Phone: (0049) (0)721 608-48894

E-mail: holger.puchta@kit.edu

Dr. Jochen Kumlehn

Address: Leibniz Institute of Plant Genetics and Crop Plant Research (IPK), Gatersleben, Corrensstraße 3, 06466 Stadt Seeland, Germany

Phone: (0049) (0)39482 5361

E-mail: kumlehn@ipk-gatersleben.de

11. Eidesstattliche Erklärung / Declaration under Oath

Ich erkläre an Eides statt, dass ich die Arbeit selbstständig und ohne fremde Hilfe verfasst, keine anderen als die von mir angegebenen Quellen und Hilfsmittel benutzt und die den benutzten Werken wörtlich oder inhaltlich entnommenen Stellen als solche kenntlich gemacht habe.

I declare under penalty of perjury that this thesis is my own work entirely and has been written without any help from other people. I used only the sources mentioned and included all the citations correctly both in word or content.

Datum / Date

Unterschrift des Antragstellers / *Signature of the applicant*

12. Appendix

List of primers used in different parts of cloning steps. Letters in the lower case show the overhangs which were added to the primer sequence.

| Primer name | Primer sequence (5' to 3') |
|------------------|---|
| Apta2-FWD | AAGTGGCACCGAGTCGGTGCTTTTTTCTAGACCCAGCTTTCTTGT ACa |
| Apta2-Rev | <u>accggt</u> GTACAAGAAAGCTGGGTCTAGAAAAAAGCACCGACTCG GTGCCACTT |
| Apta2-Rev2 | CCGACTCGGTGCCACTTCC |
| SS42 | CGACTAAGGGTTTCTTATATGC |
| ecori-35s-f1 | AAGCAGAATTCAACATGGTGGAGCACGACACA |
| ecori-35s-r1 | TGCTTAGCGAATTCCCCCGTGTCTCTCCAATG |
| PRS5A-FWD | gaattcGATGAGAGAGGAACTG |
| PRS5A-REV | gaattcGGTGAGAGAAACAGAG |
| Cas9-XVE-F | acagctatgacatgattacgaattcATAGTTTAACTGAAGGCGGGAAAC |
| XVE-Lexa-A-R | atcaattcccTCAGACTGTGGCAGGGAAAC |
| XVE-Lexa-A-F | cacagtctgaGGGAATTGATCCCCCCTC |
| LexA-Cas9-R | ttcttatccatggcgcgccgaatTCCTCTCAAATGAAATGAACTTC |
| MS2(NLS)-GFP#1 f | aagagaaaggttcagctgctATGGTGAGCAAGGGCGAG |
| GFP#1-linker1-r | atgccagagcggccgcagaCTTGTACAGCTCGTCCATG |
| linker1-GFP#2-f | agtctggcggccgctctggcATGGTGAGCAAGGGCGAG |
| GFP#2-linker2-r | atgctaccatcgatgctaccCTTGTACAGCTCGTCCATG |
| linker2-GFP#3-f | agggtagcatcgatggttagcATGGTGAGCAAGGGCGAG |
| linker2-GFP#3-f | agggtagcatcgatggttagcATGGTGAGCAAGGGCGAG |

| | |
|------------------------------|--|
| GFP#3-nos_ter-r | ggggaaattcgggggcaattTACTTGTACAGCTCGTCC |
| MS2(NLS)-mRuby#1-f | aagagaaagttgcagctgctATGGTGTCTAAGGGCGAAG |
| mRuby#1-linker1-r | atgccagagcggccgccagaCTTGTACAGCTCGTCCATC |
| linker1-mRuby#2-f | agtctggcggccgctctggcATGGTGTCTAAGGGCGAAG |
| mRuby#2-linker2-r | atgctaccatcgatgctaccCTTGTACAGCTCGTCCATC |
| linker2-mRuby#3-f | agggtagcatcgatgtagcATGGTGTCTAAGGGCGAAG |
| mRuby#3-nos_ter-r | ggggaaattcgggggcaattTACTTGTACAGCTCGTCCA |
| pDS2.0-ΔsgRNA-r | aGAGACGTCCGTCTCcaAT |
| pDS2.0-ΔsgRNA-f | AAGTGGCACCCGAGTCGGTG |
| sgRNA2.0-MS2-flip/ext-f | attgggagacggacgtctctGTTTAAGAGCTATGCTGGGCCAAC |
| sgRNA2.0-MS2-flip/ext-r | attgggagacggacgtctctGTTTAAGAGCTATGCTGGGAGCAG |
| Telomere protospacer-F | attgGGGTTTAGGGTTTAGGGTTT |
| Telomere protospacer-R | aaacAAACCCTAAACCCTAAACCC |
| Centromere protospacer1-F | attgACCTTCTTCTTGCTTCTCAA |
| Centromere protospacer1-R | aaacTTGAGAAGCAAGAAGAAGGT |
| Centromere protospacer2-F | attgTCTTCTTGCTTCTCAAAGCT |
| Centromere protospacer2-R | aaacAGCTTTGAGAAGCAAGAAGA |
| Centromere protospacer3-F | attgATATGAGTCTTTGGCTTTGT |
| Centromere protospacer3-R | aaacACAAAGCCAAAGACTCATAT |
| GFP-F | CCGACAAGCAGAAGAACGGC |

| | |
|--------|----------------------|
| GFP-R | GCGCTTCTCGTTGGGGTCTT |
| dCas-F | AGGTGGCATACCACGAGAAG |
| dCas-R | TGGTTGTAGGTCTGCACGAG |
